FEDERAL UNIVERSITY OF SANTA CATARINA
JOINVILLE TECHNOLOGY CENTER
AEROSPACE ENGINEERING

FELIPE PIMENTA PERALTA

ANALYSIS OF CUTTING PARAMETERS’ IMPACT ON THE MACHINABILITY OF ADDITIVELY MANUFACTURED POROUS INCONEL 718 FOR USE AS SUPPORT STRUCTURE IN THE MANUFACTURING OF AEROSPACE COMPONENTS

Joinville
2024

FELIPE PIMENTA PERALTA

ANALYSIS OF CUTTING PARAMETERS’ IMPACT ON THE MACHINABILITY OF ADDITIVELY MANUFACTURED POROUS INCONEL 718 FOR USE AS SUPPORT STRUCTURE IN THE MANUFACTURING OF AEROSPACE COMPONENTS

This bachelor thesis is presented to fulfill the partial requirement to obtain the bachelor’s degree in Aerospace Engineering of the Joinville Technology Center from the Federal University of Santa Catarina.

Supervisor: Antônio Otaviano Dourado, Dr.

Co-supervisor: Sebastian Schneider, M.Sc.

Joinville
2024

FELIPE PIMENTA PERALTA

ANALYSIS OF CUTTING PARAMETERS' IMPACT ON THE MACHINABILITY OF ADDITIVELY MANUFACTURED POROUS INCONEL 718 FOR USE AS SUPPORT STRUCTURE IN THE MANUFACTURING OF AEROSPACE COMPONENTS

Este Trabalho de Conclusão de Curso foi julgado adequado para obtenção do título de bacharel em Engenharia Aeroespacial, no Centro Tecnológico de Joinville, da Universidade Federal de Santa Catarina

Joinville (SC), 24 de Junho de 2024.

Banca Examinadora:

Prof. Dr. Antônio Otaviano Dourado
Orientador/Presidente

M.Sc. Sebastian Schneider
Membro(a)
RWTH Aachen

Prof. Dr. Erick Cardoso Costa
Membro(a)
UFSC

Prof. Dr. Gabriel Benedet Dutra
Membro(a)
UFSC

ACKNOWLEDGEMENTS

First of all, I would like to express my deepest gratitude to my parents, not only for their unconditional love, support, and encouragement throughout my academic and personal journey, but also for their priceless example of empathy, love, and generosity. Their belief in me has been a constant source of motivation, and I definitely would have not accomplished this without them. To my dear sister, whose support and care have always been present.

To my incredible girlfriend, my partner at anytime, her love, friendship, kindness, patience, and encouragement in so many aspects of life have been my rock throughout these years. I am so grateful to share life with with such an amazing woman. A big thank you also goes to her family, who has always been very supportive, lovely, and is very important to me.

My dear grandma Hilda (in memoriam), thank you for always being a source of inspiration, love, kindness and support. I'm sure you're always there.

To my family, cousins and friends, the old ones and the ones I had the privilege to meet in the course of graduation, thank you for your friendship and all the laughs during the challenging and funny moments. You have made this journey easier and more enjoyable.

I could not forget to thank my pets Richard, Ghost and Ferdinando for being a constant source of fun and happiness.

A big thank you goes to my co-supervisor M.Sc. Schneider, who not only suggested me the topic of this thesis, but also provided invaluable guidance, support and mentorship throughout the development of this work and during my internship at the Fraunhofer Institute (IPT). His insights, expertise, patience, and friendly relationship have been fundamental in shaping my understanding of the subject matter. I'd also like to extend my gratitude to the Fraunhofer Institute for Production Technology (IPT) for their incredible support. Their physical facilities, technical expertise, and dedicated staff were absolutely essential to this research.

I am also grateful to Prof. Dr. Dourado for his support, guidance and feedback. And a special thank you to all the professors I have been privileged to learn from and for providing invaluable knowledge and teaching during undergrad.

Finally, I would like to express my sincere gratitude to all those individuals and university employees at all levels whose dedication and commitment have been and will continue to be essential to the proper functioning and progress of our public, plural, and inclusive university.

> “ *Viver é partir, voltar e repartir*
> *Partir, voltar e repartir* ”
>
> Emicida - É Tudo Pra Ontem

ABSTRACT

Additive manufacturing (AM), especially the Laser Powder Bed Fusion (LPBF), has been gaining increasingly importance in the manufacturing of aerospace and turbomachinery components, given its advantages over conventional subtractive manufacturing, such as design freedom, integration of functions into components, and resource efficiency. In this sense, the application of LPBF has potential for both economic and environmental process optimization. Depending on the complexity of the component's geometry, AM requires the use of support structures, later removed usually by milling. The use of supports with specifically induced porosity is one option that allows improved heat dissipation, processing time, and material consumption compared to usual supports, in block or lattice shape. Widely used in the manufacturing of aeronautical parts due to its thermal and mechanical resistance, the nickel-chromium alloy Inconel 718 has been applied in the manufacturing of components via LPBF. Initial studies, however, have indicated that the machinability of AM porous Inconel 718 is inferior to that of its dense form. To broaden the understanding of this phenomenon, in this work milling trials were conducted on cubic samples of porous Inconel 718 obtained via LPBF, using uncoated tungsten carbide cutting tools with enhanced toughness. The experiments employed a fractional factorial design, wherein the effects of varying the influencing factors on cutting forces and accelerations, flank wear, chip form, and surface finishing were evaluated using analysis of variance (ANOVA). Overall, chipping could be significantly reduced, and for the first time, parameter combinations that exhibited predominantly flank wear up to the investigated feed travel were identified. These results provide cause-effect knowledge and support potential optimizations for the milling process of porous materials, with a view to their application in industry.

Keywords: Additive Manufacturing; LPBF; porous Inconel 718; milling.

RESUMO

A manufatura aditiva (AM), especialmente a fusão em leito de pó (LPBF), tem ganhado relevância na fabricação de componentes aeroespaciais e de turbomáquinas, dadas as vantagens em relação à manufatura subtrativa convencional, como liberdade de design, integração de funções e eficiência no uso de recursos. A aplicação da LPBF possui, assim, potencial de otimização econômica e ambiental do processo. Dependendo da complexidade da geometria do componente, a fabricação por AM exige a utilização de estruturas de suporte, posteriormente removidas geralmente por fresamento. O emprego de suportes com porosidade especificamente induzida possibilita melhoria da dissipação de calor, redução do tempo de processamento e do uso de material comparado aos suportes convencionais, em bloco ou malha. A liga de níquel-cromo Inconel 718, amplamente empregada na manufatura de peças aeronáuticas devido à sua resistência térmica e mecânica, tem sido aplicada na fabricação de componentes por LPBF. Estudos iniciais, porém, mostraram que a usinabilidade do Inconel 718 poroso aditivamente manufaturado é inferior à da sua forma densa. Visando ampliar o entendimento sobre esse fenômeno, neste trabalho testes experimentais de fresamento foram realizados em amostras cúbicas de Inconel 718 poroso, obtidos via LPBF, com ferramentas de corte de carbeto de tungstênio com tenacidade aumentada. Os experimentos empregaram design fatorial fracionário para avaliar, com ajuda da análise de variância (ANOVA), os efeitos da variação dos parâmetros de controle sobre as forças e acelerações no processo, bem como sobre o desenvolvimento do desgaste de ferramenta, formato do cavaco e acabamento da superfície. Em geral, o desgaste por lascamento pôde ser consideravelmente reduzido, e pela primeira vez comparado a estudos anteriores, combinações de parâmetros exibindo predominantemente desgaste de flanco até o percurso de corte estudado foram identificados. Esses resultados fornecem conhecimento de causa-efeito, fundamentam e oferecem possibilidades de otimização para o processo de usinagem de materiais porosos, visando sua aplicação na indústria.

Palavra-chave: manufatura aditiva; LPBF; Inconel 718 poroso; fresamento.

LIST OF FIGURES

LIST OF TABLES

LIST OF ABBREVIATIONS AND ACRONYMS

AM	Additive Manufacturing
ANOVA	Analysis of variance
BLISK	Blade Integrated Disk
CAD	Computer-Aided Design
CVD	Chemical Vapor Deposition
DAP	Digital Additive Production Institute RWTH Aachen
DED	Direct energy deposition
DIN	Deutsches Institut für Normung
DoE	Design of Experiments
EBM	Electron Beam Melting
IPC	Embedded Industrial PC
IPT	Fraunhofer-Institute for Production Technology
KPI	Key Performance Indicator
LPBF	Laser Powder Bed Fusion
PBF	Powder Bed Fusion
PM	Powder Metallurgy
PVD	Physical Vapor Deposition
RMS	Root Mean Square
SEM	Scanning Electron Microscope
SL	Sheet lamination
SLM	Selective Laser Melting
TDMS	Technical Data Management Streaming

LIST OF SYMBOLS

r_β	Cutting edge radius
VB_{max}	Maximal width of flank wear land
CH_{max}	Maximal width of chipping
VB_{mean}	Mean width of flank wear land
l_f	Feed travel
F_a	Active Force
acc_x	Cutting acceleration in the x-direction
acc_y	Cutting acceleration in the y-direction
S	Cutting Edge
β	Wedge Angle
A_γ	Rake face
A_α	Flank face
κ_r	Tool cutting edge angle
λ_s	Tool cutting edge inclination
ν_f	Feed velocity
ν_c	Cutting velocity
a_p	Depth of cut
γ_n	Tool normal rake angle
a_e	Radial depth of cut or width of cut
f_z	Feed per tooth
n	Spindle revolutions per minute
z	Teeth number of the tool
R_0	Tool radius
VB	Width of flank wear land
F	Resultant Cutting Force
F_p	Passive Force
F_e	Effective Force
$F_{e,n}$	Effective Normal Force
F_c	Cutting Force
$F_{c,n}$	Cutting Normal Force
F_f	Feed Force
$F_{f,n}$	Feed Normal Force
ν_e	Effective cutting speed
η	Cutting speed angle
φ	Feed motion angle
P_L	Laser power

v_s	Scanning speed
Δy_s	Hatch spacing
D_s	Layer thickness
n_r	Experimental effort
n_f	Number of factors
n_l	Number of levels
K_{IC}	Measured critical tension intensity factor
D_r	Relative density
CH	Width of chipping

CONTENTS

1 INTRODUCTION

Conventional manufacturing of aerospace components still relies on advanced machining techniques on forged and billet structures, in order to provide high precision and quality to the pieces (Klocke *et al.*, 2015). On the other hand, this technique has a high buy-to-fly ratio, which means that significant amount of time, energy, and material are consumed during the subtractive manufacturing process, resulting in a considerable volume of waste metal that is only recycled when possible, greatly impacting production efficiency and costs (Dutta; Froes, 2017).

In recent decades, the aerospace sector has been increasingly demanding lighter components that enable waste reduction in production while meeting safety and reliability standards (Najmon; Raeisi; Tovar, 2019). In this sense, the Additive Manufacturing (AM) presents itself as a promising substitute for aerospace components and turbomachinery manufacturing, due to its advantages compared to traditional subtractive methods, including design freedom, weight, cost and time reduction, improved raw material efficiency, and increased competitiveness (Angrish, 2014; Blakey-Milner *et al.*, 2021). The urge of climate change and the need for sustainable, resource-efficient, and carbon-neutral production have also accelerated the industry's search for alternatives to optimize existing production processes (Mani; Lyons; Gupta, 2014).

The Laser Powder Bed Fusion (LPBF) process, one of the innovative AM technologies, can be employed in the production of components that are often subjected to high mechanical and thermal loads. Its industrial-scale application still depends on overcoming the technological obstacles that are the subject of this work. A Blade Integrated Disk (BLISK) is a noteworthy illustrative example of the challenges in manufacturing aerospace components with complex geometries. Its sophisticated shape, curved aerodynamic sections, variable blade heights, and internal cooling ducts require the use of support structures when manufactured via LPBF. The support ensures improved stabilization and heat dissipation. However, as these structures do not contribute to any additional features, they must be removed during the post-processing phase, often through 5-axis milling (FRAUNHOFER-IPT, 2019; Svantesson, 2021). Figure 1 shows an AM-BLISK prototype obtained through LPBF process with usage of support structures.

Different structure shapes can be used to build up the support structures. Another possibility is the use of material with specifically induced porosity. When compared to conventional support structures, such as block supports, the porous support structures offer good heat dissipation in the laser entry zone during LPBF. This ensures homogeneous properties for the component while simultaneously reduces process duration, material consumption, and residual stresses introduced in the part. However, the machinability of such AM-porous materials has hardly been researched up to now (Schneider *et al.*, 2022). Pre-

Figure 1 – BLISK prototype manufactured by LPBF with use of support structure

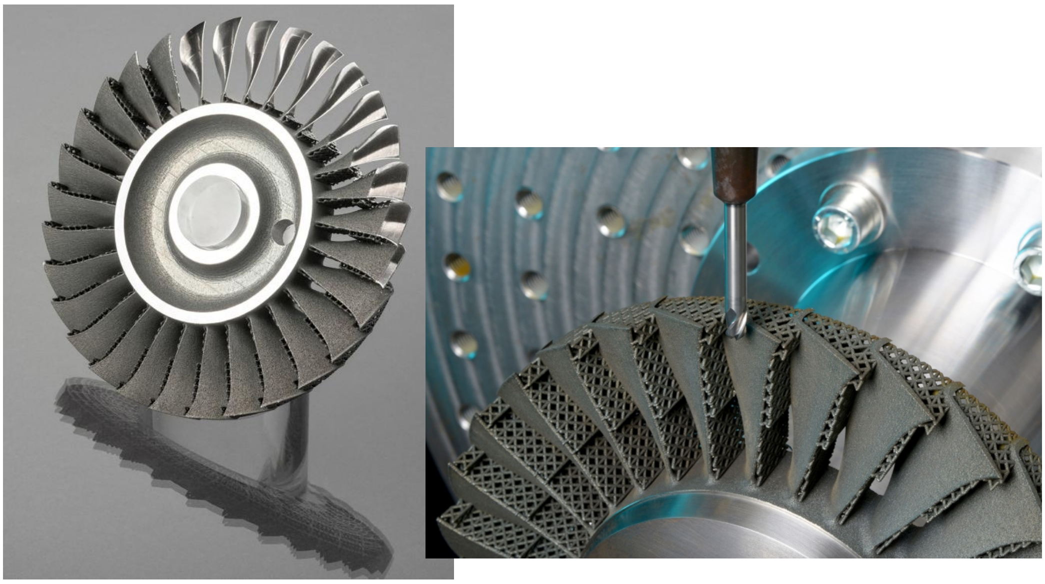

Source: Adapted from Fraunhofer-IPT (2019).

liminary milling and orthogonal cutting investigations conducted by Kirchmann (2022) and Li (2023) using AM-porous nickel-chromium based alloy, Inconel 718, showed that this material exhibits considerably poorer machinability compared to its dense form. Nevertheless, further investigations are needed to determine the influences of technological parameters on the machinability of porous Inconel 718, given its potential applications and considering its specific resistance to corrosion, high temperatures, and widespread use in the aerospace industry (Blakey-Milner *et al.*, 2021).

This work presents an investigation into the machinability of porous Inconel 718 cubic samples additively manufactured via LPBF with specifically induced porosities of 16% (material with 84% relative density) and 28% (72% relative density). The goal of this research is to assess the influence of various parameters and machining configurations on the evolution of cutting tool wear, with a particular focus on flank and chipping wear. This will be achieved by analysing machinability criteria, as forces and accelerations associated with the process, as well as the tool wear development. The parameters that have been subjected to investigation include the cutting speed, feed per tooth, radial depth of cut, feed direction, tool substrate, use of cooling fluid, and cutting edge radius. The ultimate objective is to establish cause-effect relationships between the process variables in order to minimise tool wear and prevent the development of chipping. This may have the potential to enhance the efficiency and economic viability of machining such materials and their use in the manufacture of complex aerospace components by AM.

A Design of Experiments (DoE) was set up to find out the most influential variables and parameters, based on the results of previous studies (Wood *et al.*, 2020; Kirchmann, 2022; Li, 2023). Two series of milling trials were carried out using a fractional factorial experimental design. During the tests, data on cutting forces, accelerations, evolution of cutting tool wear, chip form, and surface quality were collected and subsequently evaluated. These trials took place on the shop floor of the Fraunhofer - Institute for Production Technology (IPT) located at the Campus Melaten in Aachen, Germany, using a Makino D500 five-axis machining center.

1.1 OBJECTIVES

The following objectives are defined in the light of the economic, technological and environmental challenges associated with the machinability of porous support structures, seeking to achieve reliable and cost-effective manufacturing of aerospace components by additive manufacturing.

1.1.1 General Objective

Analyze the influence of cutting parameters and configurations on the machinability of porous AM-Inconel 718, aiming for its use as a support structure in the AM production of aerospace components.

1.1.2 Specific Goals

In addition, the specific objectives of the work are:

- Identify proper control and target variables, according with its influences on the machinability;
- Define a suitable experimental test plan using DoE based on a partial factorial experimental design;
- Identify suitable strategies for evaluating the process data acquired in the experiments;
- Assess the significance of the quantitative results through Analysis of variance (ANOVA);
- Better the understanding of cause-effect relations between the control and target variables;
- Gather conclusions that support process optimization.

2 STATE OF THE ART

To provide a better understanding and introduce the theory behind the many concepts that are going to be explored in this thesis, this chapter introduces some essential foundations and the main aspects of its theory. First of all the fundamentals of the cutting process, an overview of the cutting parameters, chip formation, and milling process, will be presented. Secondly, the cutting tools, cutting materials, and tool wear mechanisms is going to be characterized. Further, the Inconel 718 alloy and its properties, as well as the AM process, in particular the LPBF, and the machinability of conventional Inconel 718 and porous AM materials will be also discussed. Lastly, a broader view of the DoE process will be given.

2.1 FUNDAMENTALS OF CUTTING

The Deutsches Institut für Normung (DIN) defines the machining process in DIN-8580 (2022) as the process in which form is altered reducing material cohesion. This deformation is achieved by means of a relative motion between the tool and the workpiece, involving the transfer of energy. In other words, machining is the process in which layers of material are mechanically separated from a workpiece in the form of chips using a cutting tool. The procedures of the machining process are further defined by DIN-8589 (2003) and divided into two types, machining with geometrically defined cutting edges and undefined cutting edges.

During this work only the machining of geometrically defined cutting edges will be treated, therefore the term machining will be used ahead as a synonym for this kind of cutting process. In addition, all the processes in the group of geometrically defined cutting edges have in common the use of a tool, whose cutting edge number, geometry, and position are determined. In contrast, the process is called abrasive or cutting with geometrically undefined cutting edges if the geometrical features of the cutting edge can only be described statistically. Turning, drilling, and milling are examples of cutting processes while grinding is designated as an abrasive process (DIN-8589, 2003).

The cutting tool has an active part where the cutting wedges and edges are located, which is named as cutting part. The cutting wedge is idealized as having two faces, the rake and flank face, which meet each other in the cutting edge S, the angle between these two faces is the wedge angle β. Furthermore, A_γ is the face of the cutting edge where the chip runs off and A_α is the face of the cutting edge, which is turned towards the cut surface, thus this definition makes sense only in connection with the workpiece (Klocke, 2011). Figure 2 shows the idealized cutting wedge described earlier.

Figure 2 – Idealized Cutting Wedge and Process kinematics illustration

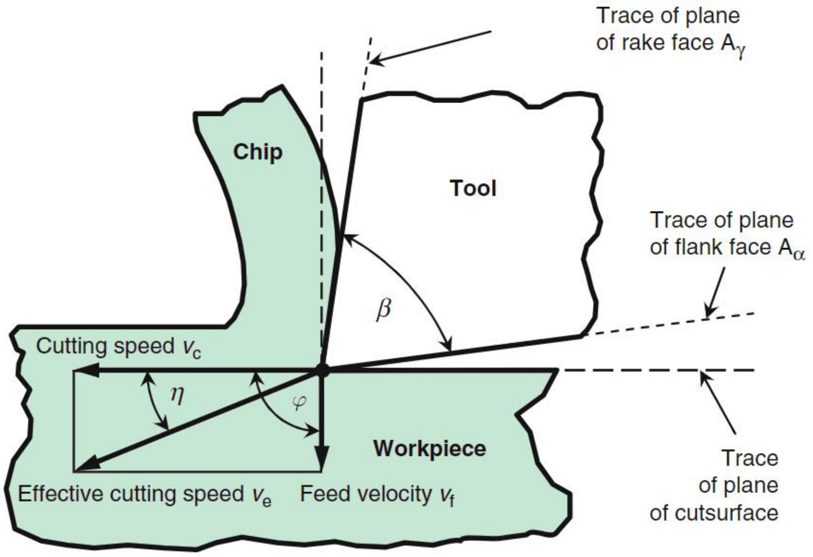

Source: Adapted from Klocke (2011).

2.1.1 Basic Process Variants

The cutting process variants can be subdivided into three main categories, according to parameters such as tool cutting edge angle κ_r, between the feed direction and the cutting edge plane, and tool cutting edge angle inclination λ_s, between the trace of the tool reference plane, perpendicular to the assumed cutting direction, and the major cutting edge S. According to Klocke (2011), the three basic cutting variants are:

- **Free, orthogonal cut**: the κ_r = 90° (orthogonal), λ_s = 0° (orthogonal), and only the major cutting edge is being engaged. This is the case for longitudinal face turning or cross-cylindrical turning.
- **Free, diagonal cut**: the κ_r can assume values different of 90° (diagonal), arbitrary values are also possible for λ_s and only the major cutting edge is engaged (free).
- **Bound, diagonal cut**: contains both previous cases also enabling the engagement of the minor cutting edge.

Furthermore, the cutting process can also be classified, conforming to Klocke (2011) in two categories:

- **Uninterrupted cut**: the cut is almost continuous, and temporal interruption is infinitely small.
- **Interrupted cut**: the cut occurs only intermittently.

Figure 3 illustrates the free, orthogonal cut and free, diagonal cut.

Figure 3 – Free, orthogonal cut (a) and free, diagonal cut (b) Illustration

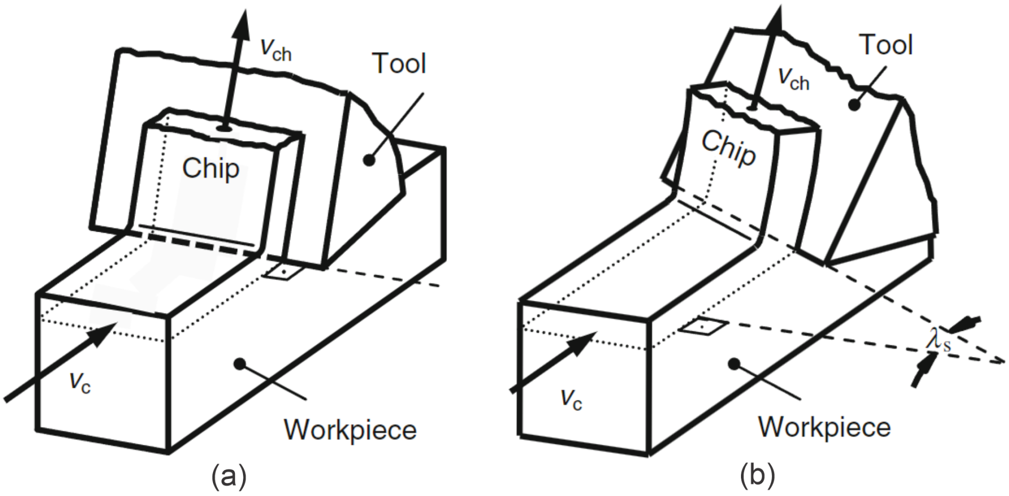

Source: Adapted from Klocke (2011).

2.1.2 Chip Formation

The chip is the result of the elastic and plastic deformation that occurs when the tool-cutting section penetrates the material. In other words, the material starts to flow after the maximum permissible material shear stress is exceeded and depending on a given cutting section geometry, the deformed material forms a chip, which flows through the rake face of the cutting section (Denkena; Tönshoff, 2011).

Furthermore, plastic deformability is not only related to the material, it can also be caused in a targeted way altering the stress. Some process variables such as the feed velocity ν_f, cut velocity ν_c, and depth of cut a_p influence the amount of stress generated. In terms of process kinematics, the direction of cutting section stress can be determined by defining the tool normal rake angle γ_n, the tool cutting edge angle κ_r, and the tool cutting edge inclination λ_s. A minimum chip thickness and depth of cut must be exceeded to ensure chip formation (Opitz; Brammertz; Kohlhage, 1963).

One same material can behave as tough or brittle depending on the direction and amount of stress, independently of how it behaves under a tension test (at room temperature and under single-axis tensile loads). This fact has a huge effect during cutting and, consequently, on chip formation. The direction of a particular stress can be set by some process parameters during cutting, such as the tool normal rake angle γ_n, tool cutting edge angle κ_r, and tool cutting edge inclination λ_s. It is important to keep in mind, that some materials as steel have a brittle behavior only at very low temperatures, while cast iron, glass, and ceramics, due to their material structures, can present brittle fracture behavior even at higher temperatures, therefore, the stress must be adjusted accordingly to the material properties and to process kinematics in both direction and amount (Klocke, 2011).

Figure 4 shows the chip formation process. The plastic deformation zone, colored, is subdivided into four areas: (a) is the zone of transition between the workpiece and the chip structure (b), where cutting is made by simple shearing. With brittle materials, small deformations on the shear plane can already lead to material detachment. However, detachment first occurs in (e) when the material has higher deformability. In addition, strong deformations occur close to the rake face (c) and cut surface (d) under simultaneous perpendicularly active pressure and high temperatures, prevalent in the contact zone. The area surrounding the transition zone on the bottom of the chip is called the "flow zone" and has a deformation texture parallel to the rake face, which gives the impression of a viscous flow process and a high degree of deformation. The chip formed from this process is called a continuous chip, but there are other chip types such as lamellar, segmented, and discontinuous chips (Klocke, 2011).

Figure 4 – Chip initiation zone

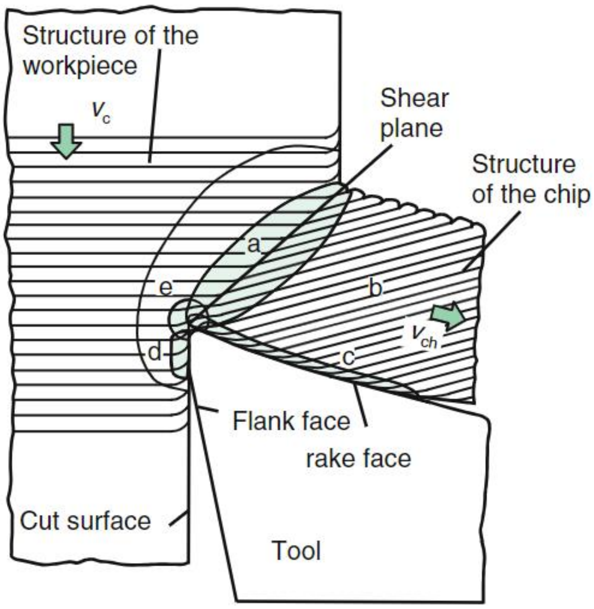

Source: Adapted from Klocke (2011).

Once the chip formation has been ensured the type of the chip is dependent on the material properties, processes parameters, range of temperature, friction, deformation, and vibration. Vieregge (1959) summarized the four principal chip types, which are illustrated in Figure 5:

- **Continuous chips** are formed when the material of the workpiece has sufficient deformability, uniform microstructure in the cutting area, no embrittlement due to deformation, and chip formation is not affected by vibrations.
- **Lammellar chips** occur when the microstructure of the workpiece material, grain structure, is not uniform, or when vibrations lead to fluctuations in chip thickness and process forces. The lamellar chips can be formed with high ν_f as well as high ν_c.

- **Segmented chips** are formed when chip segments are separated in the shear plane and then fused together due to the high temperatures of the process. They are formed when the strain rates at the primary zone cause local structural embrittlement in the microstructure of the workpiece material. This type of chip can also be formed at extremely low ν_c.
- **Discontinuous chips** occur mostly when cutting brittle materials with uneven microstructure, the chips are torn off the surface instead of being detached, which leads to damage due to small breakings on the workpiece surface. This process is composed of two main phases, stagnation and elimination. In the stagnation phase, the part of the material flowing concurrently to the cutting edge has no velocity component either on the rake or on the flank face, which leads to increasing stress and temperature values until the failure of the material. In the elimination phase, the chip segmented created on the previous phase welded with other chip segments comes off the workpiece and flows through the rake face.

Figure 5 – Types of chip and its formation according to Vieregge (1959)

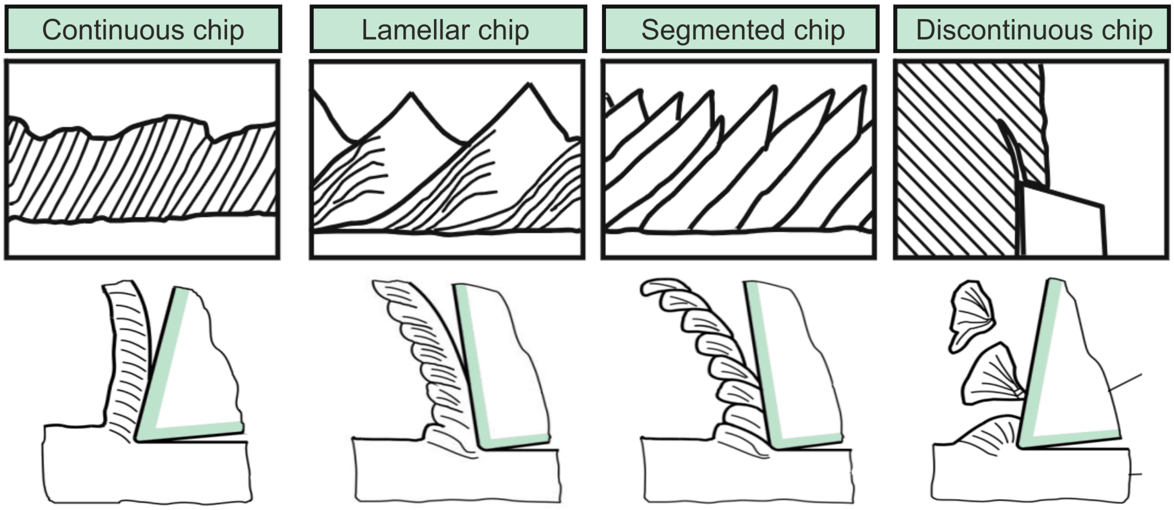

Source: Author (2024).

2.1.3 Milling Process

The kinematic engagement condition is the main difference between the various types of cutting processes, and it is defined by the tool orientation, the direction of cutting, and the direction of feed relative to the workpiece. The milling process is defined by DIN-8589 (2003) as being the machining with a predominantly circular movement of the tool cutting edges and a perpendicular or oblique feed direction in relation to the rotational axis of the tool. Furthermore, milling can be subdivided into two variants, face milling in which the tool axis is perpendicular to the workpiece surface, or peripheral milling in which the tool axis is parallel to the workpiece surface. The chip formation happens as a combination of a rotation movement of the tool and a relative movement between the milling tool and the workpiece, this movement can be linear in 3-axis milling machines or linear/rotary in 5-axis milling machines.

Another classification of the milling process is related to the direction of rotation of the milling tool and the movement of the workpiece during cutting, if both are in opposite directions at the point of contact between the tool and workpiece the process is called Up milling. Otherwise, the process is called Down milling when the feed rate vector ν_f and the cutting speed vector ν_c are pointing in the same direction at the point of contact (Youssef; El-Hofy, 2008), both classifications are illustrated in Figure 6.

Figure 6 – Chip initiation zone

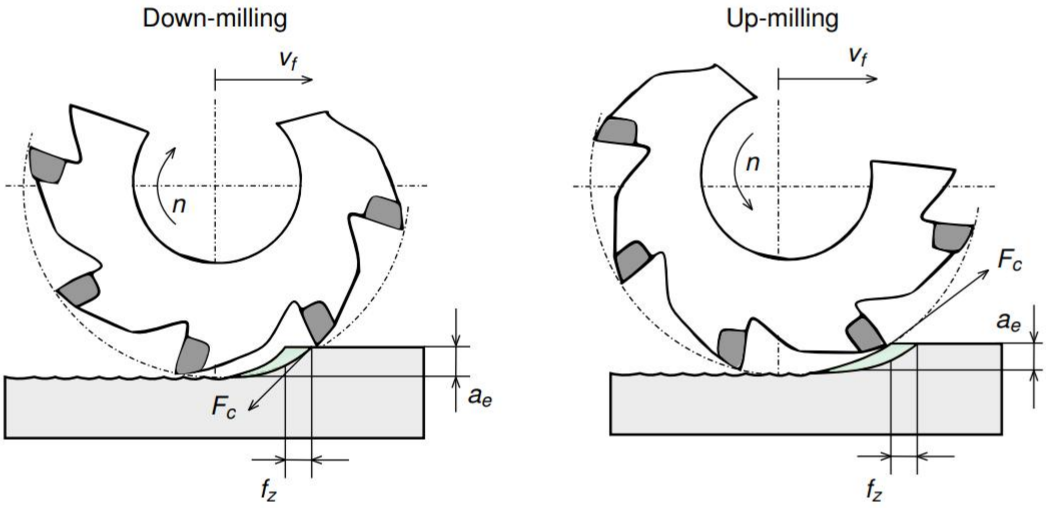

Source: Adapted from Youssef and El-Hofy (2008).

Three main operations work together to shape and refine a workpiece during the milling process, roughing, pre-finishing, and finishing. Roughing is the initial operation, where the primary goal is to remove a significant amount of material rapidly. It utilizes a robust cutting tool and aggressive cutting parameters to quickly reduce the workpiece's overall dimensions and achieve the desired shape roughly. In the pre-finishing stage, a tool with higher precision is employed to remove the remaining excess material and bring the workpiece closer to its final shape, focusing on achieving tighter tolerances and improving surface quality in preparation for the last operation. The final stage, known as finishing, involves the use of specialized cutting tools that prioritize surface quality, dimensional accuracy, and fine detail. Finishing cuts are typically performed at reduced speeds and feeds, allowing for precise contouring, smoothing, and achieving the desired surface finish (Youssef; El-Hofy, 2008; Klocke, 2011). By progressing through these three operations, the milling process enables the transformation of raw material into a precisely machined workpiece with the desired dimensions and surface characteristics.

2.1.4 Process kinematics and variables

DIN6580 (1988) gives the terminology for the chip-removing process, movements, and geometry of the chip. The technological parameters used to describe the path of the milling tool are often used by CAM programmers and machine operators during the process design. These parameters are normally found in catalogs of milling tool manufacturers, in which recommendations are given for each type of milling tool, material, and surface combination and are the most used parameters in the process layout.

The tool position, orientation, and motion in relation to the workpiece are understood as the kinematics of the milling process. The motion of the cutting edge can be essentially described as the superposition of a translational and a rotational component. Figure 7 represents the technological parameters for a ball-end milling tool, whose concept can be expanded to other peripheral milling operations. However, a universal set of parameters for describing all types of milling strategies cannot be set, because different process strategies require other parameters for describing the tool movement (Klocke, 2011; Cabral, 2015).

Figure 7 – Technological parameters for ball-end milling

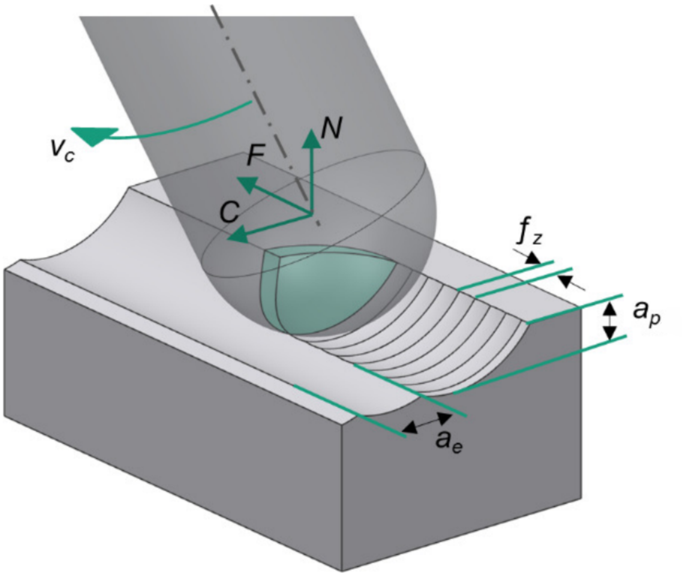

Source: Adapted from Cabral (2015).

The parameters in the technological cutting parameters according to Klocke (2011) are explained below:

- v_f or **feed velocity** is directly related to the feed rate.
- v_c or **cutting speed** is the tangential speed of the cutting edge and has important influence on temperature, power consumption and tool life.

- a_e or **radial depth of cut** is the width between two consecutive tool passes, and it's strongly related to the roughness of the generated surface.
- a_p or **depth of cut** is the tool penetration in the normal direction of the surface.
- f_z or **feed per tooth** is the translational movement of the tool for each tooth pass, and it is the parameter that has the most influence on the process forces.
- n or **spindle speed** is the number of revolutions the milling tool makes per minute.

The feed velocity can be calculated by the Equation 1 below, and it is directly related to the feed rate and spindle revolutions per minute.

$$\nu_f = z \cdot f_z \cdot n \tag{1}$$

in which z is the number of teethes present on the cutting tool. Moreover, the cutting speed ν_c is the tangential speed of the cutting edge, and it is one of the most relevant factors for process planning, affecting the chip formation mechanisms, forces, tool wear, and workpiece quality. It can be calculated by Equation 2 and it is dependent on the tool radius and on the spindle speed.

$$\nu_c = 2\pi \cdot R_0 \cdot n \tag{2}$$

2.1.5 Machinability

Machinability is defined by DIN6583 (1981) as the property of a workpiece or material that allows chip removal under specific conditions. Some criteria such as tool wear, chip shape, and surface quality are often used to assess the machinability of a material and will be briefly introduced below.

2.1.5.1 Wear

The area of the cutting edge experiences deformation, separation, and friction during the cutting process, therefore the tool materials are subject to complex loads, high compressive stress, high cutting speeds, and high temperatures. Cutting tools reach the end of their service life because of increasing wear on both rake and flank faces when using standard cutting parameters. The wear is explained as a continuous loss of material from the surface of the tool due to contact and relative motion of solid, liquid, or gaseous counter body (Klocke, 2011).

2.1.5.1.1 Wear mechanisms

The main mechanisms that explain wear are adhesion, abrasion, tribochemical reaction, and surface disruption.

- **Abrasion**: common and purely mechanical wear mechanism that occurs when two surfaces are in relative motion, in which hard particles or parts of the material penetrate the cutting tool material and simultaneously perform a tangential motion, generating scores and micro-cutting on the cutting material surface. This mechanism is enhanced by friction and associated with high temperatures on the surface (Degener *et al.*, 2019).
- **Adhesion**: is the wear mechanism in which atomic bonds are formed in the contact zone between the friction partners, workpiece, and cutting tool material, these bonds are then deformed, reinforced, and sheared off during the tangential motion of the friction partners. In other words, small particles of the machined material stick or weld to the tool. The adhesion mechanism can be caused by atomic interaction (chemical adhesion), thermally induced diffusion processes, electric exchange, electrical polarization, or mechanical snagging (mechanical adhesion) due to plastic deformation of the workpiece material under higher temperatures. When the transfer of particles between the partners is the main cause of wear, it is referred to as adhesive wear (Habig, 1980). The adhesion mechanism is also responsible for built-up edge formation when material particles accumulate in the cutting edge and rake face and are work-hardened due to high pressure and temperature (Klocke, 2011).
- **Tribooxidation**: refers to chemical reactions between the workpiece material, cutting material, and the intermediate material or surrounding medium induced by friction. This oxidation occurs at the edges of the contact zone when the surface temperature and oxidation tendency of the cutting material are high enough (Degener *et al.*, 2019). Furthermore, the reaction products can be either removed with the chip or remain stuck to the cutting material as a coating, causing wear to be increased or reduced.
- **Diffusion**: is a strongly temperature-dependent physicochemical mechanism, in which cutting material particles diffuse into the workpiece material or workpiece material penetrates the cutting material on the atomic level, reducing the resistance to wear of the cutting material. Diffusion occurs, mainly when high cutting speeds are used, leading to high temperatures and pressures in the contact zone. The diffusion of essential alloying elements can lead to decreased hardness and thus to reduced resistance of the cutting tool material to abrasion (Klocke, 2011).
- **Surface Damage**: is the result of tibological alternating stresses. The alternating mechanical stresses, in the stress surface areas, lead to structural changes, fatigue, cracking, crack growth, and even to detachment of wear particles. In contrast to abrasion, in which wear particles can be formed by a single stress process, the surface damage mechanism is usually preceded by a period in which no measurable wear is detected (Habig, 1980).

Figure 8 shows the main wear mechanisms responsible for the total wear as a function of the cutting temperature or speed. The wear processes can only be partially separated from each other since they overlap and influence each other in terms of cause and effect on wear (Klocke, 2011).

Figure 8 – Wear mechanisms influence during cutting

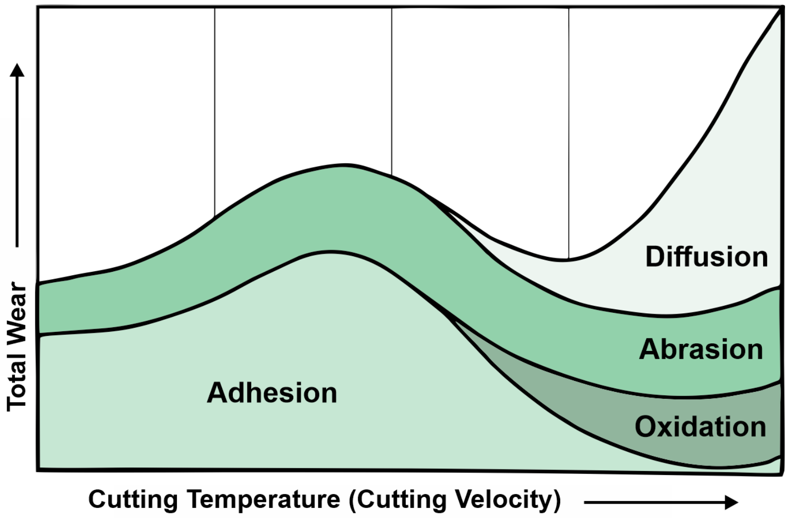

Source: Adapted from Klocke (2011).

2.1.5.1.2 Wear Forms

The tools are subjected to high mechanical and thermal stresses during the cutting process, which often exceeds the load-bearing limit of the cutting material, leading to wear and failure of the cutting edge. Due to the previously listed wear mechanisms, characteristic wear forms are formed, allowing the tool life to be determined as one of the machinability criteria. The forms of wear that are relevant in the context of this work are flank wear and chipping on the cutting edge (Dietrich, 2016).

2.1.5.1.3 Flank wear

The flank wear occurs on the flank area of the tool and can be distinguished between wear occurring on the main or secondary cutting edge. It is the most desirable tool wear condition since it is predictable and dependable, while offering a clear and well-defined relationship between flank wear and achievable tool life. Flank wear is a phenomenon that occurs during the machining of a wide range of workpiece materials. In most cases, a cutting edge will fail due to flank wear if it does not fail due to other types of wear first (SECO, 2023). The wear surface, also called wear land, is parallel to the cutting direction and spreads along the cutting edge. The width of the flank wear land is measured according to ISO3685 (1993) and can be represented as a wear parameter with the mean wear land width, VB, or with the maximum wear land width, VB_{max}, an illustration is shown on Figure 9.

Figure 9 – Width of flank wear land according to ISO3685 (1993)

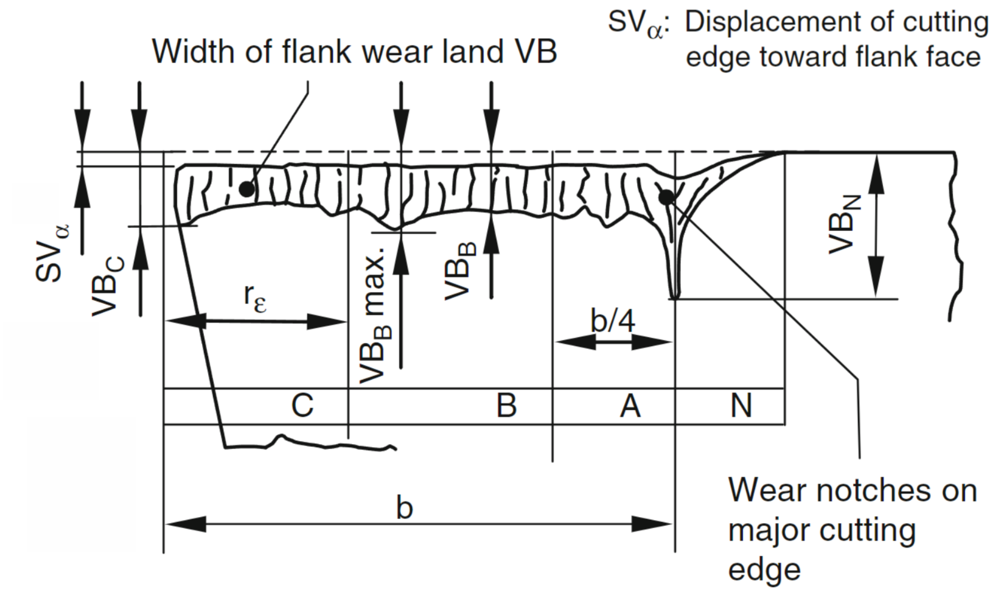

Source: Adapted from ISO3685 (1993).

2.1.5.1.4 *Chipping*

Over-stressing can also occur due to the high mechanical and thermal stress on the tools, leading to damage to the cutting edge in a process called chipping. The interrupted cut, in particular, leads to mechanical and thermal alternating stresses during milling because of the periodic entry and exit of the cutting edge on the material, increasing the concentrations of localized stress that result in cracks and chipping (Klocke, 2011). Chipping of the cutting edge is frequently attributed to vibrations in the workpiece or machine tool, or to the tool itself. It looks like small bits broken out of the cutting edge and is common in non-rigid situations. The impact between the main cutting edge and the chips can also cause cutting material chipping. Chipping is normally not desirable due to its stochastic and unpredictable nature (Kirchmann, 2022; SECO, 2023). In addition, Seco (2023) suggests some ways to minimise chipping include are proper setup of the machine tool setup, minimizing deflection, use of tougher carbide grade and stronger cutting edge geometry, reduction of the feed at the entrance or exit of the cut and increase of the cutting speed.

2.1.6 Cutting Forces

During the cutting process, various cutting forces play important roles. These forces are generated as a result of the interaction between the cutting tool and the workpiece, acting on the workpiece and engaging in a cutting point (DIN6584, 1982). The total cutting force F applied by the tool on the workpiece can be defined as the force required to overcome the elastic and plastic regimes of the workpiece's material and the frictional resistances present in the rake and flake faces of the tool.

This total force can be broken down into different components in the working plane and perpendicular to the working plane. The component perpendicular to the working plane, defined by the vector ν_c and ν_f, is the passive force F_p and it is not involved in the power during machining. The component that generates power during cutting is called active force F_a and it is also in the working plane. Furthermore, the active force can be decomposed into an effective direction, effective force F_e, and perpendicular to the effective direction, effective normal force $F_{e,n}$, as well as a subdivision into cutting direction, cutting force F_c, perpendicular to the cutting direction, cutting normal force $F_{c,n}$, the feed force F_f in the feed direction and the feed normal force $F_{f,n}$ perpendicular to the feed force, Figure 10 illustrates the cutting force components (Degener *et al.*, 2019).

Figure 10 – Cutting forces components Illustration

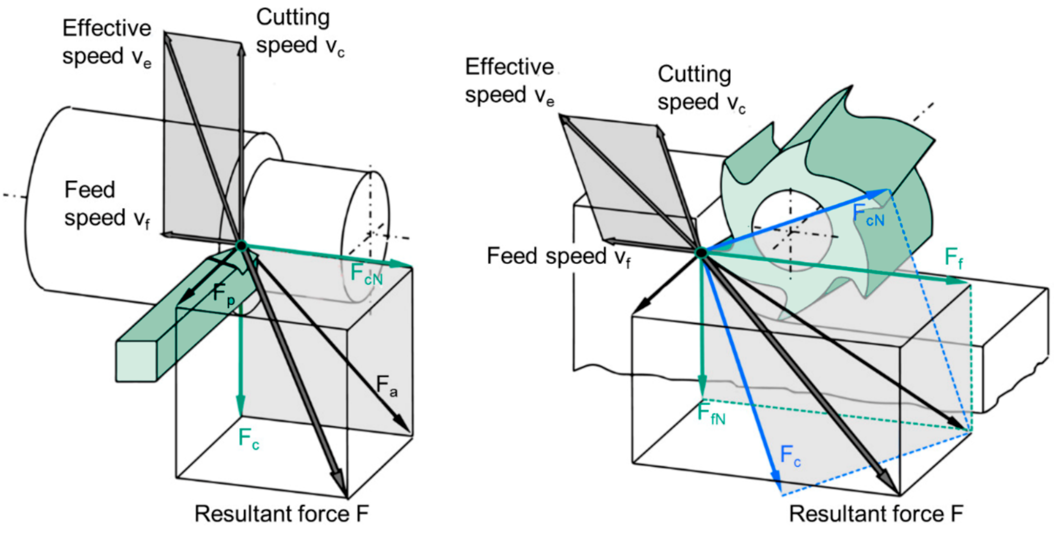

Source: Adapted from DIN6584 (1982).

The influences of the forces F_c, F_f and F_p on the cutting parameters ν_f, ν_c and a_p are qualitatively shown in Figure 11. While the feed rate ν_f increases, the force components also increase. For the variation of the force components due to increasing in cutting speed ν_c, the extreme values can be explained by built-up edge formation. On the other hand, the decrease in force components at increasingly ν_c results from the decrease in the strength of the material, as a consequence of temperature rise. Finally, the cutting force components increase proportionally to a_p, when a_p is greater than, the corner radius of the tool R_0 (Klocke, 2011).

Understanding and controlling these cutting forces are crucial in machining opera-

Figure 11 – Qualitative influence of feed, cutting velocity, and depth of cut on components of resultant force depending

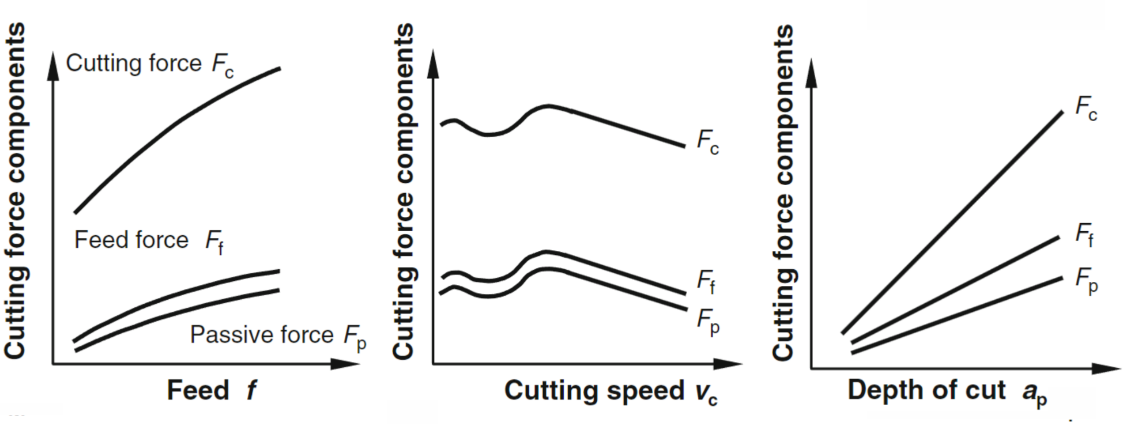

Source: Adapted from Klocke (2011).

tions. Excessive cutting forces can lead to various issues, including tool wear, poor surface finish, dimensional inaccuracies, machine tool deflection, and increased energy consumption. To optimize the cutting process, it is essential to select appropriate cutting parameters, use cutting tools with suitable geometries, ensure proper tool material and condition, and consider workpiece material properties. By effectively managing cutting forces, manufacturers can achieve efficient and reliable machining operations while maintaining the desired quality and productivity (Klocke, 2011).

2.2 CUTTING TOOLS

The selection and utilization of cutting tools and materials are vital aspects of modern machining processes, playing a crucial role in achieving efficient and accurate material removal. With advancements in manufacturing technologies and the ever-increasing demands for higher productivity and precision, the field of cutting tools and materials has witnessed significant developments. This section examines the influence of workpiece materials and their properties on tool selection and machining strategies. Understanding the state of the art in cutting tools and materials is crucial for optimizing machining processes, improving productivity, and meeting the challenges posed by modern manufacturing requirements.

2.2.1 Cutting Tool Geometry

Solid-body milling tools are the most used tools in multi-axis milling operations. The tool geometry can be characterized by its macroscopic geometry and by the cutting geometry. End mills and ball-end tools are the most used type of tools used in practical milling applications. The end mill tools are commonly used for roughing operations, while the ball-end used to be mainly used for finishing operations due to their small area of contact with the workpiece surface (Cabral, 2015).

A simplified description of the process kinematics is shown in the idealized illustration, Figure 2, summarizing the spatial velocity fields in one point, the cutting point, where the velocity fields are represented by vectors. In this model, the workpiece is assumed as fixed, and the resulting velocity vector is ν_e, which can be split in the cutting velocity ν_c in the cutting direction and feed velocity ν_f in the feed direction. Two angles are also defined in relation to the velocity directions, η as the angles between ν_e and ν_c, and φ between ν_c and ν_f (Klocke, 2011).

In the majority of the cases, there is a curved transition between the flank and the rake face, described by the cutting edge radius r_β (DIN6582, 1988). The cutting edge can also be chamfered and the three main types of cutting edge profiles are shown in Figure 12.

Figure 12 – Types of cutting edge profiles

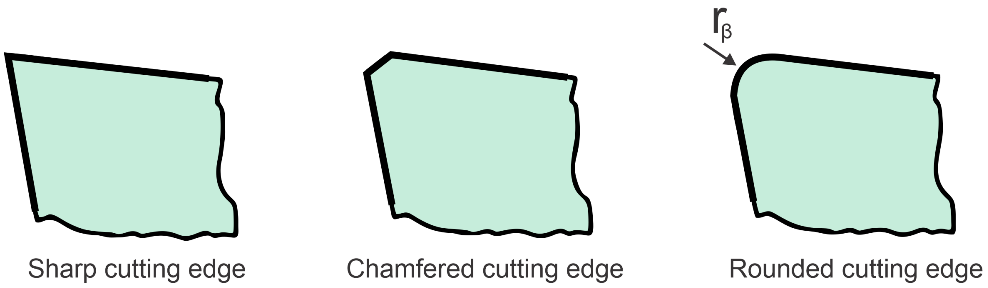

Source: Adapted from DIN6582 (1988).

Usually, more complex tools are used with several cutting wedges, one example of such a cutting wedge, composed of one major cutting wedge and one minor cutting face is presented in Figure 13. The major cutting edge is always turned towards the cut surface, while the minor cutting edge is towards the machined face (Klocke, 2011).

2.2.2 Cutting Edge Preparation

Modern production demands high productivity and high process reliability. For this reason, the selection of an appropriate shape for the cutting edge is very relevant to improving wear resistance, tool life, surface quality, and performance during machining operations. Different approaches of cutting edge preparation including coating, cutting edge rounding, and pre-treatment, among others can be applied to improve the cutting process. For this work, two forms of cutting-edge preparation, cutting-edge rounding, and coating, are relevant for the experimental part and will be explained in the next two sections (Klocke, 2011; Denkena; Biermann, 2014).

Figure 13 – Representation of cutting edges and faces

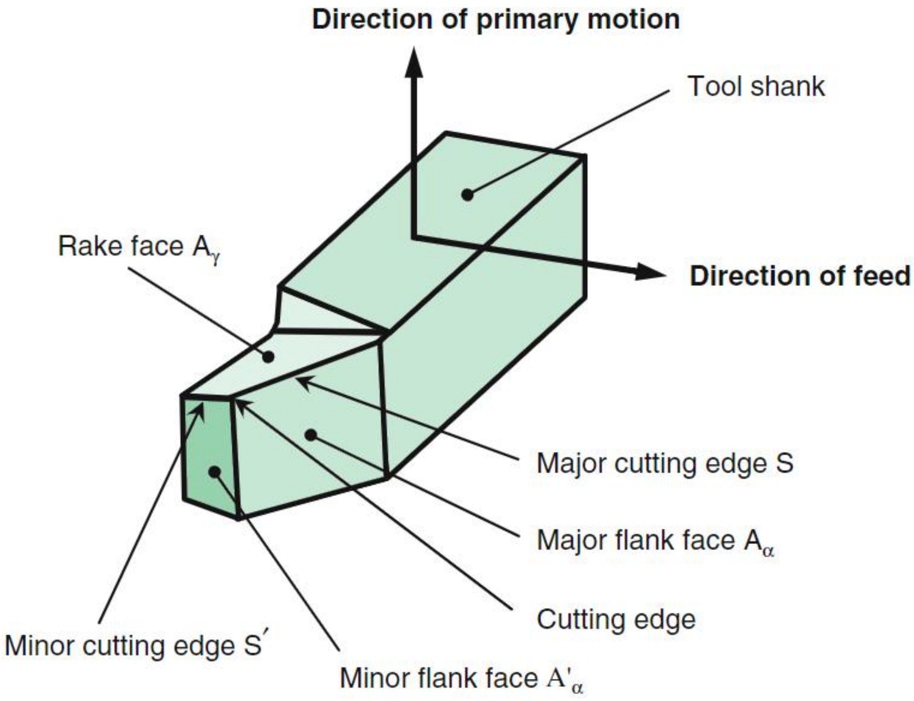

Source: Adapted from Klocke (2011).

2.2.2.1 Cutting Edge Rounding

The cutting edge rounding process in milling cutting tools is the intentional rounding of the sharp cutting edge of the tool in order to improve the tool's performance, extend its life, and improve the quality of the machined surface, this process is also known as edge honing. The process and technologies to prepare the edge profile are dependent on the geometric requirements. Common preparation methods are grinding, brushing, dry and wet abrasive jet machining, drag finishing, brush-polishing, magneto abrasive machining, abrasive flow machining, laser machining, and electrical discharge machining, among others. Figure 14 illustrates some of these processes (Denkena; Biermann, 2014; Klocke, 2011).

Each of these processes is precise and controlled, allowing manufacturers to achieve the desired cutting-edge rounding with a high level of accuracy. The choice of the process depends on factors such as tool material, desired level of sharpness, and intended application of the tool. Additionally, the process should be performed by skilled operators or using automated systems to ensure consistent results and maintain the overall quality and performance (Denkena; Biermann, 2014).

The cutting edge radius r_β plays a significant role in the durability of the cutting tool, especially when dealing with extra hardened materials such as nickel alloys (Denkena; Biermann, 2014). Celaya *et al.* (2019) and Ondřej, Miroslav and Tomáš (2018) showed in their work that the cutting edge preparation, cutting edge rounding in particular, had a pos-

Figure 14 – Schematic overview of cutting edge preparation technologies

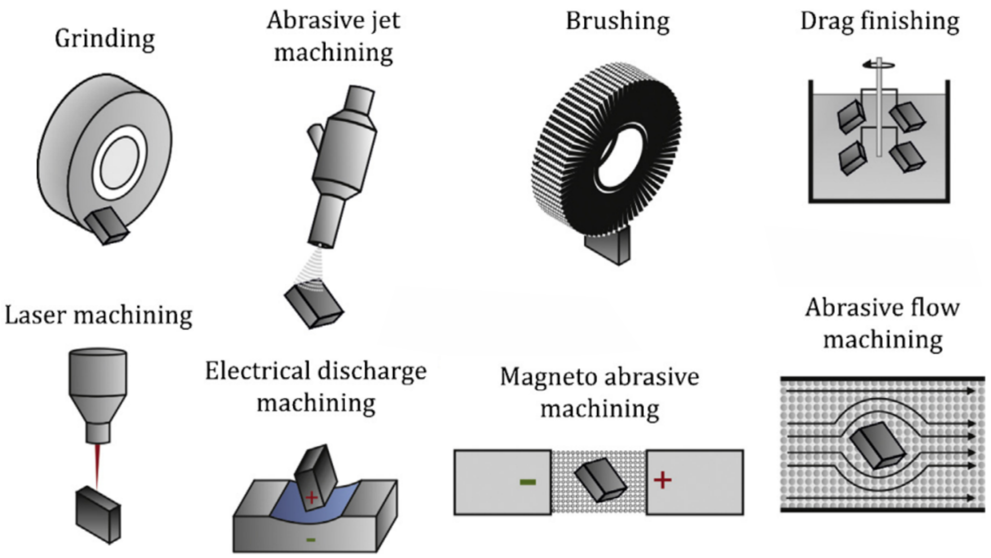

Source: Adapted from Denkena and Biermann (2014).

itive effect on flank wear development, contributing to extend the tool life when machining Inconel 718.

2.2.2.2 Coating

The coating process of milling tools involves applying a thin layer of a specialized material to the surface of the cutting tool. The coating acts as a protective barrier, enhancing the performance and extending the tool's life, increasing tool's hardness, reducing the tool's friction coefficient, and improving the tool's heat resistance. Generally, the abrasive and adhesive wear are reduced when applying a coating resulting in higher tool life for both prepared and non-prepared tools (Denkena; Biermann, 2014).

Before applying the coating, a cleaning process to remove any contaminants or residues that might hinder the proper adhesion of the coating material is applied, using ultrasonic baths, chemical treatments, or other suitable methods. There is a range of coating materials available, each offering specific benefits based on the tool's application and the material being machined. Common coating materials include titanium nitride (TiN), titanium carbonitride (TiCN), titanium aluminum nitride (TiAlN), diamond-like carbon (DLC), among others. Soon after the material selection, two main types of coating processes can be applied, the Physical Vapor Deposition (PVD) and Chemical Vapor Deposition (CVD). PVD is one of the most commonly methods used, this process uses a vacum chamber to deposit a thin layer of material onto the tool's surface, throughout the vaporization and condensation of the coating material, adhering as a coating layer. On the other hand, in the CVD the material is vaporized and then reacts with a gas in the chamber forming the coating layer, this process is used typically for high-temperature applications, once it can produce coating with high degree of hardness. CVD coatings tend to be thicker and have higher wear resistance compared to PVD coatings. Some Post-Coat treatments can optionally be employed in order to improve the coating's mechanical and tribological characteristics, such as tempering, annealing, or surface smoothing (Bartolomeis *et al.*, 2021; Denkena; Biermann, 2014).

2.2.3 Cutting Tool Materials

The cutting tool materials should have some properties to resist the stresses placed on them during cutting, such as hardness, pressure and oxidation resistance, bending and edge strength, toughness, inner bonding and high-temperature strength, the small propensity to diffusion and adhesion, abrasion resistance and reproducible wear behavior. Concurrently the materials used for cutting tools can be summarized in order of increasing hardness and wear resistance as tool steels, cemented carbides, cutting ceramics, and super-hard cutting tool materials made of boron nitride and diamond (Klocke, 2011), this relation is shown in Figure 15.

Figure 15 – Schematic classification of several cutting tool materials

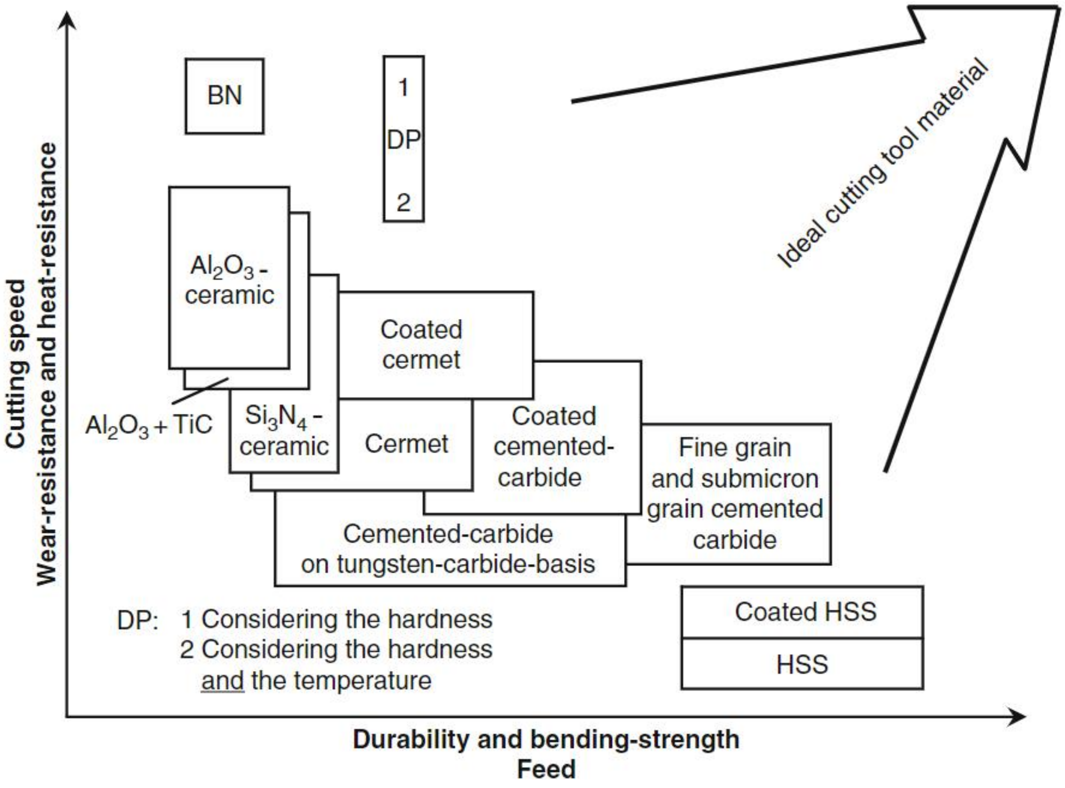

Source: Klocke (2011).

2.2.3.1 Cemented Carbide

The cemented carbides are composite materials formed of carbides of transition metals merged in a soft metallic binder phase made of cobalt and/or nickel. The carbides are on the boundary between metals and ceramics and can combine the properties of both a metal, such as electrical conductivity, and undergo plastic deformation and those of ceramics, such as high-temperature resistance and hardness (Hornbogen; Eggeler; Werner, 2011). Some of the advantages of cemented carbides are good structural uniformity, high hardness, pressure resistance, and high-temperature wear resistance, which allow the cemented carbides at 1000℃ to have the same hardness as high-speed steel at room temperature. Changing the amounts of hard material and binder it is possible to manufacture cemented carbides with specific desired properties (Schedler, 1988). The components of cemented carbides and their properties are listed below according to Klocke (2011):

- **WC or mono tungsten carbide** is the most important hard material phase in technical sintered cemented carbides. WC-Co cemented carbides result in high inner bonding and edge strength, due to the solubility of WC in Co. Its application is limited at higher temperatures, because of the dependency on dissolution and diffusion.
- **TiC or titanium carbide** has considerable high-temperature wear resistance but fragile bonds and edge strength, due to its low tendency to diffusion, it is normally used when cutting steel materials with high cutting speeds and can be joined with WC to make a composite carbide.
- **TaC or tantalum carbide** in small amounts has a grain-refining effect, which improves toughness and edge strength.
- **NbC or niobium carbide** has similar effects as TaC, they usually appear as mixed crystal (Ta, Nb)C in cemented carbides.
- **TiN or titanium nitride** is the component that determines the properties in all modern cermets. Because of the TiN's low solubility in steel and thus it is more resistant to diffusion than titanium carbide. Nitrogen is known to cause an increase in wear resistance.
- **Co or cobalt** is used as a binder metal for cemented carbides based on tungsten carbide, due to the high level of solubility of WC in cobalt and to the good wettability of tungsten carbide crystals by the molten WC-Co binder phase.
- **Ni or nickel** is used as a binder for cermets, because of its improved wettability of hard materials, however since nickel is more easily deformable than cobalt, Co is also added with nickel as a binder in cermets to increase the temperature-resistance of the material.

2.3 NICKEL ALLOY 718 (INCONEL 718)

Inconel 718 is a high-strength, corrosion-resistant nickel-based superalloy that finds extensive applications in the aerospace industry. Its exceptional mechanical properties, combined with its resistance to high temperatures and aggressive environments, make it a top choice for critical aerospace components (Schneider *et al.*, 2022). This kind of material is widely used in the fabrication of aircraft engine parts, including turbine discs, compressor blades, and combustion chambers. The alloy's ability to retain its strength and integrity even at elevated temperatures allows engines to operate efficiently and reliably in extreme conditions. Moreover, Inconel 718's resistance to fatigue and creep makes it well-suited for gas turbine rotors, ensuring prolonged service life and safety in aircraft propulsion systems. Beyond engines, this superalloy is utilized in aerospace applications such as aerospace fasteners, rocket motors, and structural components for space exploration, due to the combination of mechanical properties and resistance to harsh environments (Bartolomeis *et al.*, 2021; Li, 2023).

The Inconel 718 is a precipitation-hardening nickel-chromium alloy with substantial amounts of iron, niobium, and molybdenum, in combination with small portions of aluminum and titanium, the material can also be found under the short name NiCr19Fe19Nb5Mo3 and the material number 2.4668, and its composition is shown on Table 1 below, according to DIN10088-1 (2014).

Table 1 – Chemical composition of Inconel 718

Element	Mass fraction (%)	Element	Mass fraction (%)
C	0.02 - 0.08	Co	1.0
Si	0.35	Al	0.3 - 0.7
Mn	0.35	Cu	0.3
P	0.015	Nb + Ta	4.7 - 5.5
S	0.015	Ti	0.6 - 1.2
Cr	17.0 - 21.0	B	0.002 - 0.006
Mo	2.80 - 3.30	Fe	Remnant
Ni	50.0 - 55.0		

Source: DIN10088-1 (2014).

The properties displayed by Inconel 718 contribute to its widespread use in aerospace applications. One of its key attributes is its high tensile strength, enabling it to withstand heavy mechanical loads and stresses at both room and elevated temperatures up to 700 ℃. With a melting point of approximately 1350 ℃, Inconel 718 can maintain its structural integrity even under extreme heat encountered in aerospace engines and rocket propulsion systems. Furthermore, the alloy possesses excellent corrosion resistance, making it highly resistant to oxidation and attack from various corrosive agents, including acids and alkalis. This property is crucial for components exposed to aggressive environments during flight. Additionally, Inconel 718 offers good weldability and formability, allowing for ease of manufacturing complex shapes and components, its combination of strength, corrosion resistance, and high-temperature capability makes it an indispensable material in the aerospace industry, where reliability and performance under demanding conditions are paramount (SUPER-METALS, 2016; Schneider *et al.*, 2023).

Despite of its well-seen properties, nickel-based alloys are very difficult to machine thanks to their properties, such as high strength, low thermal diffusion, and work hardening, resulting in poor machinability, low material removal rates, abrasive and diffusion wear, and low tool life (Akhtar *et al.*, 2014). Thus, the improvement of the machining process of Inconel 718 has become a challenge, in which some approaches such as cutting parameters and tool optimization may be fundamental to achieve it (Celaya *et al.*, 2019).

2.4 ADDITIVE MANUFACTURING (AM)

Unlike the conventional subtractive manufacturing process, additive manufacturing is an incremental layer-by-layer manufacturing process based on a common feedstock, normally powder or wire, that is melted or fused by a heat source and solidifies to produce the final geometry based on a digitally defined heat source trajectory (Herzog *et al.*, 2016). The AM processes are classified by DIN-8580 (2022) as primary forming processes since the three-dimensional pieces are produced from shapeless or shape-neutral starting material. The process starts with the creation of a 3D model using a Computer-Aided Design (CAD) software. This digital model is then sliced into thin horizontal layers, and the AM machine is responsible for interpreting each layer and to deposit material accordingly. As the material is added layer by layer, the object gradually takes shape, adhering to the previous layers. Figure 16 illustrates the main differences between the conventional subtractive and additive manufacturing processes.

According to ASTM-F2792 (2012) AM process are classified into seven different categories, Direct energy deposition (DED), Sheet lamination (SL) (by ultrasonic), Powder Bed Fusion (PBF), material extrusion, binder jetting, material jetting and vat photopolymerization. In recent years droplet printing and arc-based AM processes (gas tungsten arc, plasma arc, and gas metal arc) have been also added to the list. DED and PBF are the most used processes for manufacturing metal parts in the industry and PBF will be further explained in the next section (Tepylo; Huang; Patnaik, 2019; Herzog *et al.*, 2016).

The AM process has several advantages such as the reduced lead time and associated cost in the production of complex geometries, the ability to design and manufacture complex geometries with intricate internal structures, design freedom, and possibility to optimize the material distribution, reducing mass while maintaining the mechanical and other performance requirements. AM enables, furthermore, on-demand and localized production, which is particularly beneficial for industries requiring rapid response to market demands. However, there are also also challenges to consider regarding the limited material selection

Figure 16 – Comparison between the conventional subtractive and AM processes

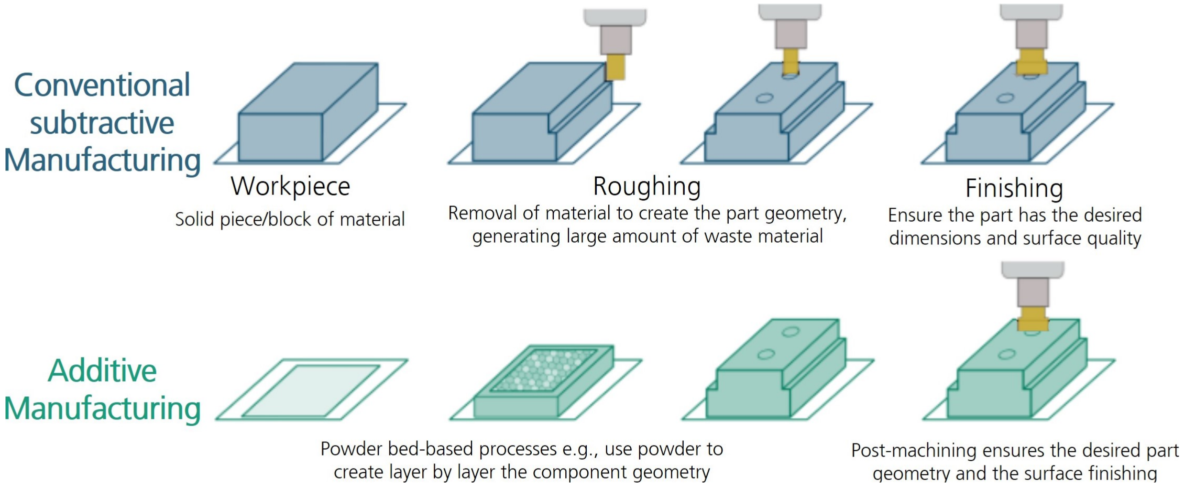

Source: Adapted from Tepylo, Huang and Patnaik (2019).

and post-processing requirements to achieve the desired surface finishing and properties. The quality control, repeatability, and scalability of AM process for high-volume production are topics that are still under development and should be further refined (Herzog *et al.*, 2016; Gibson *et al.*, 2021).

Despite of the challenges, the AM technologies and processes have revolutionized the manufacturing landscape over the past decades, driving innovation and reshaping different industries in the years to come (Angrish, 2014). By the year 2017 nearly 18,2% of the total market-share of the AM-market was related to the aerospace sector, which shows an established, but also growing panorama for the application of AM in the sector. Estimations indicate that the revenues from the AM-market are going to surpass $100 billion within the next two decades, mostly coming from the aerospace industry. In this sense, leading companies in the aerospace sector use nowadays thousands of additive manufactured pieces in their daily production (Najmon; Raeisi; Tovar, 2019; Angrish, 2014).

2.4.1 Laser Powder Bed Fusion (LPBF)

The Powder Bed Fusion (PBF) is one out of seven additive manufacturing processes according to the ISO52900:2021 (2021). It includes two types of processes dependent on the energy source, the Laser Powder Bed Fusion (LPBF), also known as Selective Laser Melting (SLM), and Electron Beam Melting (EBM). The LPBF is a layer-by-layer process, in which a recoater dispenses a thin layer of metal powder on top of the build platform in an inert-gas flushed build chamber to minimise the risk of oxidation. Then a laser scans along the flat surface of the thin layer of powder, melting the metal powder according to the corresponding cross-section from the loaded CAD model. This process is repeated by lowering the building platform by one layer thickness, applying a new thin layer of powder and melting the powder using the laser source's thermal energy. The tracks created by the process can be stacked to form the desired three-dimensional component (Schleifenbaum *et al.*, 2010; Svantesson, 2021).

The parameters for building up the layers are selected in such a way that the lower layer is melted again on the surface in order to metallurgically bond the respective layers together. Furthermore, support structures are required to avoid local hardening, stresses, distortions and cracks during the process. These structures are removed after the manufacturing and heat treatment of the component by milling during post-processing phase (Gibson *et al.*, 2021). The support structures may also be applied to stabilize thin-walled components areas, as blades, that are prone to vibrations during post-processing (Svantesson, 2021). Figure 17 illustrates the schematic structure of the LPBF process.

Figure 17 – Schematic illustration of the LPBF process

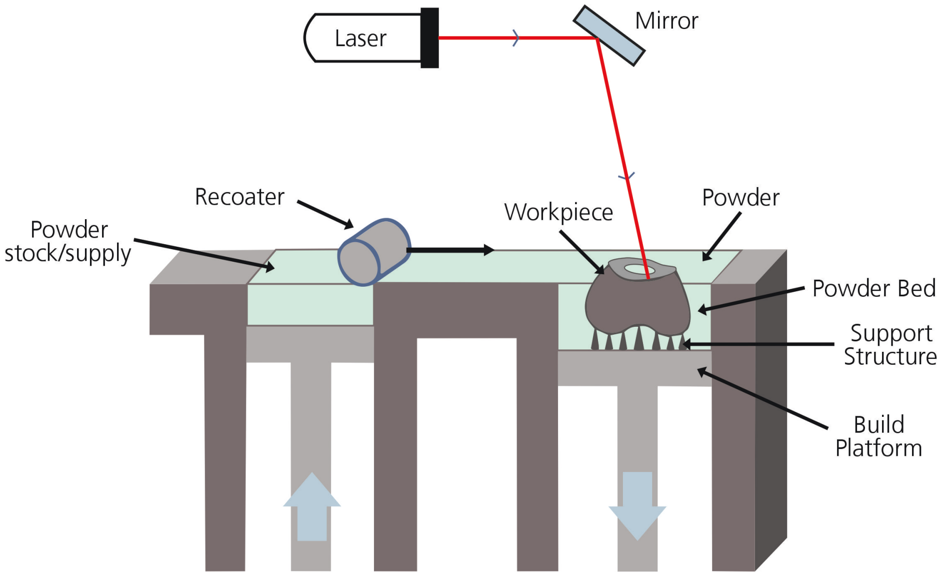

Source: Author (2024).

The main process parameters of LPBF control the energy input during manufacturing, strongly influencing the quality of the manufactured parts. The workpiece density, surface condition and dimensional accuracy are especially influenced by the amount of energy input. Some of the main LPBF process parameters are: laser power (P_L), scanning speed (v_s), hatch distance (Δy_s), layer thickness (D_s) and AM build direction(Gibson *et al.*, 2021). These parameters are schematically shown in Figure 18.

Once the components have been manufactured, they must be cleaned of powder residue and separated from the build platform, further post-treatments, such as infiltration or heat treatment may also be required in order to improve the material properties (Gibson *et al.*, 2021). The additive manufacturing usually does not achieve the necessary dimensional accuracy or surface quality demanded for the parts, which requires subtractive finishing,

Figure 18 – LPBF process parameters

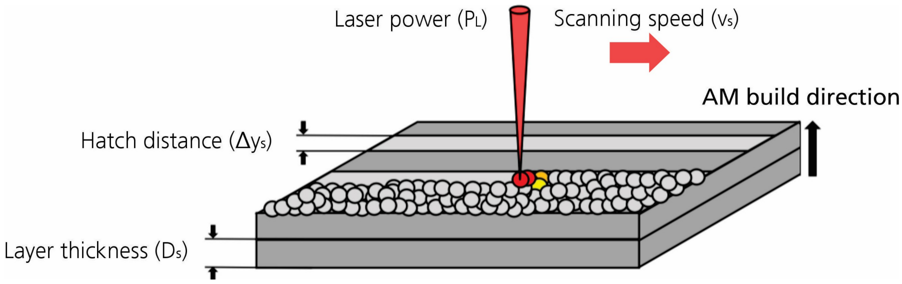

Source: Adapted from Gibson *et al.* (2021).

support structures are also removed during finishing (Schneider *et al.*, 2023). Depending on the type of process, the post-process can be very time-consuming and cost-intensive (Lachmayer; Rettschlag; Kaierle, 2021).

2.4.1.1 Support structures

The support structures are extra material added underneath or nearby the part in order to ensure its good printability during AM process. The supports are crucial for dissipating heat away from the melt pool and assure clamping of the part to the build platform, besides that, the supports absorbs process forces and thermally induced residual stresses (Järvinen *et al.*, 2014). In the AM-manufacturing of complex component geometries the support structures help to stabilize the overhangs generated by the geometry, they are often used if the angle between the part geometry and the building platform falls below a limit value of 45 °. Moreover, supports may be also necessary for the vibration damping of thin-walled or vibration-prone areas of the component. The orientation of the component has direct influence on the design of the support structures and must be taken into account during AM process (Svantesson, 2021). Different customization levels for the support structure are possible by adjusting several parameters based on the basic geometries for supports (Krol; Zaeh; Seidel, 2012). Figure 19 shows different types of support structures.

Figure 19 – Basic forms of support structures

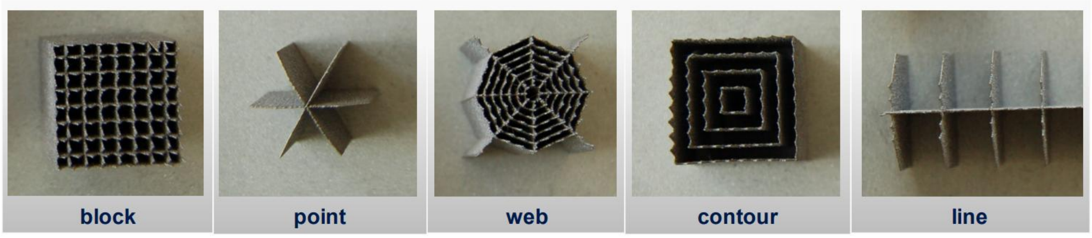

Source: Krol, Zaeh and Seidel (2012).

2.5 MACHINABILITY OF CONVENTIONAL AND AM-INCONEL 718

Inconel 718 is a high strength and thermal resistant Nickel-based alloy extensively used in the aerospace, automotive and energy industries. It is considered a hard-to-cut material due to the extreme toughness and work hardening characteristic of the alloy, at the same time that it is commonly associated with high tool wear and high time an cost expenditure during machining. The manufacturing method applied to obtain a component made from Inconel 718 plays an important role on the formation of the microstructure and mechanical properties of the material, these include conventional methods as forging an casting, as well as additive manufacturing process (Rahman; Seah; Teo, 1997; Volpato; Tetzlaff; Fredel, 2022).

Previous investigations revealed that forged Inconel 718 presented higher concentration of TiC and NbC carbides in comparison with additively manufactured material, which can lead to higher tool wear. The direction-dependent properties of the AM-Inconel 718 showed to influence the feed direction during machining. Greater fluctuations of the thermo-mechanical loads on the cutting tool were found during the machining of the AM-material (Bartolomeis *et al.*, 2021; Khanna *et al.*, 2021). Ducroux *et al.* (2021) investigated the machinability of wrought and AM-Inconel 718 during milling, it was found that forces are lower in all directions when milling AM-Inconel 718 compared to wrought Inconel, this could be explained by the differences of microstructure. Abrasion on the flank face was the main tool wear mechanism, which led to firstly flank wear and secondly to notching on the cutting edge. In addition, the tool life when milling AM-Inconel 718 showed to be twice longer in comparison with milling of wrought Inconel. Similar results were obtained during turning experiments in additivelly manufactured Inconel 718 (Chen *et al.*, 2021).

2.6 MACHINABILITY OF POROUS AM-INCONEL 718

Porosity can occur or be artificially induced by influencing factors during LPBF process. By applying a laser beam with high energy input, the powder evaporates and pores are formed. Alternatively, a low energy input leads to inclusion of unmelted powder in pores, if the melt pools do not overlap, then powder-filled pores can be formed (Kumar *et al.*, 2019; Valdez *et al.*, 2017). The cutting mechanism of porous materials differs from that of dense materials, and there is limited literature covering the machinability of AM-porous materials manufactured by LPBF (Schneider *et al.*, 2022). Porosity affects chip formation, thermal conductivity, process temperature, strength, and surface quality after machining. Therefore, cutting theories have been proposed to evaluate the machinability of porous materials (Tutunea-Fatan; Fakhri; Bordatchev, 2011; Li, 2023).

Since the porous materials obtained by powder metallurgy have a comparable level of porosity to the alloys produced by LPBF, and both are classified in the category of metallic materials, the 3 predominant theories in the literature, which explain the influence of pores on the machinability of powder metallurgically produced materials, can also be used as a theoretical basis for understanding the phenomenon on materials with induced porosity obtained by LPBF (Tutunea-Fatan; Fakhri; Bordatchev, 2011; Li, 2023). The 3 main cutting theories, interrupted cutting, deformation cutting and the thermal conductivity theory (Tutunea-Fatan; Fakhri; Bordatchev, 2011; Hu *et al.*, 2016), are briefly explained below.

- **Interrupted cutting theory**
  During the cut of porous materials, the cutting tool periodically enter and exit the material due to the pores. This leads to an intermittent engagement and disengagement of cutting edge with the workpiece, producing a periodic change in cutting force determined by the spatial pore distribution of the material. The cutting forces are, therefore, cyclical and dependent on the random occurrence of pores and solid material. These loading and unloading cycles of the cutting edge lead to alternating mechanical and thermal loads, which cause thermal and mechanical fatigue stress on the tool, inducing micro cracks and wear of the tool. This has, consequently, negative impact on tool life (Tutunea-Fatan; Fakhri; Bordatchev, 2011; Šalak; Danninger; Selecká, 2005). Figure 20 schematically shows how the cutting edge is, for variable periods of time, either fully engaged or fully disengaged depending on its relative position within material structure.

  Figure 20 – Interrupted cutting mechanism

  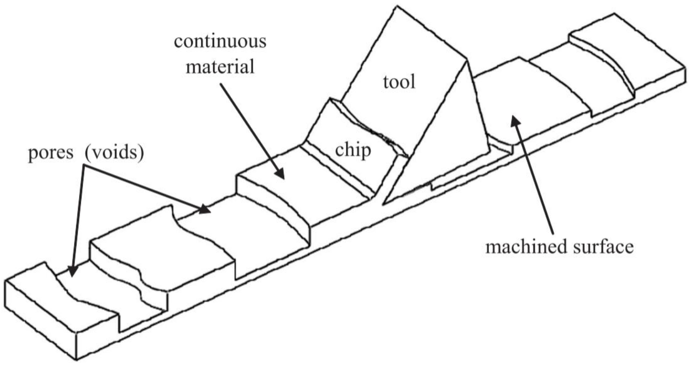

  Source: Tutunea-Fatan, Fakhri and Bordatchev (2011).

- **Deformation cutting theory** According to this theory, the hardening effect, which occurs when machining metallic materials, can play also a role during the machining of porous metallic materials. When metallic materials are machined, a hardened edge zone is formed on the surface of the material due to plastic deformation of the grains and entanglement of the dislocations caused by the mechanical load of the cutting tool on the workpiece surface. This phenomenon leads to significantly higher strength and hardness, and lower plasticity and toughness, creating a hardened layer that makes machining of metallic components more difficult (Klocke, 2011).

In the machining of porous metallic materials, the material particles are compressed into the pores by the cutting edge's constant pressure on the surface. The pores are then closed due to local deformation and material transport. This results in a continuous layer with minimal or no pores at all after machining. Consequently, the cutting edge cuts trough an almost dense layer of material instead of the porous material. In addition, as the porosity increases, the thickness of compacted layer also increases and the microhardness of the compacted edge zone decreases, which leads to lower cutting forces when compared with dense materials (Tutunea-Fatan; Fakhri; Bordatchev, 2011; Šalak; Danninger; Selecká, 2005; Li, 2023). Figure 21 illustrates the deformation cutting mechanism.

Figure 21 – Deformation cutting mechanism

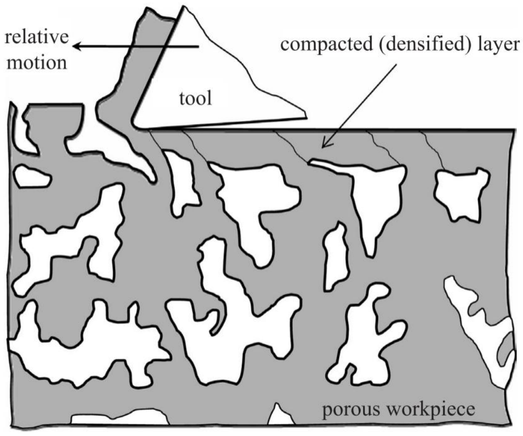

Source: Tutunea-Fatan, Fakhri and Bordatchev (2011).

- **Thermal conductivity theory**
  The theory of thermal conductivity explains the poorer machinability of porous materials by using the linear relationship between conductivity and porosity. As porosity increases, thermal conductivity decreases, leading to slower heat dissipation in the cutting zone. This, in turn, increases the temperature locally at the cutting edge, accelerating tool wear. High temperatures can also spark oxidation and other chemical reactions, which have a negative impact on tool wear (Šalak; Danninger; Selecká, 2005).

The conclusions and insights gathered by the two previous sets of studies from Kirchmann (2022), Schneider *et al.* (2022) and Li (2023), Schneider *et al.* (2023), which investigated the machinability of porous Inconel 718 obtained via LPBF in milling and orthogonal cut, respectively, were mainly used as starting point for this work. The investigation of Kirchmann (2022) and Schneider *et al.* (2022) on milling compared the impact of control variables as cutting speed (v_c), feed per tooth (f_z), width of cut (a_e), and the feed direction relative to the AM build direction on target variables as flank wear, active force, surface quality and chip form when machining the 72%, 84% and 100% relative density samples using DoE. Their main conclusions were that after initial feed travel with only flank wear, chipping wear becomes dominant when machining the porous variants, while uniform flank wear was seen for the 100% dense variant. The reason for chipping was seen due to the strongly alternating loads observed on the active force for the porous variants, which increased with higher porosity. Chipping showed to be even more severe for the 84% than for the 72% material. The chips shape of the porous materials presented a disrupted structure with perforations. However, the significance of the effect of the influencing variables on the target variables was not assessed due to a lack of a significance analysis. Furthermore, the high mechanical alternating loads observed in the force signals appear to support the interrupted cutting theory, which explains these oscillations by the constant entry and exit of the cutting edge in the pores.

Moreover, the investigation conducted by Li (2023) and Schneider *et al.* (2023) sought to enhance the comprehension of the fundamental principles underlying the machinability of porous Inconel 718 obtained by LPBF. This was achieved through a more rigorous material science related approach, which involved the conducting of experimental trials on orthogonal cut in the 72%, 84% and 100% relative density samples based on DoE according to Taguchi method. The impact of various process parameters, as cutting direction, cutting-edge radius (r_β), cutting speed (ν_c), unreformed chip thickness, on the target parameters, as cutting force, cutting normal force, chip underside temperature, chip shape and machined surface, was investigated. The results were consistent with previous findings, indicating that cutting force and cutting normal force decreased with increasing porosity. Additionally, the standard deviation of force components and acceleration amplitudes demonstrated that the tool cutting edge experienced higher mechanical alternating loads. It can be reasonably assumed that, on average, a lower temperature load is present with increasing porosity. The interrupted cutting theory was found to be the most probable explanation for the alternating mechanical load mechanism observed during the cutting of porous materials. The significance of the investigated influencing on the target parameters could be determined through the ANOVA, which allowed the establishment of cause-effect relationships between them for the orthogonal cut process.

2.7 DESIGN OF EXPERIMENTS (DOE)

The Design of Experiments (DoE) is a standardized statistical procedure for conducting and analyze experimental investigations. Its aim is to determine the correlations between the influencing and target variables while minimizing the number of experiments required. It has three fundamental principles: randomization, replication, and blocking. The influencing variables, also refereed as factors, are independent and can be specifically changed. The setting of the factors are named values or levels. The impact of a factor on the system is called effect. There are two type of effects, the main effect refers the pure impact of the effects, while the interaction effects denote the effects of a factor that are dependent on the setting of another factor (Antony, 2003).

A full factorial experiment is a design in which two or more factors, each with discrete possible levels, are tested across all possible combinations of levels and factors. In a full factorial experiment, the experimental effort (n_r) can be calculated from a relation between the number of factors (n_f) and the number of levels (n_l) (Oimoen, 2019), given by the Equation 3:

$$n_r = {n_l}^{n_f} \tag{3}$$

To investigate the influence of various parameters with reduced experimental effort and improved economic and time feasibility, a fractional factorial design can be applied. This design analyzes only a subset of the full experimental design, resulting in different mixing structures of the main effects and interactions. These can be evaluated according to the resolution level of the design. There are four standardized resolution levels that indicate which interactions are mixed with the main effects and provide information on whether a clear assignment of an effect can be determined (Gunst; Mason, 2009; Antony, 2003).

An important characteristic of a fractional design is its resolution, which refers to its ability to distinguish main effects and low-order interactions from each other. The resolution is indicated by roman numerals, and it increases with the number. The fractional designs of resolution III, IV, and V are considered the most important. Resolutions below III are not useful, while resolutions above V are wasteful for two-level factors. This is because the additional effort required goes into estimating very high-order interactions that rarely occur in practice and do not provide practical benefits in most cases (Ledolter; Swersey, 2007). Table 2 shows the resolution level according to the number of runs needed and the number of factors of the experimental design, the upper resolution levels are highlighted in green and yellow, and the lower resolution levels in red.

Table 2 – Fractional factorial design available resolution levels

	Factors													
Run	2	3	4	5	6	7	8	9	10	11	12	13	14	15
4	Full	III												
8		Full	IV	III	III	III								
16			Full	V	IV	IV	IV	III	III	III	III	III	III	III
32				Full	VI	IV	IV	IV	IV	IV	IV	IV	IV	IV
64					Full	VII	V	IV	IV	IV	IV	IV	IV	IV
128						Full	VIII	VI	V	V	IV	IV	IV	IV

🟥 Resolution level III 🟨 Resolution level IV 🟩 Resolution level V or higher

Source: Adapted from Minitab (2023b).

3 METHODOLOGY

After Chapter 2 presented the theoretical basis for comprehending the milling process, the impact of various parameters and cutting tool geometry on the machining process, as well as an overview of the machinability of both dense and porous AM-Inconel 718, this chapter outlines the experimental methods and procedures followed in this work. These steps were undertaken to further develop a cause-effect knowledge about the milling process of porous AM-Inconel 718. The ultimate goal is the proposal of process enhancements with a view to the application of such material in support structures during the manufacturing of AM-aerospace parts.

First, based on the analysis of the state of the art, preliminary investigations, and industry standards certain control and target variables were defined. The control variables selected for investigation include cutting speed (ν_c), radial depth of cut (a_e), feed per tooth (f_z), cutting edge radius (r_β), cutting tool substrate (Cobalt content in tungsten carbide), feed direction relative to AM build-up direction, and use of coolant. The target variables defined are the tool wear, cutting forces and accelerations in the x, y, and z directions, chip form and surface finishing. A trial plan is then designed with the help of DoE to identify the influences and effects of the individual control variables on the targeted variables.

To make the trials logistically feasible, a fractional factorial experimental design is chosen where each factor assumes only two different values, reducing the number of combinations to be investigated. A sequence of two milling trial sets is then defined, each one with a 7×2 factorial design, which means 8 different combinations of parameters, for each of the two relative densities (72% and 84%) of porous AM-Inconel-718 samples obtained via LPBF. The second trial plan of the sequence is obtained after applying a folding method to the first trial plan. The goal is to minimize plan saturation and enable the assessment of the control factor's significance levels of influence on the targeted factors. Due to the folding, in this case, it is possible to increase the accuracy of the trial plan from level III to level IV.

Furthermore, the sensors placed on the machine tool record cutting forces and accelerations during the trials. A set of feed travel values and volume of machined material is established as a reference for collecting chips and light microscopic images of the flank faces of the cutting tool. Later, the chips and collected pictures are analyzed, and the width of the flank wear land (VB) and chipping (CH) of each cutting edge of the cutting tools are measured, to obtain the development of flank wear as a function of the volume of machined material. Besides that, a VBScript routine treats the cutting forces and acceleration signals and chooses the corresponding values for the feed travel ranges that have been accordingly defined.

Finally, statistical software and methods are utilized to conduct quantitative evaluations of all the processed data. A qualitative evaluation of the workpiece, tool, and chips is carried out. The influences and level of significance of the manipulated variables on the cutting forces, accelerations, and flank face wear are investigated, aiming process optimizations to the milling of porous AM-Inconel 718 that might prevent chipping wear. Figure 22 schematically illustrates and overviews the methodology of the research, showing the step-by-step workflow to accomplish its objectives.

Figure 22 – Schematic overview of the methodological strategy

Source: Author (2024).

3.1 WORKPIECE MANUFACTURING VIA LPBF

The porous AM-Inconel 718 workpieces investigated in this thesis were manufactured by the Digital Additive Production Institute RWTH Aachen (DAP) using the LPBF process. The powder used for the fabrications of the probes is the MetcoAddTM 718C from OC Oerlikon Metco Add GmbH. This kind of powder is obtained due to the argon atomization process, whereby the flow stream of the melted alloy is atomized at high speed by the impact of argon gas atomization in a vacuum, in such a way that fine droplets are formed and quickly solidify into solid powder particles when flying. The raw material batch is characterized by a particle size D50 of 38.1 µm of spherical particles with isolated satellites (Li, 2023).

For the LPBF process an EOS M290 system from EOS GmbH was used. Its build chamber has a volume of 250 x 250 x 325 mm^3, and its high-speed scanner can reach up to 7 m/s. The system also has a F-theta lens with a focus diameter of 100 µm and an Nd-YAG Laser (Neodymium-doped yttrium aluminium garnet), a single mode fiber laser with a wavelength of 1064 nm and a maximum power of 400 W. Argon is used as the shielding gas. A total of 8 cuboid workpieces, half of them with 84% relative density and the other half with 72%, were fabricated on the same build platform and later heat-treated. The LPBF-produced samples measure around 46.3 x 50 x 60 mm^3 and were obtained using a laser scanning strategy in layers rotated by 67°, as schematically showed by Figure 23, where AM build-up direction is perpendicular to the build-up platform.

Figure 23 – Schematic structure of the workpiece

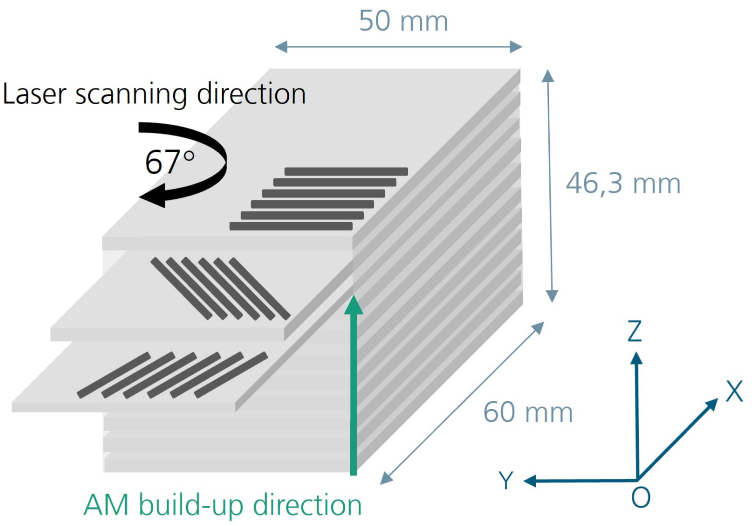

Source: Author (2024).

The fabrication parameters and conditions are summarized in Table 3. A standard heat treatment, according to AMS5662P (2022), was carried out on the pieces including solution annealing at 980 °C for 1 hour, followed by quenching in air, argon, or water. A second treatment for precipitation hardening was subsequently carried out at 720 °C for 8 hours, followed by cooling in the furnace at approximately 50 K/h and at 620 °C for 8 hours with cooling in air or argon (Li, 2023).

Table 3 – LPBF parameters for the manufacturing of porous Inconel 718 probes

Workpiece Nr.	**Relative density (D_r)** [%]	**Laser power (P_L)** [W]	**Scanning speed (v_s)** [mm/s]	**Hatch distance (Δy_s)** [μm]	**Layer thickness (D_s)** [μm]	**LPBF Time** [%]*
H, B, C, G	84%	285	960	200	80	30
E, D, F, A	72%	370	1500	200	80	20

* Regarding the time required to manufacture 100% dense Inconel 718 via LPBF process.

Source: Schneider *et al.* (2022).

Lastly, the 8 cubic-shaped probes were removed from the mounting platform, C45 substrate, by sawing. Fissures were observed on the workpiece surface, likely caused by residual stresses and deformation during the LPBF process. To minimize the influence of fissures on the trials, two workpieces of each relative density (72% and 84%) with fewer visible fissures were selected for the experiments. Figure 24 shows in (a) the workpieces on the build-up platform and in (b) the two final workpieces after removal, and heat treatment.

3.2 MATERIAL CHARACTERIZATION

Tensile tests for the two different relative density variants, 72% and 84%, of AM-Inconel 718 used in this work were carried out by Schneider *et al.* (2022). The mechanical tests were conducted by TPW Prüfzentrum GmbH following the standards of ISO 6892-1:2009. In opposition to 100% dense AM-Inconel 718, the two porous variants obtained by LPBF show anisotropic mechanical properties, and it was observed that the stiffness is greater in the direction parallel to the AM build-up direction than in the direction perpendicular to the build-up direction. The tensile strength parallel to the AM build-up direction showed to be at least 40% lower than that perpendicular.

Furthermore, the strength of AM-Inconel 718 decreases significantly as the relative density decreases. Tensile tests indicate that a reduction in relative density from 100% to 84% results in a decrease in tensile strength of approximately 60% in the direction parallel to the AM build-up and 50% perpendicular to it. The decrease in tensile strength is even more pronounced when the relative density is reduced from 100% to 72% in AM-Inconel 718, with a decrease of approximately 80% parallel to the AM build-up direction and 70% perpendicular to it. Meanwhile, both porous materials exhibited brittle properties, whereas the 100% dense material displayed ductile properties (Schneider *et al.*, 2022). Table 4 shows the tensile strength values for both the parallel (||) and perpendicular ($\perp$) directions to the AM build-up direction.

Figure 24 – AM-Inconel 718 probes with induced porosity obtained via LPBF

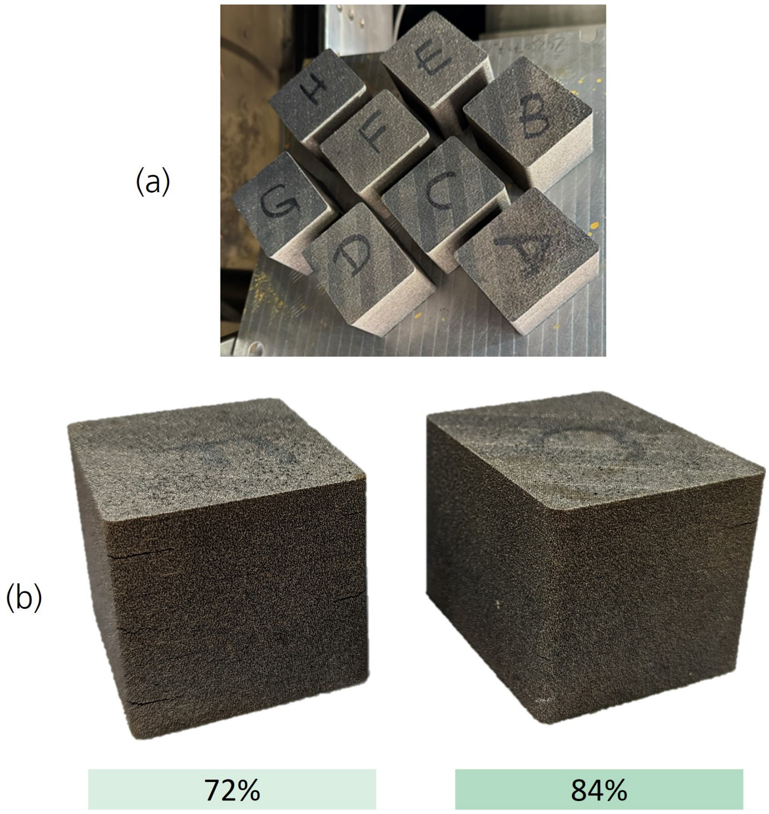

Source: Author (2024).

Table 4 – Mechanical properties of porous Inconel 718 obtained via LPBF

Relative density (D_r) [%]	**Tensile strength ||** [MPa]	**Tensile strength ⊥** [MPa]
100%	1504	1576
84%	585	814
72%	291	415

Source: Schneider *et al.* (2022).

The material structure of the heat-treated 84% porous Inconel 718 is shown in Figure 25. The anisotropy of the morphology of the material can be clearly seen in the figure and it was described by Li (2023). In the XOZ or YOZ planes, section (a) of the figure, due to different laser scanning strategies in the LPBF process, within each material layer no obvious material distribution pattern can be identified. In the XOY plane (b), however, there is a more regular grid-like structure, where each track of material layer is parallel to each other. The microstructure of the material presents also anisotropy. During the solidification process, the heat is predominantly directionally removed, leading to the formation of numerous long columnar crystals along the AM build-up direction with many acicular δ-phase in them, while in the XOY plane, there is a more homogeneous distribution of grain boundaries (Li, 2023).

Figure 25 – Microsections of the 84% porous Inconel 718

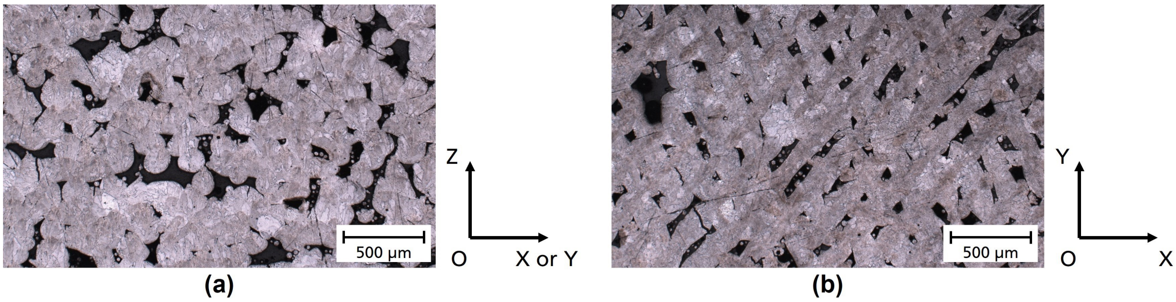

Source: Adapted from Li (2023).

The investigations conducted by Li (2023) also obtained SEM images from the lattice-shaped material structure of dense and porous Inconel 718 obtained via LPBF. This kind of electron microscopy technique allows the acquisition of images from the sample topography achieving resolutions better than 1 nm. In the porous materials, the material tracks are parallel to each other in the same material layer, and two neighboring material layers connect to each other by overlapping, as joints. It is also clearly visible the presence of remaining metal powder in the pores of the material, which were not or not completely melted during the LPBF process. Besides that, many cracks occur on the surface of the two porous variants in comparison with the dense one due to the residual tensile stress in the material (Li, 2023). This residual stress arises from the non homogeneous solidification process under a strong temperature gradient and high cooling rate, leading heat to preferably dissipate along the track, generating the tensile stresses at the solidification front (Kaya *et al.*, 2021). In addition, the 72% relative density material showed more cracks than the 84%. Figure 26 presents the comparison between the SEM pictures obtained from the dense and porous surfaces of Inconel 718 obtained via LPBF process.

Figure 26 – SEM images of the AM-Inconel 718 variants

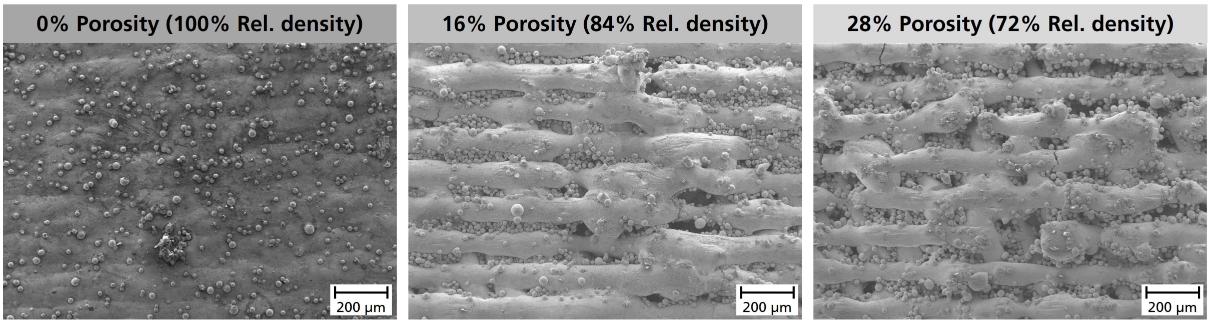

Source: Adapted from Li (2023).

3.3 CUTTING TOOL SELECTION AND CHARACTERIZATION

Schneider *et al.* (2022) conducted previous investigations on the machinability of porous AM-Inconel 718 manufactured by LPBF. Their findings showed that chipping was the predominant type of wear during milling, which is highly undesirable. The focal aim of the tool selection in this work is to minimize chipping wear when milling porous Inconel 718. To achieve this, the effect of different hard metal substrates applied to the cutting tool, as well as the influence of cutting-edge rounding on machinability will be explored.

The cutting tools are usually made of cobalt tungsten carbides (Co-WC), which possess elevated hardness, and consequently high wear resistance as one of their most important properties (Klocke, 2011). The wear resistance, specifically related to the abrasion wear mechanism, can be measured by quantifying the volume removal on the carbide piece according to ASTM-B611 (2017). This is achieved by pressing a carbide piece against an abrasive rotating disk while keeping the number of revolutions, test time, and normal force on the steel disk constant. According to Klocke (2011), wear resistance, hardness, and compression strength increase as grain sizes become finer and cobalt concentrations decrease. Conversely, toughness increases with larger WC-grain sizes and cobalt concentration, as shown in Figure 27.

Figure 27 – Factors influencing the wear resistance of hard metals

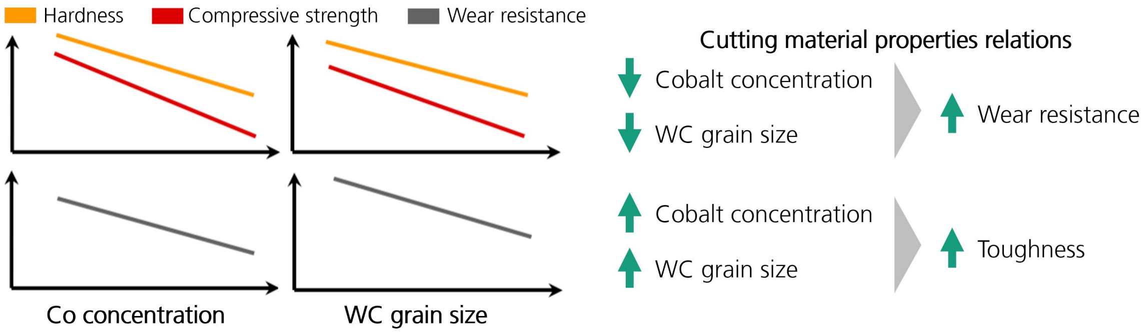

Source: Adapted from Klocke (2011).

To minimize chipping wear when milling porous AM-Inconel 718 without compromising tool wear resistance, it is desirable to select cutting tools made of hard metals with higher toughness and acceptable wear resistance. The hypothesis is that using a Co-WC with higher Co concentration and smaller WC grain size can achieve this. The available rod substrates on the market were searched on the catalogs from companies like CERATIZIT S.A. and EXTRAMET AG. Two potential tool hard metal substrate types, CTS24Z and CTS30D from CERATIZIT, were identified and then selected. These hard metal substrates are classified as submicron grades, because of their small WC grain size, between 0.5 and 0.8 µm. Additionally, the CTS24Z and CTS30D alloys have higher Co concentrations, 12% and 15% respectively, which provides increased toughness, especially compared to the

CTS20D substrate used by Kirchmann (2022) and Li (2023) in their studies. The CTS24Z is described by the manufacturer as a special high-performance grade for high-temperature alloys with high toughness, while the CTS30D with extremely high fracture toughness for particular unstable and difficult applications (CERATIZIT, 2020). Table 5 presents the properties and characteristics of both substrates, CTS24Z and CTS30D, which can be compared with the CTS20D substrate.

Table 5 – Characteristics of the two hard metal substrates

Grade	**Co concetration** [m %]	**Density** [g/cm^3]	**Hardness** [HV30]	**Transverse rupture strength** [MPa]	**K_{IC} (Shetty)** [MPa · m$^{1/2}$]
CTS20D	10	14.10	1600	4000	10.4
CTS24Z	12	14.10	1570	4000	11.3
CTS30D	15	13.84	1400	4300	13.2

Source: CERATIZIT (2020).

Besides that, the relationships between toughness (K_{IC}), wear resistance, and cobalt concentration are shown in Figure 28.

Figure 28 – Influences between properties of Co-WC hard metals

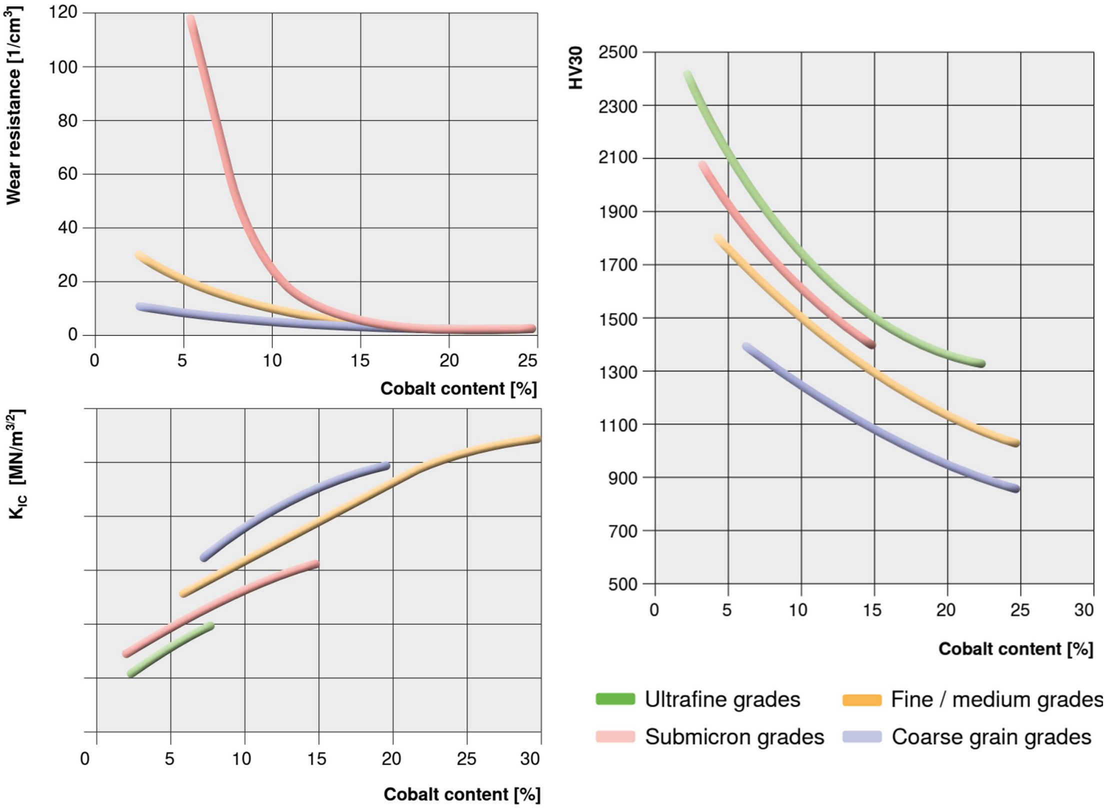

Source: Adapted from CERATIZIT (2020).

Cutting edge preparation, particularly rounding, might have positive effects when milling dense Inconel 718. It helps to increase edge strength, minimize chipping, eliminate defects, improve tool life, surface quality, precision, and chip flow (Celaya *et al.*, 2019; Klocke, 2011). However, the influence of cutting edge rounding on the machining of LPBF porous Inconel 718 is still unclear. In order to investigate this influence, two different values of cutting edge radius, 9 μm, and 14 μm, were selected to be applied on the cutting edges for the trials. Previous investigations conducted by Schneider *et al.* (2022) used end mills with 10 μm of r_β. The purpose of this set of two r_β values is to determine whether increased edge rounding can influence machinability of porous AM-Inconel 718 and whether it is significant compared to the other parameters investigated in this work.

The company Präwest Präzisionswerkstätten Dr.-Ing. Heinz-Rudolf Jung GmbH & Co. KG provided the uncoated tungsten carbide end mills, which were made using the CTS24Z and CTS30D substrates, with Co content of 12% and 15% respectively, from CERATIZIT. Tools with cutting edge radius (r_β) of 9 μm and 14 μm were produced for each substrate. The end mill tools have a diameter of 8 mm and four cutting edges. The cutting edge radius of four different tools of each set of substrates and r_β were measured with the help of the 3D surface measuring device MikroCAD premium, Figure 29. The four cutting edges of each tool were measured and evaluated, to check if the measured geometry matched the manufacturer's specifications.

Figure 29 – Setup for r_β measurement on a 3D surface measuring device

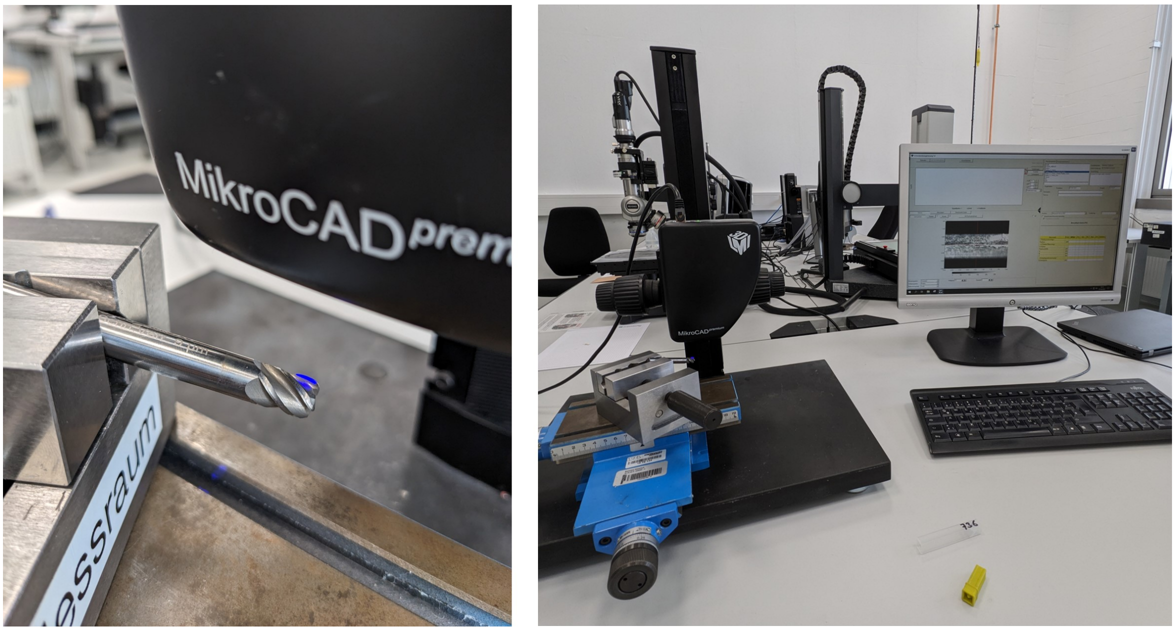

Source: Author (2024).

The average value of the r_β for each cutting tool was calculated using the results of the measurements of r_β for each cutting edge. Then, the mean r_β values of the tools with the same set of parameters were used to calculate the average r_β for each set of tools. Finally, these values were compared with the manufacturer's specifications. Figure 30 shows an example of r_β measurement, while Table 6 presents the final mean value for the measurement and a comparison with the manufacturer's specifications. Ultimately, the tool was held using a clamping unit from REGO-FIX AG, consisting of an HSK 63 collet tool holder (hollow shank taper) with a collet chuck.

Figure 30 – Example of cutting edge radius (r_β) measurement

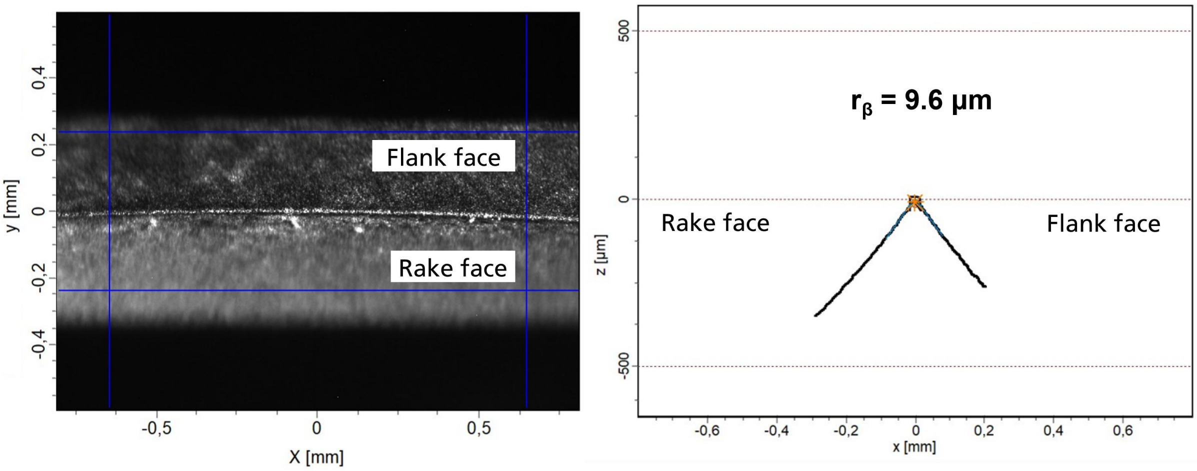

Source: Author (2024).

Table 6 – Measured r_β sampling

Tool set configuration	**Average of the measured r_β** [µm]
CTS24Z, r_β = 9 µm	11.61
CTS24Z, r_β = 14 µm	13.89
CTS30D, r_β = 9 µm	12.74
CTS30D, r_β = 14 µm	13.88

Source: Author (2024).

As seen in Table 6, the cutting edge preparation was not as precise as specified. Consequently, identifying and comparing the effects and significance of cutting edge radius (r_β) on the response may not be straightforward.

3.4 TEST PLANNING ACCORDING TO DOE

A fractional factorial experimental design was chosen to investigate the impact of different parameters and reduce the experimental workload in accordance with statistical Design of Experiments (DoE) principles. The factors that affect the process can be controlled as input parameters, while the output parameters describe the selected qualities of the product. In the scope of this work, various variables can affect the process. These include factors related to the workpiece, such as porosity, geometry parameters, laser scanning strategy, and heat treatment, as well as factors related to the cutting tool, such as carbide substrate, cutting edge radius, geometry, and surface treatment. Additionally, cutting parameters, such as cutting speed, depth of cut, and feed per tooth, among others, may also have an impact.

3.4.1 Trial A

Foremost, 7 influencing variables, also known as factors, were selected based on preliminary works from Wood *et al.* (2020), Kirchmann (2022) and Li (2023), and the state of the art. The factors selected are the **relative density (**D_r**)**, related to the workpiece, the **hard metal substrate** and **cutting edge radius (**r_β**)**, related to the tool, as well as the machine-side adjustable process parameters, **cutting speed (**ν_c**)**, **feed per tooth (**f_z**)**, **radial depth of cut (**a_e**)**, **feed direction relative to the AM build-up direction**, and a factor related to a process boundary condition, as the **use or not of coolant**. The experimental plan has two levels of parameters for each factor, which means that for each control parameter two different values are tested. Table 7 provides the selected factors and their level values. The values of the factors were chosen based on prior research and current industry standards.

Table 7 – Selected control parameters and their Levels

Relative density (D_r)	**Cutting tool substrate**	**Cutting edge radius (r_β)* [μm]**	**Cutting speed (ν_c)** [m/min]	**Feed per tooth (f_z)** [mm]	**Radial depth of cut (a_e)** [mm]	**Feed direction**	**Use of coolant**
72%	CTS24Z	9	30	0.030	1.0	‖	No
84%	CTS30D	14	45	0.045	1.5	⊥	Yes

* The r_β values presented here represent the planned specification. After measurement, it was shown that they deviate on average from the specified value (see Table 6).

Source: Author (2024).

Both selected feed directions, illustrated in Figure 31, are related to the AM build-up direction. Since the mechanical properties of porous AM-Inconel 718 differ depending on the direction of analysis in relation to the AM build-up direction, this factor may also influence machinability.

The experimental fractional factorial plan was originally conceived with seven factors. The relative density was deliberately omitted to allow the comparison of different initial values with the same parameter sets. As a result, the trial plan consisted of 8 test runs for each material porosity, *i.e.*, the same set of parameters was tested for both 84% and 72% relative density samples. The total experimental effort resulted in 16 runs, twice the

Figure 31 – Feed directions relative to the AM build-up direction

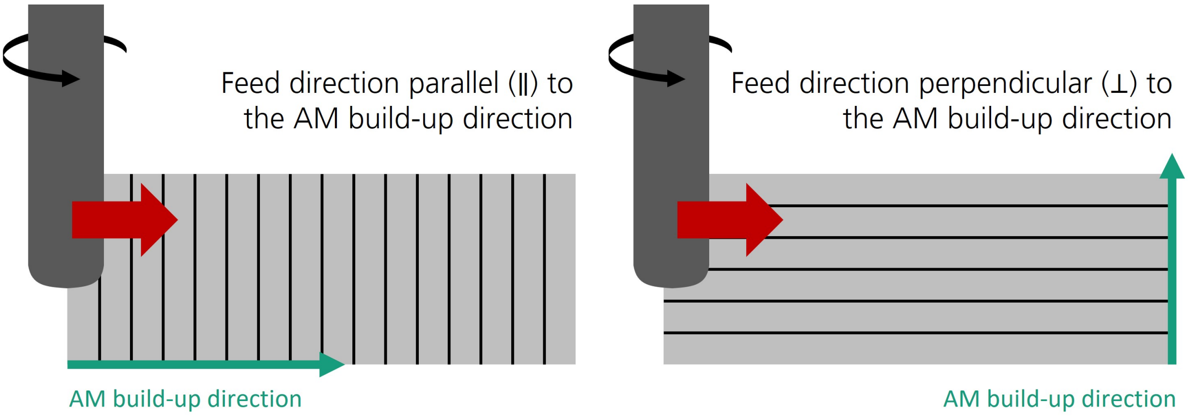

Source: Author (2024).

trial plan, one for each material porosity. This initial design had a resolution level III and is shown in Table 8.

Table 8 – Experimental Test Plan for trial A

Parameter set	**Cutting tool substrate**	**Cutting edge radius (r_β)** [µm]	**Cutting speed (v_c)** [m/min]	**Feed per tooth (f_z)** [mm]	**Radial depth of cut (a_e)** [mm]	**Feed direction**	**Use of coolant**
1	CTS24Z	14	30	0.030	1.5	∥	Yes
2	CTS30D	14	30	0.045	1.0	∥	No
3	CTS30D	9	45	0.030	1.5	∥	No
4	CTS24Z	9	45	0.045	1.0	∥	Yes
5	CTS30D	9	30	0.030	1.0	⊥	Yes
6	CTS24Z	9	30	0.045	1.5	⊥	No
7	CTS24Z	14	45	0.030	1.0	⊥	No
8	CTS30D	14	45	0.045	1.5	⊥	Yes

Source: Author (2024).

The output variables selected to be observed and further analyzed during and after the tests are some of the criteria used to evaluate machinability. The quantitative variables are the cutting forces, especially the active force, accelerations, flank wear land width (VB), and chipping width (CH). The qualitative variables to be analyzed are tool wear mechanisms, chip form, and workpiece surface quality after milling. The control and target variables selected are summarized in Figure 32.

Figure 32 – System Analysis according to DoE

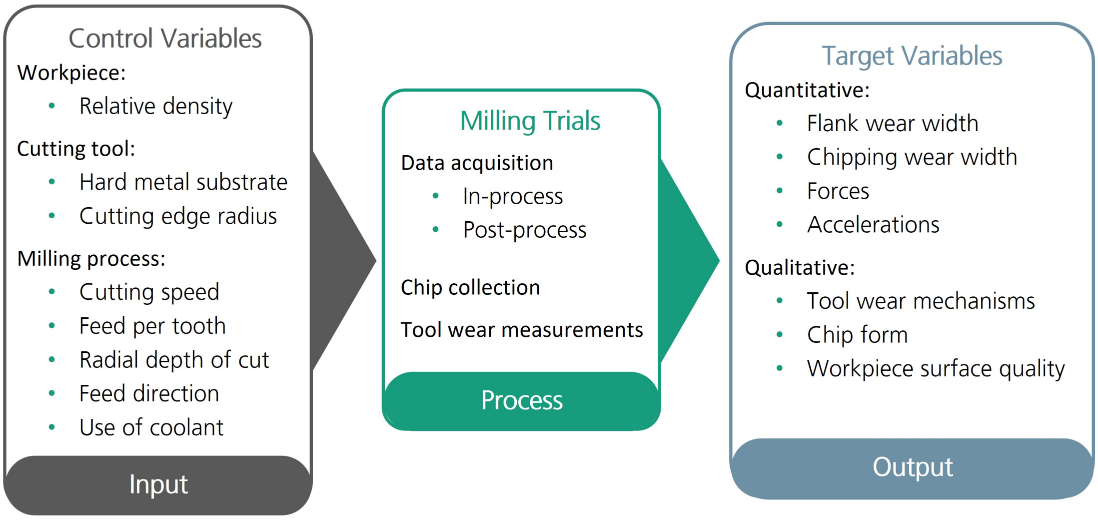

Source: Author (2024).

3.4.2 Trial B

The initial idea was to conduct Trial B as a second experiment with only two control parameters for both material porosities, selected from the seven control parameters tested in Trial A, depending on the level of significance obtained from the results of Trial A. However, a quick analysis of the output from Trial A revealed that the initial fractional factorial design was saturated, making it impossible to calculate the level of significance using only the runs from Trial A. As a result, the original plan for Trial B was abandoned. To reuse the data obtained in trial A and to determine the level of significance, influence, and interactions of the control variables on the outputs, a folding method was applied to all factors in the fractional factorial design of trial A. Table 9 displays the complete set of parameters for trials A and B. Trial A remains unchanged, while trial B is the result of folding the trial A design.

To fold the fractional design, additional runs need to be added to the original trial plan. These tests will be similar to the initial DoE. The follow-up test sections mirror the original test runs, except that the level value of all factors is systematically switched, meaning that the signs on all factors are reversed on the doubled runs (Gunst; Mason, 2009). In other words, the new folded trial plan adds the same number of runs as the initial plan, but for each new run, the factors assume the exact opposite level values of their original parameter set. "Fractionating" a design can reduce the number of tests, while folding a fractional design doubles its size to separate confounded interactions and main effects (Antony, 2003). Folding designs are useful supplements to highly fractionated designs. They are effective in resolving aliasing issues when an analysis of a fractional factorial experiment indicates that some aliased effects are statistically significant (Gunst; Mason, 2009). Applying fold-

Table 9 – Complete experimental Test Plan for trials A and B

	Parameter set	**Tool substrate**	**Cutting edge radius (r_β) [μm]**	**Cutting speed (v_c) [m/min]**	**Feed per tooth (f_z) [mm]**	**Radial depth of cut (a_e) [mm]**	**Feed direction**	**Use of coolant**
Trial A	1	CTS24Z	14	30	0.030	1.5	‖	Yes
	2	CTS30D	14	30	0.045	1.0	‖	No
	3	CTS30D	9	45	0.030	1.5	‖	No
	4	CTS24Z	9	45	0.045	1.0	‖	Yes
	5	CTS30D	9	30	0.030	1.0	⊥	Yes
	6	CTS24Z	9	30	0.045	1.5	⊥	No
	7	CTS24Z	14	45	0.030	1.0	⊥	No
	8	CTS30D	14	45	0.045	1.5	⊥	Yes
Trial B	9	CTS30D	9	45	0.045	1.0	⊥	No
	10	CTS24Z	9	45	0.030	1.5	⊥	Yes
	11	CTS24Z	14	30	0.045	1.0	⊥	Yes
	12	CTS30D	14	30	0.030	1.5	⊥	No
	13	CTS24Z	14	45	0.045	1.5	‖	No
	14	CTS30D	14	45	0.030	1.0	‖	Yes
	15	CTS30D	9	30	0.045	1.5	‖	Yes
	16	CTS24Z	9	30	0.030	1.0	‖	No

Source: Author (2024).

ing to the fractional factorial design of trial A doubles the number of runs from 8 to 16 and increases the design's resolution from level III to IV. The 8 new runs and their parameter combinations are now tested in trial B. The trial B plan was conducted for both investigated material porosities, resulting in an additional experimental effort of the same size as that of Trial A.

3.5 EXPERIMENTAL SETUP AND DATA ACQUISITION

In this work, porous Inconel 718 probes manufactured using LPBF were subjected to milling tests in an experimental setup at the Fraunhofer-IPT shop floor to investigate the effects of selected control variables on the machinability of the materials. A Makino D500 5-axis vertical machining center was used to carry out the milling tests. This machine has a spindle speed (n) up to 20000 min^{-1} and a maximum power of 18.5 kW. The controller used by the machining center is a Professional 6 CNC type FS31i-B series from Fanuc Deutschland GmbH.

The workpieces were clamped using a bench vise from Schunk GmbH & Co. KG, and aligned according to the required feed motion direction. A new tool was used for each trial run, mounted using a clamping unit type HSK 63 and an automatic clamping unit from REGO-FIX AG. The projected tool length was 20 mm, after each tool change, the tool length was measured and checked by the machine to meet the configured length. To measure the target variables, the machine was equipped with a dynamometer platform, mounted on the machine bed, and an accelerometer, placed on the spindle. Figure 33 provides an overview of the internal and external experimental setup at the shop floor of Fraunhofer Institute (IPT), including the directions of measurement for the dynamometer and acceleration sensors.

Figure 33 – Overview of the internal and external experimental setup at IPT's Shop Floor

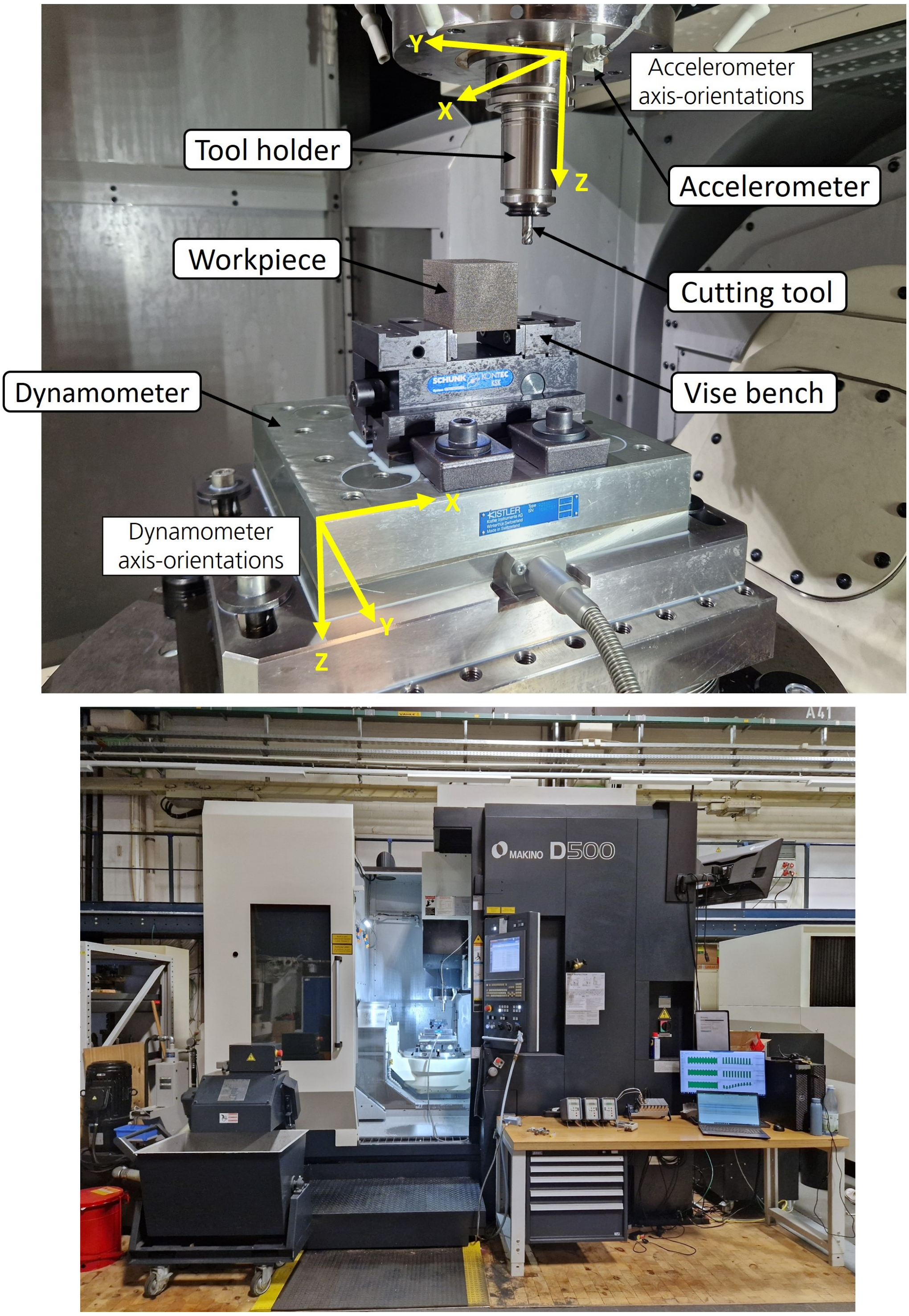

Source: Author (2024).

The frontal part of the bench vise was used to align the workpiece. Each time a workpiece had to be replaced, the upper, left, and front surfaces of the new workpiece were measured with the help of a measurement probe from RENISHAW. The measured points on each of the named surfaces were then replaced on the G-program, this step ensures that the cutting tool always cuts the right amount of material and will travel over the expected position.

The depth of cut (a_p) remained constant at 3 mm throughout the tests. Additionally, the milling was performed in paths, where each path corresponds to the feed travel distance (l_f) of the tool after one complete crossing of the workpiece, from one side to the other. Because the workpieces are cuboid-shaped with unequal edge sizes, and the probe's position during machining depends on the feed direction, the path length is always equal to the length of the workpiece edge that is parallel to the feed direction. When the feed direction is parallel to the AM build-up direction, the path length is 46.3 mm, and when it is perpendicular, the path length is 50 mm. Figure 34 illustrates the path length and volume of material removed per path, highlighted in red.

Figure 34 – Schematic illustration of the feed path length and volume removed/feed path

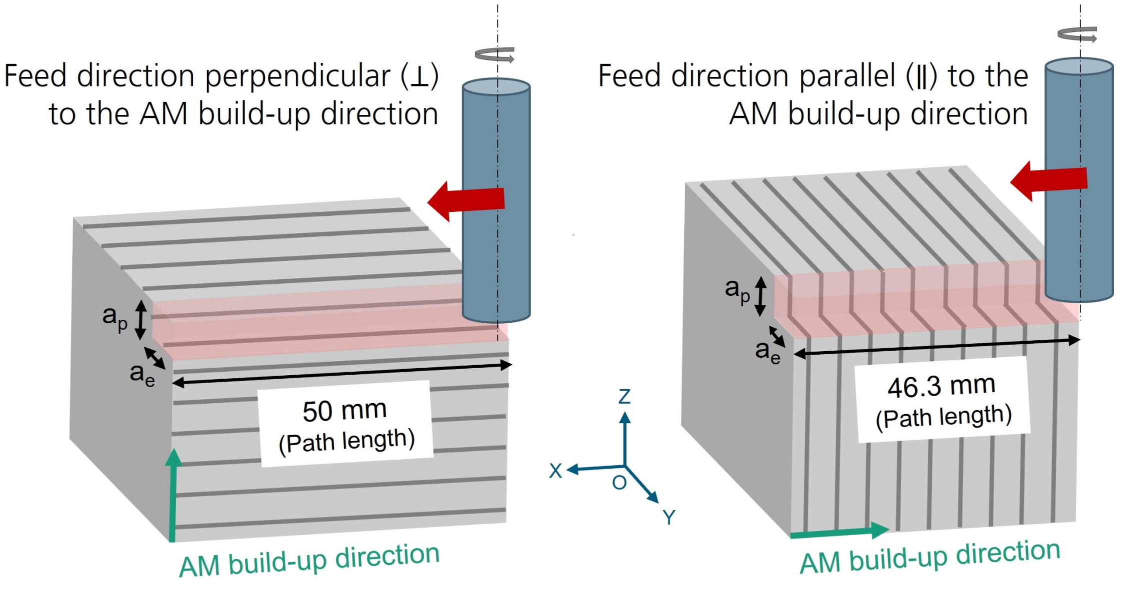

Source: Author (2024).

The tool life is usually evaluated based on the tool feed travel distance (l_f) and the volume of the machined material. Equation 4 can be used to easily calculate the machined volume by multiplying the radial depth of cut with the depth of cut and feed travel.

$$V = a_e \cdot a_p \cdot l_f \tag{4}$$

To ensure an accurate comparison of wear development and machinability, a criterion was established based on the feed travel distance (l_f) for collecting chips, acquiring microscopic images of the tool cutting edges, record and processing of forces and accelerations. This criterion was also used in previous investigations, as in Kirchmann (2022), and allows for comparison of results across studies. To analyze chipping width criteria (CH), the same machined volume was used as a basis for comparing different parameter sets.

The machined volume of 7200 mm^3 was selected as the benchmark for comparing the CH results. To achieve the same volume of machined material, a larger overall feed travel (l_f) is required for a_e equal to 1.0 mm compared to a_e of 1.5 mm. Additionally, the influence of feed direction on the feed travel must be taken into account. The strategy for each value of a_e and feed direction varies. Table 10 shows the strategy adopted for trials A and B for data collecting.

Table 10 – Data collecting strategy for trial A and B

a_e [mm]	**Nr. of paths**	**Path length** [mm]	**Nr. of accumulated paths**	**Feed travel l_f** [mm]	**Machined volume** [mm^3]	**Forces and accelerations**	**Tool wear documentation**	**Chips collection**
1.0	4	46.3	4	185.2	555.6	Yes	Yes	Yes
	11		15	694.5	2083.5	Yes	Yes	No
	20		35	1620.5	4861.5	Yes	Yes	No
	17		52	2407.6	7222.8	Yes	Yes	No
	4	50	4	200	600	Yes	Yes	Yes
	10		14	700	2100	Yes	Yes	No
	18		32	1600	4800	Yes	Yes	No
	16		48	2400	7200	Yes	Yes	No
1.5	4	46.3	4	185.2	833.4	Yes	Yes	Yes
	11		15	694.5	3125.25	Yes	Yes	No
	20		35	1620.5	7292.25	Yes	Yes	No
	4	50	4	200	900	Yes	Yes	Yes
	10		14	700	3150	Yes	Yes	No
	18		32	1600	7200	Yes	Yes	No

Source: Author (2024).

Table 10 also highlights the equivalent feed travel distances (l_f) and machined volume for the corresponding data acquisition and analysis, which are color-coded for easy reference. To compare flank tool wear, process forces, and accelerations, three values of l_f (200, 700, and 1600 mm) were chosen. This allows for an overview of the milling process and a comparison of the influence of different parameter combinations from the initial to the end phase of the milling trials.

3.5.1 Measurement of Cutting Forces

Figure 35 schematically illustrates the force measurement system used in the trials. The cutting forces were recorded using a piezoelectric multi-component force platform (type

9255B) from Kistler. The 3-component dynamometer was fixed to the machine's workbench and was rustproof and protected against penetration from cooling agents. During the trials, a bench vise was fixed to the measurement platform, where the workpiece was attached. The measurement platform is connected to a splitter box type 5407A from Kistler via cable. This box divides the 3-component signal into three separate signals, one for each direction. The component signals are then connected via cable to a charge amplifier type 5011 from Kistler. A separate charge amplifier is used for the respective force components in the x, y, and z directions. The charge amplifier converts the electrical charge produced by the piezoelectric sensors into a proportional voltage signal. The amplifiers had a built-in low pass filter that allowed signals below the cut-off frequency of 3 kHz to pass through without attenuation. The voltage level was adjusted to +/- 10 V in the charge amplifiers to match the input signal of the A/D converter (KISTLER INSTRUMENTE AG, 2009; KISTLER INSTRUMENTE AG, 2005).

Figure 35 – Schematic illustration of the force measurement system

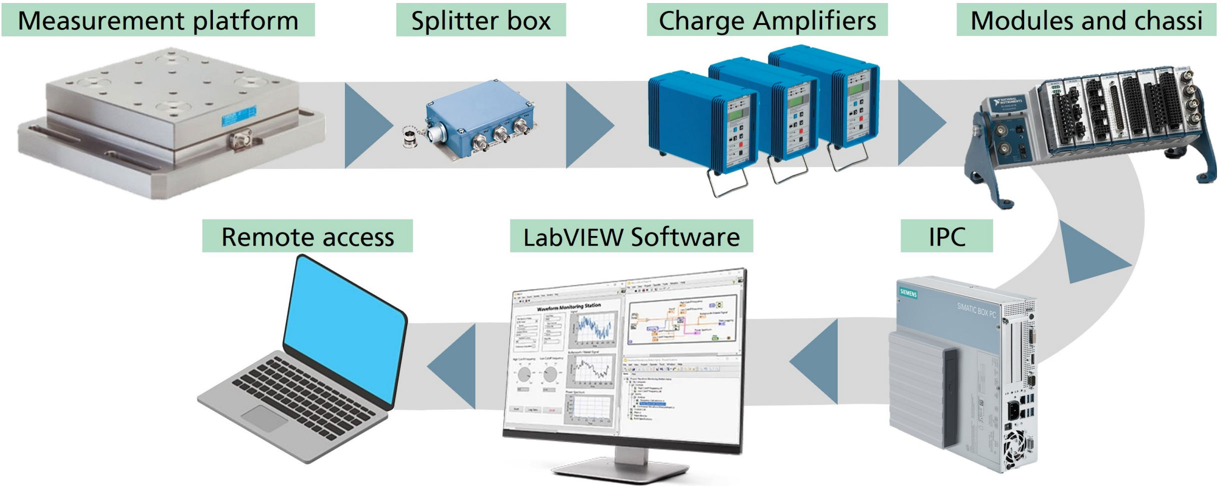

Source: Author (2024).

Each output signal from the charge amplifiers were then connected to a NI9234 A/D measurement card module converter from National Instruments, which process and convert the signals of the respective force component. The converter has a band with of 16 bits and a maximum sampling rate of 10 MHz (NATIONAL INSTRUMENTS, 2024). The measurement card was attached to a chassis cDAQ-9178 also from National Instruments, in which the converted signals were then transferred to a measuring Embedded Industrial PC (IPC) in the machine via USB cable. The data was acquired and saved using the LabView software interface from National Instruments. The sampling frequency was set to 40 kHz. The charge amplifiers were equipped with a remote control, which allowed resetting the signal to the zero level before starting each measurement. The data was recorded following the defined feed travel distances. The IPC was remotely accessed to control and monitor the data acquisition.

3.5.2 Measurement of Process Accelerations

In a similar way to the acquisition of forces, the process accelerations were gathered using an accelerometer sensor model 356A15 from PCB Piezotronics. This sensor can be magnetically attached to metallic surfaces and was placed on the bottom part of the machined spindle, close to the cutting tool holder. Besides, the connection between the sensor and the cable was covered with an insulating rubber plaster and plastic bags to prevent contact with lubricant during the trials. The cable was connected to a National Instruments measurement card NI9234, which was then attached to the chassis. Follow-up occurs in a comparable way as for the process forces.

3.6 TOOL WEAR MEASUREMENTS

In accordance with the previously defined data collection strategy, pictures of the tool's cutting edges were captured for the specified feed travel distances. They were obtained using a digital microscope VHX-6000 from Keyence GmbH, which can achieve magnification of up to 5000x. To evaluate the flank wear land width (VB) and chipping width (CH), pictures of each of the four cutting edges of the tool were captured with magnification levels of 100x and 200x. After reaching the planned feed travel distance, the tool holder was unclamped from the machine spindle and taken out of the machine. The cutting edges of the tool were then cleaned of any contamination from coolant and material particles using compressed air and a soft brush. Finally, the tool was optically inspected using the microscope.

3.7 CHIP COLLECTION AND SURFACE QUALITY INSPECTION

The chips were, in the same way, collected only after achieving the defined feed travel. During the milling process with use of coolant, a sieve was placed near the component to collect the chips. However, when cutting dry, without lubricant, the chips accumulated above the workpiece and could be easily collected. The VHX-6000 digital microscope was used for image inspection and acquisition at magnification levels of 30x and 100x.

An evaluation of surface quality is particularly relevant for finishing processes and may also be useful for roughing processes to improve process understanding (Schneider *et al.*, 2022). Therefore, pictures of the machined surface of the workpiece were taken at the end of the experiment for each feed direction and material relative density. The digital microscope used for capturing the images of the cutting edges, chips and machine surface is shown in Figure 36.

Figure 36 – Digital microscope for image acquisition of cutting edges, chips and machined surface

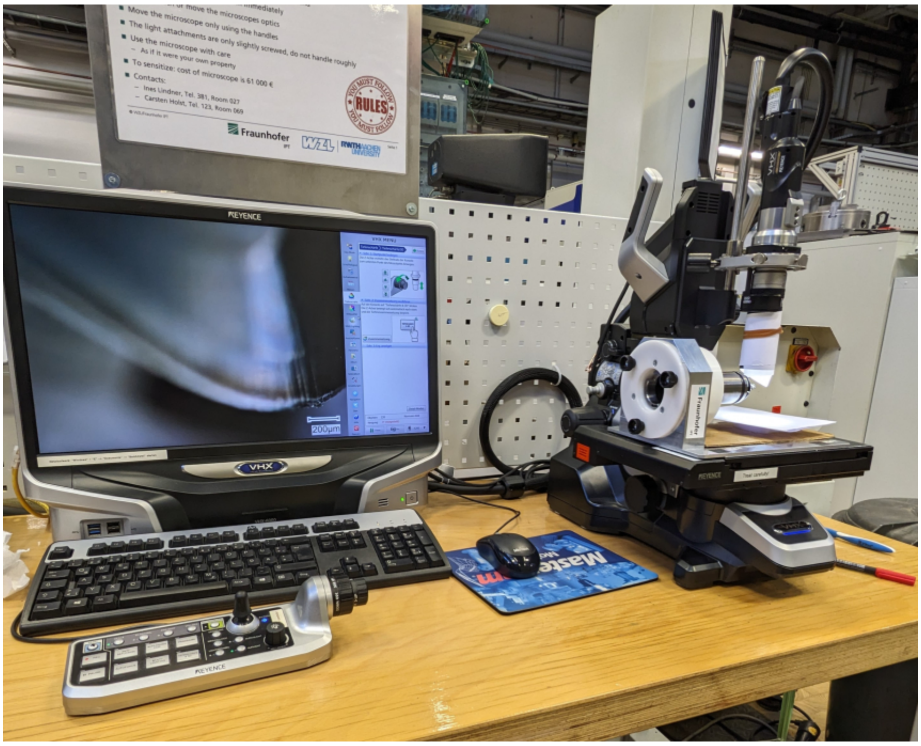

Source: Author (2024).

3.8 PROCESSING OF THE ACQUIRED DATA

To ensure precise results and reliable data analysis, it is necessary to process the raw data. This processing is crucial to ensure the quality and accuracy of the acquired data in describing the experimental trials. During processing, each Key Performance Indicator (KPI) selected to describe the target variable was calculated for further evaluation.

3.8.1 Processing of measured forces

A Technical Data Management Streaming (TDMS) file was created by LabView software for each force measurement, recorded in Newtons (N). These files contain data channels for each measured data and can be opened, visualized, and processed using NI DIAdem 2022 Q2 software. Figure 37 displays an example of the measured signal for the cutting force in the x direction during the milling of the first 200 mm of feed travel. Each signal pick represents the machining of one complete path, during which the cutting tool is engaged on the workpiece. When the signal approximates to zero, the tool is disengaged and travels freely, moving from one side of the workpiece to the other to initiate the machining of the next path. An initial analysis of the raw data on the forces identified some unusual signal behaviors, including signal drifts and offset. These behaviors may be caused by a defective cable connecting the dynamometer platform to the splitter box or by the nature of the piezoelectric sensor itself. In the figure, each of the four signal peaks represents a complete path where the tool is engaged in the workpiece and the process forces of interest occur. In this example, one feed path has a length of 50 mm.

Figure 37 – Example of unprocessed signal for cutting force in the x direction

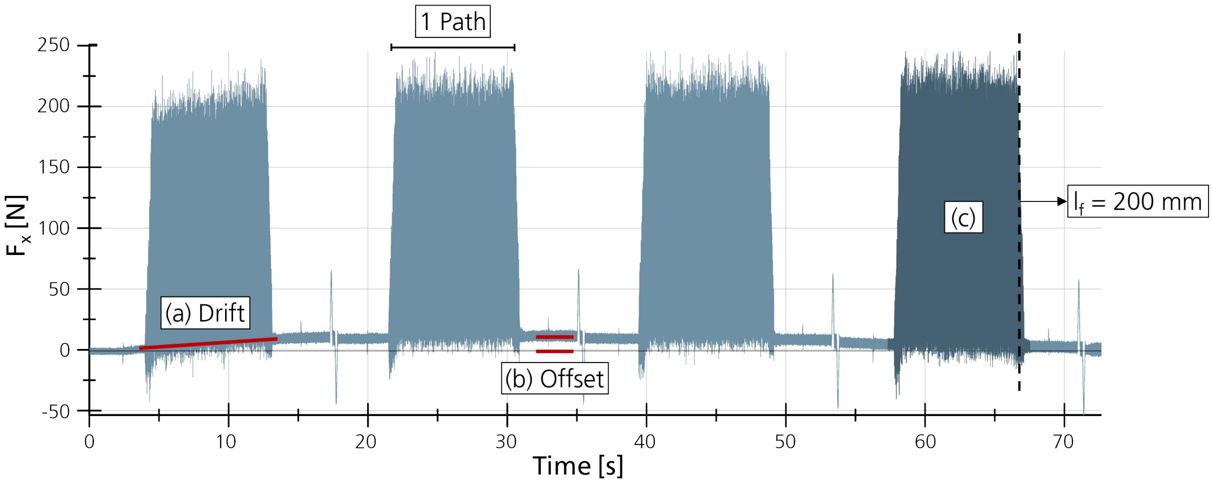

Source: Author (2024).

The measured data reveals several characteristics. Section (b) identifies an offset between the zero signal level (after resetting) and the "zero" level immediately after the tool is disengaged. Linear regression of data points in different intervals also shows that the measured data tends to present unreasonable drifts, as in section (a). Additionally, the signal interval representing the selected feed travel distances for analysis should be manually trimmed in NI DIAdem for further signal corrections and calculation of the KPIs. Section (c) of the figure shows the signal interval representing where a feed travel distance of 200 mm is achieved. After selecting the signal interval and applying Drift and Offset corrections, an additional strategy to avoid signal fluctuations during tool engagement and disengagement was defined. To obtain the KPIs for analysis, only the middle 80% of the newly selected signal interval will be used, disregarding the first and last 10%. The analysis was performed using a VBScript script executed within the software DIAdem 2022, following six consecutive steps:

1. Linear regression between the 100 first and last points of the trimmed interval to obtain information about the drift of the signal;
2. Elimination of the drift;
3. Averaging the 100 first values of the corrected interval to obtain the offset distance between the calculated mean value and the zero level;
4. Elimination of the offset;

5. Elimination of two unstable measured areas, first and last 10% of the new corrected interval, based on the sampling rate of the force platform;
6. Calculation of KPIs, as the maximum, minimum, mean cutting force, and the standard deviation of the final interval.

The procedure described above was executed for the signals in the x and y directions for all tested sequences and defined feed travel distances. Figure 38 displays the signal preview after the treatment process in (a), while (b) illustrates the orientation of the x, y, and z directions in the force measurement platform.

Figure 38 – Signal after treatment and orientation of the force measurement platform

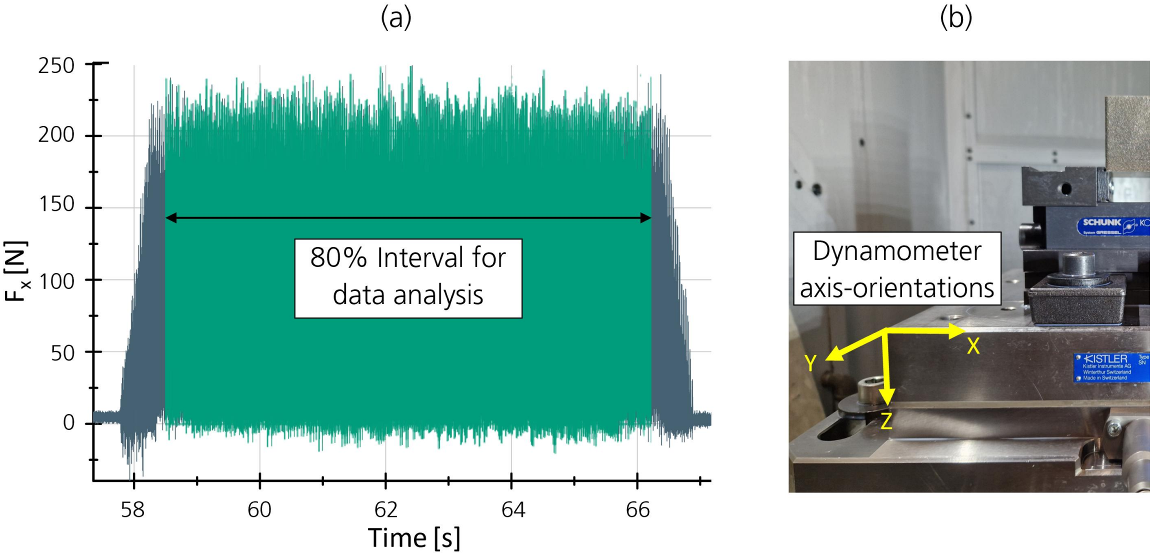

Source: Author (2024).

The active force (F_a), which generates the power during machining, is the focus of the analysis of this work and was used to assess the cutting force. It can be easily obtained from the measured feed force (F_x) and normal force (F_y) by the Equation 5. From the minimum, maximum, mean, and standard deviation values calculated for F_x and F_y, the same KPIs can be obtained for the active force through this equation.

$$F_a = \sqrt{F_x^2 + F_y^2} \tag{5}$$

3.8.2 Processing of measured accelerations

When machining porous Inconel 718, the cutting tool frequently engages and disengages due to the material's porosity. This causes abrupt changes in mechanical loads, leading to oscillations and vibrations (Li, 2023). To measure these changes, an accelerometer was placed on the machine spindle, near the cutting tool holder, and acceleration values were recorded in the x, y, and z directions. These values can be used to draw conclusions about the vibrations affecting the tool during the process. The acquired data was recorded similarly to the forces in TDMS files, then visualized and processed using DIAdem software. The same time ranges used to evaluate the forces were used to extract the acceleration intervals. No drift or offset corrections were necessary for the acceleration signals. After comparing the statistical values, the Root Mean Square (RMS) was selected for evaluation. The RMS, given in units of acceleration (g = 9.8 m/s^2), is proportional to the square root of the vibration power over the sectional distance. Therefore, it can be used as the target value to describe the vibration amplitude or "level" (Li, 2023). Figure 39 shows in (a) an example of the acceleration treatment signal process in the x direction, and the axis orientations of the acceleration sensor are illustrated in (b).

Figure 39 – Trimmed acceleration signal in the x direction and the accelerometer axis-orientations

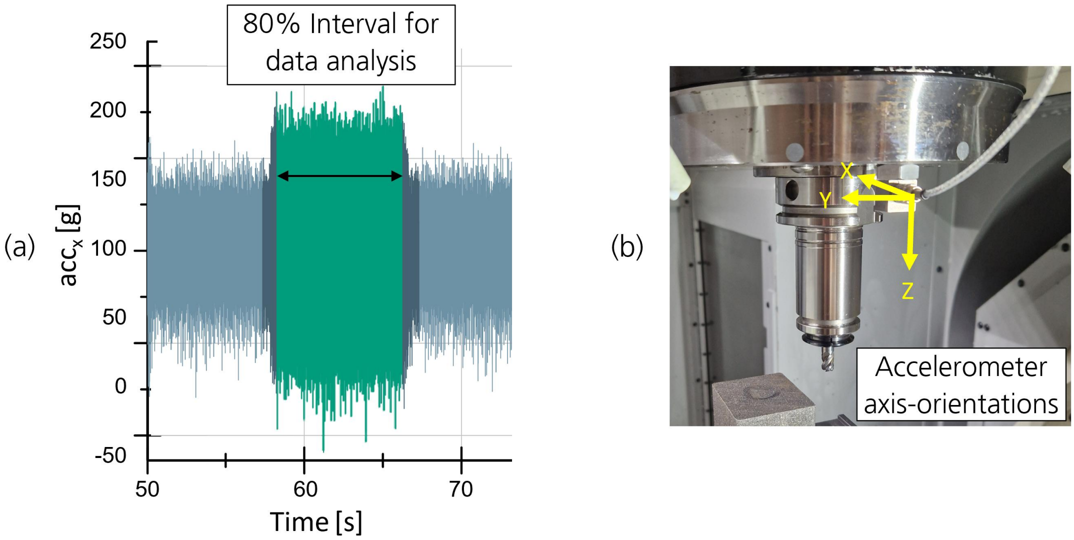

Source: Author (2024).

Since the purpose of the RMS is to get a better insight into the amplitude of the vibrations during the process, only the accelerations in the x and y-directions were analyzed. The x-direction in this case refers to the direction normal to the feed motion direction, associated with the radial depth of cut parameter (a_e), while the y-direction refers to the feed motion direction. The vibrations are expected to be more pronounced in these two directions, while in the z-direction, since the depth of cut (a_p) remains constant throughout the test runs, no major variations between parameter sets should be seen.

3.8.3 Flank wear land and Chipping

Tool flank wear and chipping were analyzed using two criteria defined by ISO8688-2 (1989). The maximum tool flank wear width (VB_{max}) was measured on the flank face from a parallel line to the cutting edge. The four VB_{max} values were then averaged and the result is referred to as VB_{mean}. This process was repeated for each tool at the defined feed travel. The measurements were performed using the data communication software of the Keyence VHX 6000 digital microscope. The VB_{max} is the maximum distance between two parallel reference lines. One line represents the original cutting edge, *i.e.*, without smeared material, while the other crosses the point of maximum VB and is parallel to the first line. In some cases, the original cutting edge must be estimated. Moreover, the maximum chipping width (CH_{max}) was defined as the maximum chipping width of the four cutting edges, measured and calculated according to Equation 6. Although (CH_{max}) is not a known standard value in the literature, it was used here to obtain a quantitative tendency with respect to chipping.

$$CH_{max} = \max(CH_{max,1}, CH_{max,2}, CH_{max,3}, CH_{max,4}) \tag{6}$$

Figure 40 shows two examples of how VB_{max} and CH_{max} measurements were taken for each cutting edge.

Figure 40 – Examples of VB_{max} and CH_{max} measurements

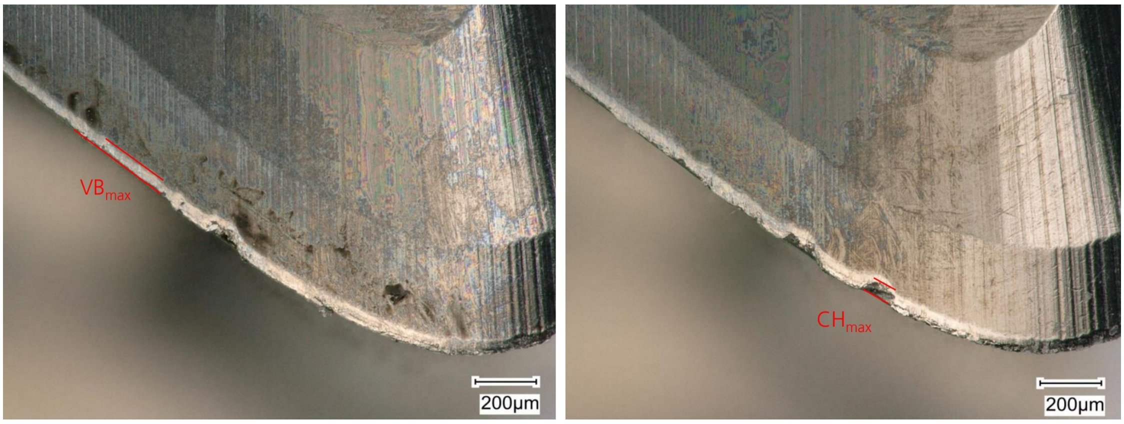

Source: Author (2024).

During the measurements, the presence of wear caused by the adhesion mechanism was many times observed. This kind of tool wear may lead to inaccurate flank wear measurements, which might make it harder to identify the effects of the control parameters on the tool flank wear.

3.8.4 Main effect and Interaction diagrams

After gathering all the quantitative target variables, it was time to evaluate the data. The processed KPIs (mean active force, RMS of the accelerations, mean flank wear width and maximum chipping width) for the defined feed travel distances were directly entered into Minitab statistical software as response variables. With the help of the software, the statistical parameters, as well as, the interaction of the two different relative densities of Inconel 718 with other manipulated variables and main effect diagrams of the relative density on each target variable were generated.

The interaction diagrams show whether an effect on the response of a target variable caused by one control factor depends on the level of another control factor. These diagrams refer to the change in the effect of one manipulated variable on the target variable when another manipulated variable is changed. On the other hand, the main effects diagram graphically shows the mean values of the response variables for each of the factor levels. In other words, the main effect refers to the tendency and degree of change of the target variable with one manipulated variable while all other manipulated variables are held constant. It is commonly used when the difference between the mean values of the levels for an individual factor should be examined (MINITAB, 2023c; MINITAB, 2023d).

3.8.5 Analysis of variance (ANOVA)

The statistical method called ANOVA proposed by the British statistician Ronald Fisher was applied in this work to determine the significance of mean differences on an independent target variable caused by two or more independent control variables. The idea behind ANOVA is to split the variance, or total variance, of the measured data according to the causes of the variation. ANOVA compares and quantitatively estimates the influences on the target variable of different control variables group or different levels of the same control variable and the error effects within the group, *e.g.*, measurement errors of the sensors (Gelman *et al.*, 2005; Li, 2023). There are three primary assumptions in ANOVA: the responses for each factor level have a normal population distribution, these distributions have the same variance, and the data are independent (Mathews, 2005).

The level of significance of the control variables on the target variables was also calculated through the statistical software Minitab. The p-value indicates the probability that the variance caused by the manipulated variable is significant. During the analysis, a 95% confidence interval with a confidence level α of 0.05 was used. Therefore, a p-value smaller than or equal to 0.05 means a statistically significant influence of the manipulated variable on the target variable (Mathews, 2005).

4 RESULTS AND DISCUSSION

The results presented in this chapter are the product of the analysis using data collected during the experimental milling trials on porous AM-Inconel 718 samples. The data was processed following the methodological procedures described in section 3.8. The quantitative statistical analysis of variance (ANOVA) based on the general linear model of the target variables (VB_{mean}, CH_{max}, mean F_a, and RMS values of the acc_x and acc_y), obtained or derived from the trials, is presented for each of the factors in the specified feed travel distances. Additionally, the interactions between the selected control variables as well as the main effect analysis of porosity on the target variables are discussed. Finally, a qualitative analysis of chip formation and quality of the machined surface is performed using microscopic images.

4.1 TOOL WEAR

Tool flank wear and chipping were measured at the defined feed travel distances during the trials according to the collecting strategy (Table 10). To simplify the presentation of results and increase conciseness, the ANOVA results, interaction, and main effect diagrams will be displayed only for the initial 200 mm and final 1600 mm. After analyzing the results for all feed travel distances, the results right at the beginning and at the end of the experiment domain seem to give a good representation of the process. In this context, it can be expected that the tool will initially experience minimal wear, while at the end, the influence of tool wear will be significant on milling process. For each ANOVA performed, the model fit to the data and the residual plots were checked to ensure that they were consistent with the assumptions of the analysis.

4.1.1 Flank wear

The quantitative results of the analysis of variance (ANOVA) for the mean flank wear land width (VB_{mean}) and the initial feed travel l_f = 200 mm are shown in Table 11. The left column lists the factors or control variables, for each a series of values obtained from ANOVA are presented. The total degrees of freedom (DF) indicate the amount of information a term uses, while the adjusted sum of squares (Adj. SS) measures the variation for different components of the model. Moreover, the adjusted mean squares (Adj. MS) calculate the amount of variation explained by a term, and the F-value is the test statistic used to determine the relationship between the term and the response (MINITAB, 2023e).

The statistical software Minitab uses the values previously described to calculate the p-value, which determines the statistical significance of the factors and is particularly relevant for the purpose of this work. The table's final column displays the percentage contribution of each factor to the response of the VB_{mean}. The contribution is obtained by dividing the factor's Adj. SS by the sum of the Adj. SS of all factors.

Comparing the p-values given by Table 11 with the 95% selected confidence interval (α = 0.05), the ANOVA shows that the relative density and use of coolant factors have a significant influence on the VB_{mean}, once their p-values, 0% and 0.6%, respectively, are way smaller than 5%. The contribution values also show how much each of these factors contributes to the response, 57.6% and 22%, respectively. The p-value corresponding to 6.4% (8.9% contribution) for the cutting speed v_c is close to the 95% limit of the confidence interval, in such a way that a significant influence on the VB_{mean} can also be assumed Li (2023), Klocke (2011). The remaining factors do not impact the response of the target variable significantly, their p-values are far from the 95% confidence limit.

Table 11 – Result of the analysis of variance for VB_{mean} after l_f = 200 mm

Factors	**DF**	**Adj. SS**	**Adj. MS**	**F-value**	**p-value**	**Contribution** [%]
Rel. Density (D_r)	1	113.439	113.439	24.33	0.000	57.6
Hard Metal Substrate	1	8.768	8.768	1.88	0.184	4.5
Cutting edge radius (r_β)	1	6.799	6.799	1.46	0.240	3.5
Cutting speed (v_c)	1	17.627	17.627	3.78	0.064	8.9
Feed per tooth (f_z)	1	0.158	0.158	0.03	0.855	0.1
Radial depth of cut (a_e)	1	2.127	2.127	0.46	0.506	1.1
Feed Direction	1	4.689	4.689	1.01	0.326	2.4
Coolant	1	43.361	43.361	9.30	0.006	22.0
Error	23	107.248	4.663			
Total	31	304.217				

Source: Author (2024).

Figure 41 presents the interaction plots of the control variables as a function of the two relative densities (72% and 84%) and the main effects plot of the relative density. The interaction diagrams are only shown for v_c and coolant, as they are the significant factors in this analysis. The direction of feed motion was also included because it will become a significant factor at the end of the trial, after l_f = 1600 mm, however for the initial 200 mm it has no significance. Overall, VB_{mean} values were higher when machining porous AM-Inconel 718 with 84% relative density compared to the 72% relative density material. The interaction plots always show the curve of the 84% relative density material above the 72% material. This can also be quickly accessed by looking at the main effects diagram, which shows that increasing the relative density leads to increased tool flank wear. The higher flank wear in 84% material is assumed to be due to greater forming work required to cut denser materials (Schneider *et al.*, 2022).

This behavior is consistent with the findings of previous studies from Kirchmann (2022). The interaction plot for v_c indicates that as the cutting speed increases from the lower to the higher level, VB_{mean} slightly increases for the 72% material, but increases substantially from 23.1 to 25.6 μm for the 84% relative density material. For the coolant, as expected, when the workpieces were machined with the use of lubricant the VB_{mean} was substantially lower. The curves of the two Inconel 718 variants run almost parallel to each other on the interaction plots. This suggests no interactions between the controlled variables. The greater the difference in slope between the lines, the higher the degree of interaction. Moreover, a slope of 0 degrees in the interaction curve indicates that the manipulated value does not influence the target variable (MINITAB, 2023a; Meyer; Krueger, 2005).

Figure 41 – Interaction and main effects diagrams for VB_{mean} after l_f = 200 mm

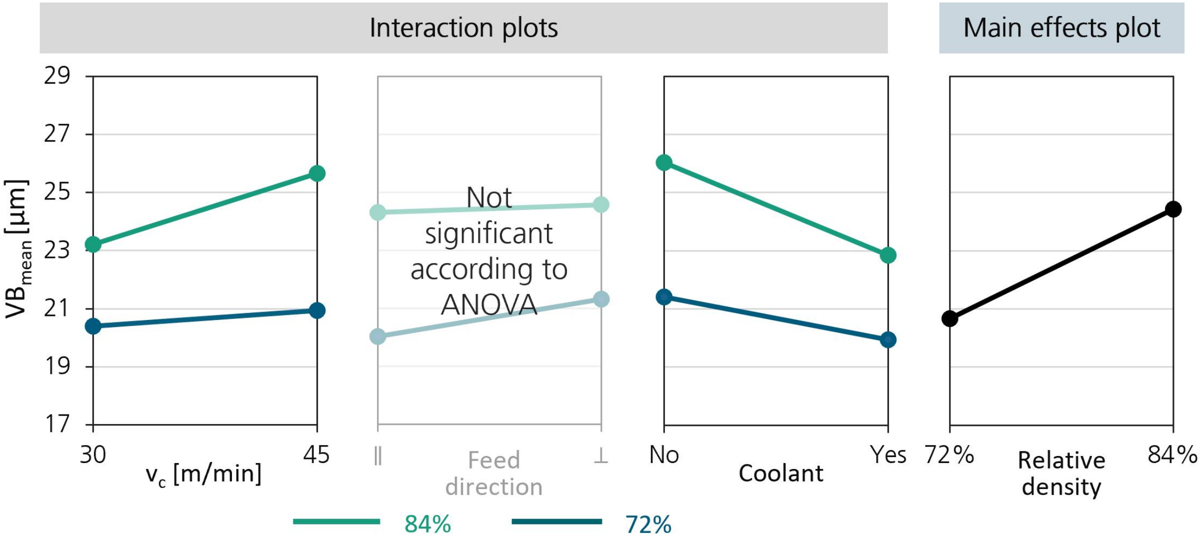

Source: Author (2024).

Table 12 presents the ANOVA results for l_f = 1600 mm. The results show that VB_{mean} increases due to expected tool wear development, as the cutting edges machined a greater volume of material compared to the initial 200 mm feed travel. The table also indicates that porosity (63% contribution) and cutting speed (13.4% contribution) remain significant factors, and feed direction (14.4% contribution) now also affects the response of the target variable. In addition, even though the use of coolant was initially a significant factor, it no longer affects the response, as evidenced by the sudden increase in its p-value.

By analyzing the interaction and main effects plots in Figure 42, the same overall trend of increasing VB_{mean} as the factor level increases, which was observed for the initial 200 mm feed travel, is also seen for the cutting speed and feed direction factors. The VB_{mean} increases more when v_c is increased for the 72% relative density material than for the 84%. However, VB_{mean} increases at almost the same rate for both porosities when changing the feed motion direction from parallel to perpendicular to the AM build-up direction. Although, the use of coolant is no longer a significant factor in the analysis for l_f = 1600 mm, its interaction plot shows unusual behavior. When milling the 72% relative density material,

Table 12 – Result of the analysis of variance for VB_{mean} after l_f = 1600 mm

Factors	DF	Adj. SS	Adj. MS	F-value	p-value	Contribution [%]
Rel. Density (D_r)	1	733.16	733.158	21.09	0.000	63.0
Hard Metal Substrate	1	79.16	79.16	2.28	0.145	6.8
Cutting edge radius (r_β)	1	0.02	0.022	0.00	0.980	0.0
Cutting speed (v_c)	1	156.07	156.07	4.49	0.045	13.4
Feed per tooth (f_z)	1	12.92	12.916	0.37	0.548	1.1
Radial depth of cut (a_e)	1	3.02	3.02	0.09	0.771	0.3
Feed Direction	1	168.04	168.04	4.83	0.038	14.4
Coolant	1	11.48	11.484	0.33	0.571	1.0
Error	23	799.55	34.763			
Total	31	1963.41				

Source: Author (2024).

the expected trend of decreasing flank wear using lubricant is reversed, which, at a first sight, seems counterintuitive. For the 84% relative density material, the predictable trend for the use of coolant is kept. These two different trends for the same factor might have probably led to a decrease in the level of significance of this control variable.

Figure 42 – Interaction and main effects diagrams for VB_{mean} after l_f = 1600 mm

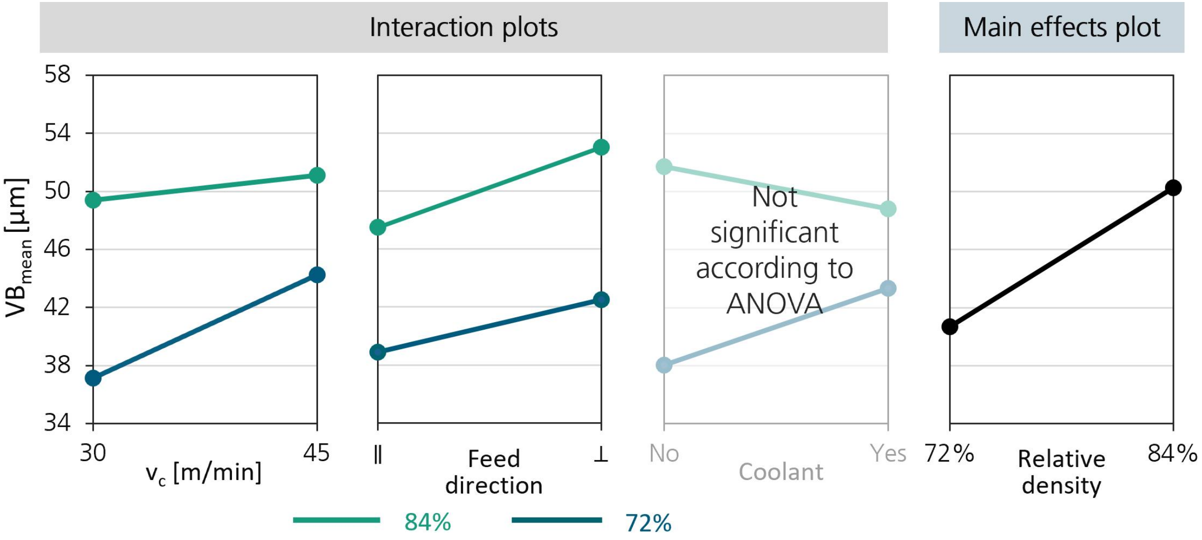

Source: Author (2024).

Besides that, the microscopic images also showed the occurrence of adhesion-type wear on the cutting edges. The adhesive wear appears due to high temperature and pressure during cutting, which causes welding to occur between the fresh surface of the chip and the rake and flank face of the tool (Bhushan, 2013; Klocke, 2011). The adhesive layer created in this process was observed multiple times in the microscopic images captured for the measurement of the flank wear land (VB). This layer can often cause incorrect measurement of VB due to confusion between the flank wear mark and the adhesive layer (Hrechuk; Bushlya, 2023). Scanning electron microscopes (SEM) images were taken to better identify the adhesion wear. Figure 43 shows a representative SEM image of the cutting edge of one cutting tool used on the trials, the adhesion phenomenon is indicated.

Figure 43 – SEM images of the cutting tool edge showing the adhesion phenomenon

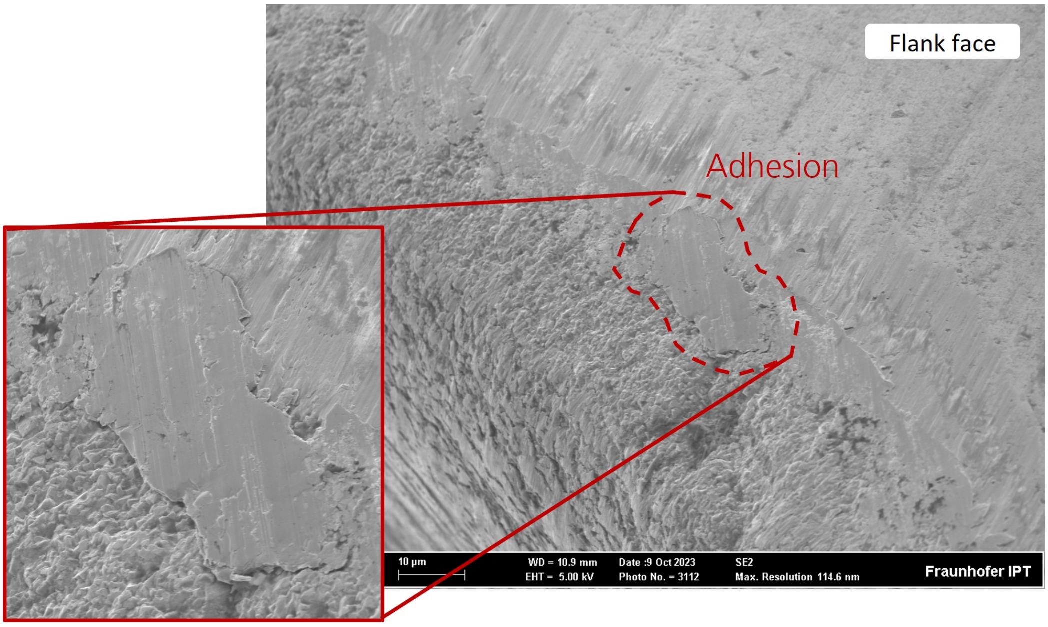

Source: Author (2024).

This work intentionally uses partially comparable parameter sets to those employed in the investigation from Kirchmann (2022). Microscopic images of the tool cutting edges from these sets can be visualized, described, and compared to the results obtained in previous studies. Figure 44 displays the most representative image of the four cutting edges of the tool after defined feed travel distances for both material porosities and parameter set 1. Overall, for both porosities, 72% and 84% relative density materials, there was almost no chipping detected for l_f= 200 and 700 mm, while for l_f = 1600 mm chipping started to be noticeable. The flank wear increased continuously with an increasing feed travel for both materials, as expected. Additionally, the flank wear appeared to affect the 84% material more, as it presented a higher flank wear land compared to the 72% material. These results can be compared to those observed by Kirchmann (2022, p. 66). In particular, the results obtained with parameter set 1 in this study are comparable to the results obtained with parameter set 7 in the previous investigation.

Since Kirchmann (2022) used only four control variables in his work: cutting speed (ν_c), feed per tooth (f_z), radial depth of cut (a_e), and feed motion direction, to the cases in which these variables assume the same values in both works, the results can be partially compared. The figures highlight the factors which are consistent across both studies.

Figure 44 – Tool wear evolution after defined feed travel distances using parameter set 1

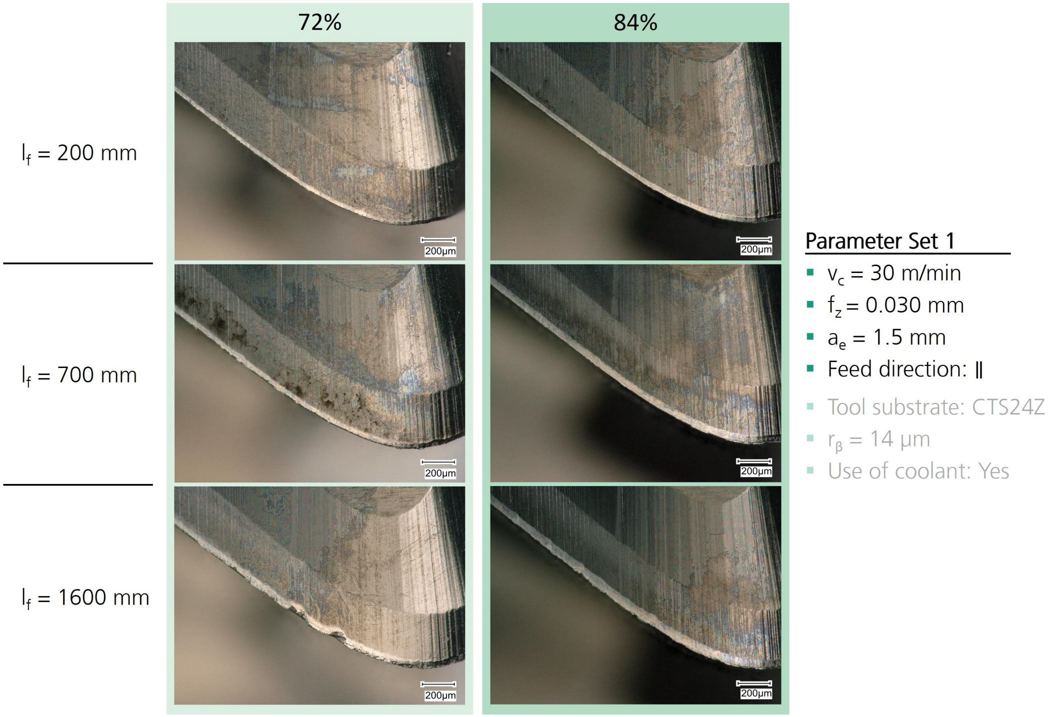

Source: Author (2024).

Generally, the main difference observed between the two studies was the early presence of strong chipping wear immediately after l_f = 800 mm, which increased with higher feed travel distances, in contrast to the almost constant flank wear and modest chipping observed in this work, notably after l_f = 1600 mm. One possible reason for this difference could be attributed to the use of tougher tool substrates in this study compared to the carbide substrates, commonly used for machining Inconel 718, employed by Kirchmann (2022). As described in section 3.3, tool substrates with higher cobalt concentration and, therefore, higher toughness were deliberately chosen to minimize chipping wear, which appears to have been successful in this study. Although two different r_β were used here, the analysis suggests that the influence of cutting edge rounding was not significant, which might be caused by imprecision in the cutting edge preparation process, revealed in section 3.3.

The parameter set 5 can also be partially compared to parameter set 1 from Kirchmann (2022, p. 58). The tool wear development after defined feed travel distances for parameter set 5, presented in Figure 45, indicates that flank wear is the dominant wear type, with higher VB values observed for the machining of the 84% material. However, chipping wear starts to appear sporadically after 700 mm for the 72% relative density material and more consistently along the cutting edge after milling the 84% material. Chipping wear slightly increases after 1600 mm when machining both materials. In addition, the chipping wear pattern at the end is very similar in both cases. In these two comparisons, the cutting speed (ν_c) has the lower factor level of 30 m/min.

Figure 45 – Tool wear evolution after defined feed travel distances using parameter set 5

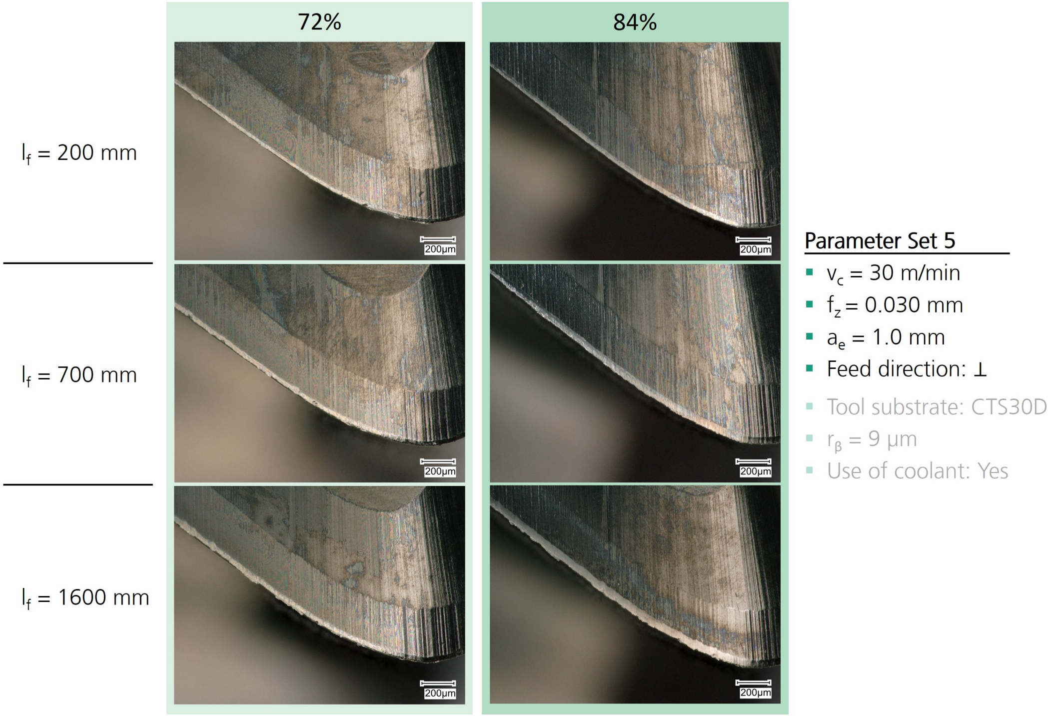

Source: Author (2024).

A correlation can also be made across studies for the two partially comparable cases in which ν_c assumes the higher factor level of 45 m/min. Figure 46 shows images of representative cutting edges after defined feed travel distances machined using parameter set 14. Even though flank wear is the dominant wear and increases with the feed travel distance for both porous materials, chipping appears to be more intense with higher cutting speed. Chipping occurs in an isolated manner along the cutting edge after 700 mm, and the frequency of chipping increases after 1600 mm for both material porosities. When compared to the parameter set 5 from Kirchmann (2022, p. 64), it is noticeable that chipping could be significantly reduced, particularly for the initial feed travel distances and when machining the 84% relative density Inconel 718.

Figure 47 shows the images of the tool cutting edges after the defined feed travels using parameter set 10. The chipping wear appears to affect the cutting edges more strongly when machining the 72% relative density material, particularly at the end. Chipping starts sparsely after 700 mm for both porosities but increases significantly after a feed travel distance of 1600 mm. Flank wear also increases as the feed travel increases, but becomes difficult to measure at the end. The results in this case are very close to those obtained by Kirchmann (2022, p. 61) using the comparable parameter set 4 of his study.

Figure 46 – Tool wear evolution after defined feed travel distances using parameter set 14

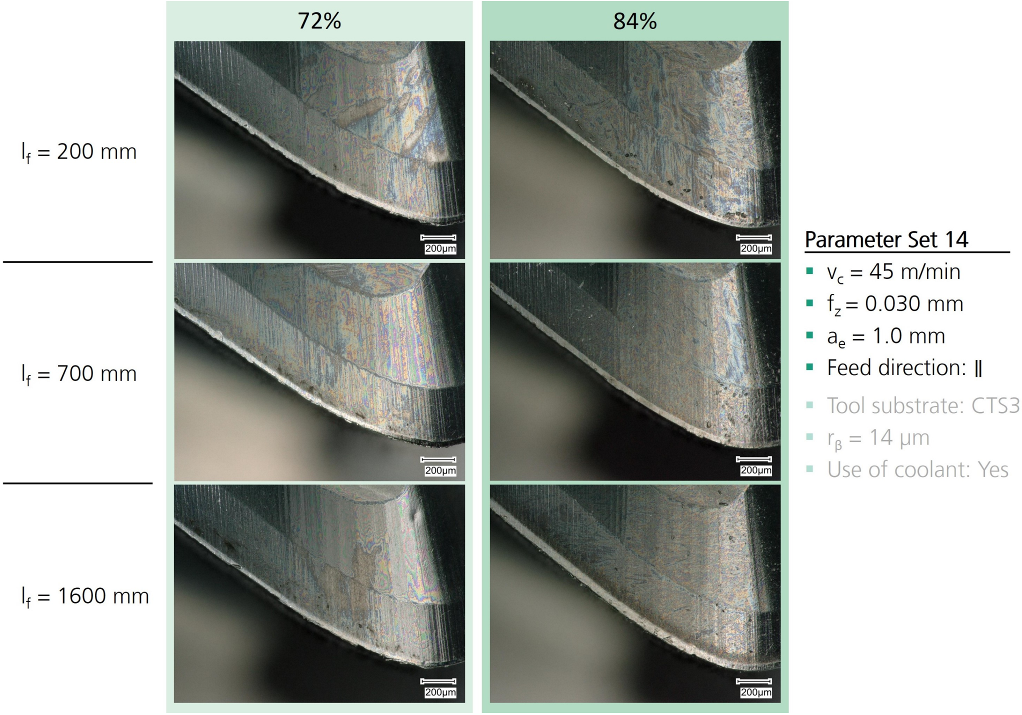

Parameter Set 14
- v_c = 45 m/min
- f_z = 0.030 mm
- a_e = 1.0 mm
- Feed direction: ∥
- Tool substrate: CTS30D
- r_β = 14 µm
- Use of coolant: Yes

Source: Author (2024).

Figure 47 – Tool wear evolution after defined feed travel distances using parameter set 10

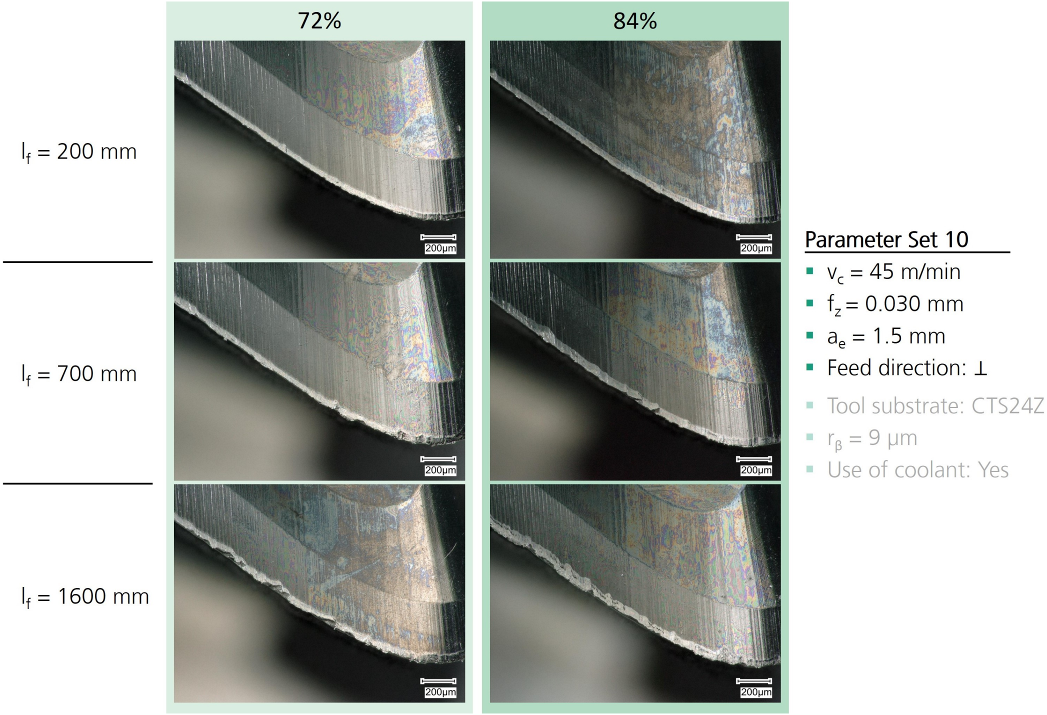

Parameter Set 10
- v_c = 45 m/min
- f_z = 0.030 mm
- a_e = 1.5 mm
- Feed direction: ⊥
- Tool substrate: CTS24Z
- r_β = 9 µm
- Use of coolant: Yes

Source: Author (2024).

4.1.2 Chipping

Chipping can also be used to complementary assess machinability according to ISO8688-2 (1989). It is defined as the deterioration of the cutting edge where parts of the edge break away. As shown in subsection 3.8.3, the value of the maximum chipping width (CH_{max}) for each cutting edge was measured, and then the maximum value of the four edges was selected for each tool in the defined feed travel. The analysis for the CH criterion was made only for one defined volume of machined material. In the trial, the tools achieved approximately the same amount of machined material volume after different feed travel distances due to use of two different values of a_e, 1.0 and 1.5 mm. Chipping measurements were then taken at l_f = 2400 mm when a_e = 1.0 mm and at l_f = 1600 mm when a_e = 1.5 mm, resulting in an approximate volume of machined material of 7200 mm^3 in both cases.

The ANOVA was performed to determine the influence of the control variables on chipping wear evolution. Table 13 shows that three factors are relevant to the response: hard metal substrate (32.2% contribution), radial depth of cut a_e (22.5% contribution), and use of coolant (28.7% contribution). The tool substrate and coolant usage fall within the 5% significance interval with p-values less than 0.05. The p-value of a_e is close to the 95% confidence interval limit and is assumed to have a significant impact.

Table 13 – Result of the analysis of variance for CH_{max} after V = 7200 mm^3

Factors	**DF**	**Adj. SS**	**Adj. MS**	**F-value**	**p-value**	**Contribution** [%]
Rel. Density (D_r)	1	9.74	9.735	0.23	0.633	1.6
Hard Metal Substrate	1	199.85	199.85	4.80	0.039	32.2
Cutting edge radius (r_β)	1	7.67	7.673	0.18	0.672	1.2
Cutting speed (v_c)	1	5.99	5.994	0.14	0.708	1.0
Feed per tooth (f_z)	1	18.53	18.529	0.45	0.511	3.0
Radial depth of cut (a_e)	1	139.49	139.487	3.35	0.080	22.5
Feed Direction	1	60.97	60.968	1.46	0.238	9.8
Coolant	1	178.09	178.086	4.28	0.050	28.7
Error	23	957.43	41.628			
Total	31	1577.76				

Source: Author (2024).

As expected, given the initial hypothesis of the tool selection that tool substrates with higher Co concentration and higher toughness would result in a reduction in chipping wear, the cemented carbide substrate factor had the most significant influence on the response of chipping. The influence of the coolant on the reduction of thermal and mechanical loads was also expected to be a relevant factor in the response of chipping. The a_e appeared to have a considerable contribution to the process, but further analysis is required through interaction plots.

Figure 48 presents the interaction and main effects diagrams for the significant factors for chipping according to ANOVA. The two lines, representing the 72% and 84% relative density variants of AM-Inconel 718, intersect, indicating that the tool substrate and relative density factors are not independent and have a more complex interaction. The results show that the substrate CTS30D, with higher Co concentration, successfully had lower values of chipping than the CTS24Z variant, demonstrating the potential of these types of tool substrates in mitigating chipping wear. This chipping wear reduction was more pronounced when machining the 72% material with the CTS30D substrate tool. The chipping width decreased from 34.2 to 26.7 μm, a reduction of 22%. In contrast, machining the denser material only resulted in a 7.5% reduction.

Figure 48 – Interaction and main effects diagrams for CH_{max} after V = 7200 mm^3

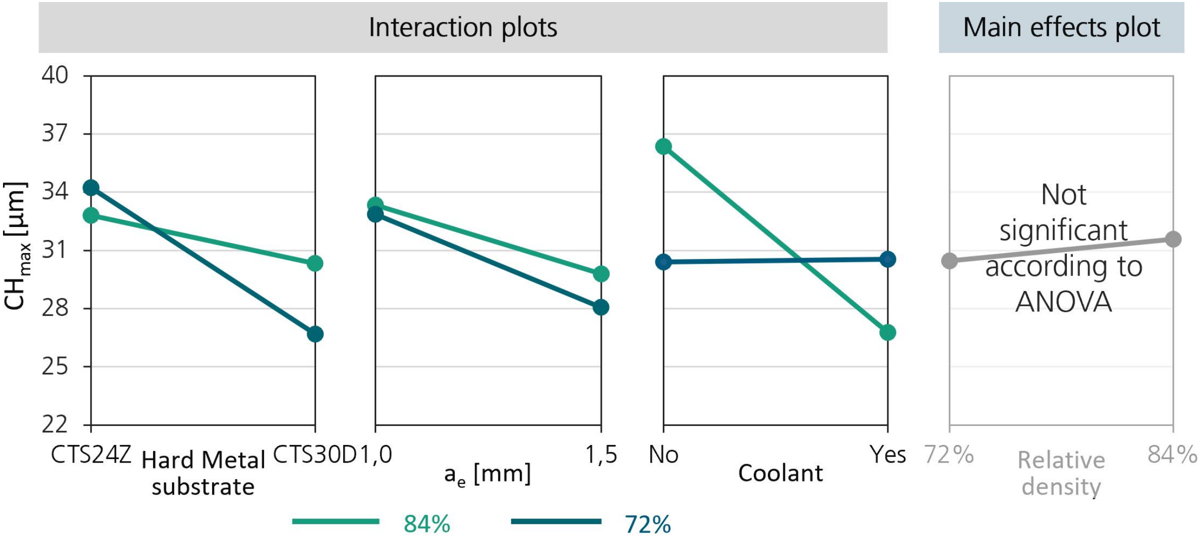

Source: Author (2024).

Furthermore, the use of coolant appears to reduce chipping wear by 26.2% when machining the 84% relative density AM-Inconel 718, while it remained almost stable when machining the 72% material. The effectiveness of the coolant in reducing VB and CH appears to be lower with the 72% relative density material compared to the 84% variant. This could be due to the possibility of the coolant draining through the pores of the material, resulting in less lubrication and cooling in the cutting area. Alternatively, it could be a consequence of the chip formation being less clean in the 72% variant and thus the coolant being less effective as other forming mechanisms dominate.

Increasing the radial depth of cut a_e from 1.0 to 1.5 mm resulted in a decrease in CH for both material porosities. The lines on the plot remain almost parallel, indicating some independence between the variables. As mentioned earlier, at a_e = 1.5 mm, the tools had to travel a shorter distance to achieve the same volume of machined material. This appears to be more effective than cutting the same volume at a lower a_e, even though the trend of decreased chipping wear with increasing a_e may seem counterintuitive at first glance, as larger a_e values typically result in increased tool wear (Khan *et al.*, 2022). It is important to note that the measurements of CH were taken in a range of larger feed travel distances in which wear is consistently present. This makes the interaction between factors and the response more complex. In addition, the ANOVA results indicate that relative density was not a significant factor in the response, but from the main effects plot, the 84% material variant showed to be slightly more affected by chipping than the 72% relative density AM-Inconel 718, which was also observed by Kirchmann (2022). Lastly, for the first time in comparison with previous research, parameters sets in which flank wear was the dominant type of wear up to the investigated feed travel distances were identified. Examples of this behavior were observed in the case of parameter sets 2 and 14, when they were applied in the machining of the 84% variant. The resulting chipping was minimal, and flank wear was uniform and dominant up to the investigated feed travel (Appendix A).

4.2 CUTTING FORCES

The cutting forces in the x, y, and z directions were acquired during the trials on the specified feed travel distances. However, only the forces in the x and y directions have been used in order to calculate the mean active force F_a, the object of analysis in this work, as shown in subsection 3.8.1. The results of the ANOVA, interaction, and main effects plots are going to be presented below.

4.2.1 Active force

The cutting forces are a common metric used for assessing machinability of materials, due to its direct relation with tool wear and process reliability, in this work only the active force F_a in the working plane was used for the process evaluation, since its components generate the power during machining (KISTLER, 2024; DIN6584, 1982). To maintain conciseness, the mean F_a results are presented for the early 200 mm and final 1600 mm feed travel distances, as done in the discussion of flank wear results. Table 14 displays the ANOVA results, indicating that the relative density (13.8% contribution), cutting edge radius r_β (1.8% contribution), feed per tooth f_z (20% contribution), radial depth of cut a_e (57.4% contribution), and use of coolant (5.7% contribution) significantly influence the response (α = 0.05, p $\leq$ 0.05) of the mean F_a after a 200 mm feed travel distance. The largest contributors were a_e and f_z.

The interaction and main effects plots of the five most significant factors show that the mean F_a values for the 84% material were almost 15.7% higher than those for the 72% relative density AM-Inconel 718, Figure 49. The lines representing both material porosities also run parallel to each other, indicating no interaction between the two control variables displayed on the interaction diagrams. Increasing the cutting edge radius r_β from 9 to 14 μm

Table 14 – Result of the analysis of variance for mean F_a after l_f = 200 mm

Factors	DF	Adj. SS	Adj. MS	F-value	p-value	Contribution [%]
Rel. Density (D_r)	1	4942.9	4942.9	53.78	0.000	13.8
Hard Metal Substrate	1	327.8	327.8	3.57	0.072	0.9
Cutting edge radius (r_β)	1	662.7	662.7	7.21	0.013	1.8
Cutting speed (v_c)	1	145.0	145.0	1.58	0.222	0.4
Feed per tooth (f_z)	1	7151.6	7151.6	77.81	0.000	20.0
Radial depth of cut (a_e)	1	20562.2	20562.2	223.73	0.000	57.4
Feed Direction	1	6.0	6.0	0.06	0.801	0.0
Coolant	1	2024.8	2024.8	22.03	0.000	5.7
Error	23	2113.8	91.9			
Total	31	37936.9				

Source: Author (2024).

resulted in an increase of 5.8% and 5.1% in the mean F_a when cutting the 84% and 72% materials, respectively. This can be attributed to stronger friction processes and ploughing in the area of the cutting edge rounding (Klocke, 2011). In principle, the oscillations and vibrations can be significantly reduced by selecting a suitable cutting edge radius r_β, which can result in a better surface finishing (Klocke, 2011). Ideally, when the r_β is increased, the blunt cutting edge prevents the cutting edge from engaging the workpiece, resulting in an increase in cutting force and a reduction in vibration (Li, 2023). It is very important to note that, as mentioned in section 3.3, the actual r_β values were not as precise as the specified values, which may make it more challenging to assess its significance on the process.

Figure 49 – Interaction and main effects diagrams for mean F_a after l_f = 200 mm

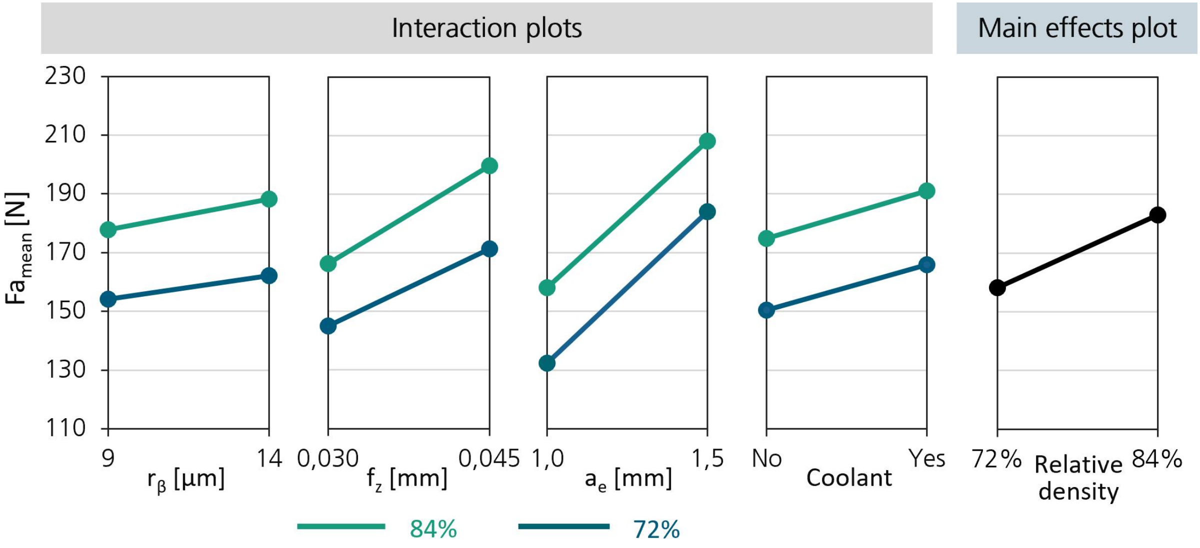

Source: Author (2024).

After l_f = 200 mm, for all cases, an increase in the factor level leads to an increase in the mean F_a. These findings are in line with the principles of cutting technology (Klocke, 2011) and previous observations made by Kirchmann (2022) and Li (2023). Increasing the radial depth of cut a_e, from 1.0 to 1.5 mm, had a greater impact on the mean F_a, resulting in a 39% increase when cutting the 72% material and a 31.5% increase when cutting the 84% material. Further investigation is required to explain the increase in the mean F_a observed for both material variants when using coolant. One hypothesis is that the interaction between the two primary effects of lubrication and cooling during the use of lubricants may be a contributing factor. Good lubrication can lead to a reduction in the power converted into heat, which in turn means that less heat needs to be dissipated. Conversely, more intensive cooling of the chip formation zone can result in an increase in the forming strength of the material, which in turn may lead to an increase in the force and power required to cut the material (Denkena; Tönshoff, 2011).

For the final feed travel distance of 1600 mm, Table 15 shows the results of the ANOVA, indicating that the relative density (13.2% contribution), feed per tooth f_z (12.1% contribution), radial depth of cut a_e (60% contribution), and use of coolant (13.1%) factors still significantly affect the response of the mean F_a. The cutting edge radius r_β, however, became insignificant, with its significance level also decreasing after 700 mm of machined feed travel. The evolution of the significance of r_β in the response of the mean F_a is consistent with the expected behavior of r_β, which tends to be modified due to tool wear influence after higher feed travel distances. The a_e remains as the control variable with greater contribution to the response, followed by relative density, f_z and use of lubricant.

Table 15 – Result of the analysis of variance for mean F_a after l_f = 1600 mm

Factors	DF	Adj. SS	Adj. MS	F-value	p-value	Contribution [%]
Rel. Density (D_r)	1	9224	9224	29.66	0.000	13.2
Hard Metal Substrate	1	196.2	196.2	0.63	0.435	0.3
Cutting edge radius (r_β)	1	66.4	66.4	0.21	0.648	0.1
Cutting speed (v_c)	1	86.3	86.3	0.28	0.603	0.1
Feed per tooth (f_z)	1	8446.1	8446.1	27.16	0.000	12.1
Radial depth of cut (a_e)	1	41814.7	41814.7	134.47	0.000	60.0
Feed Direction	1	736.5	736.5	2.37	0.137	1.1
Coolant	1	9139.9	9139.9	29.39	0.000	13.1
Error	23	7152.3	311			
Total	31	76862.4				

Source: Author (2024).

Figure 50 shows the interactions and main effects diagrams sequentially for the four remaining significant factors after 1600 mm of machined feed travel. As expected, higher factor levels resulted in increased mean F_a values. In general, the mean F_a values were 17.2% higher for the 84% compared to the 72% relative density material. The radial depth of cut a_e played a major role in the response of mean F_a. A change in the factor level from 1.0 to 1.5 mm resulted in a 40.5% increase in the mean F_a for the 84% material and a 40.7% increase for the 72% material.

Figure 50 – Interaction and main effects diagrams for mean F_a after l_f = 1600 mm

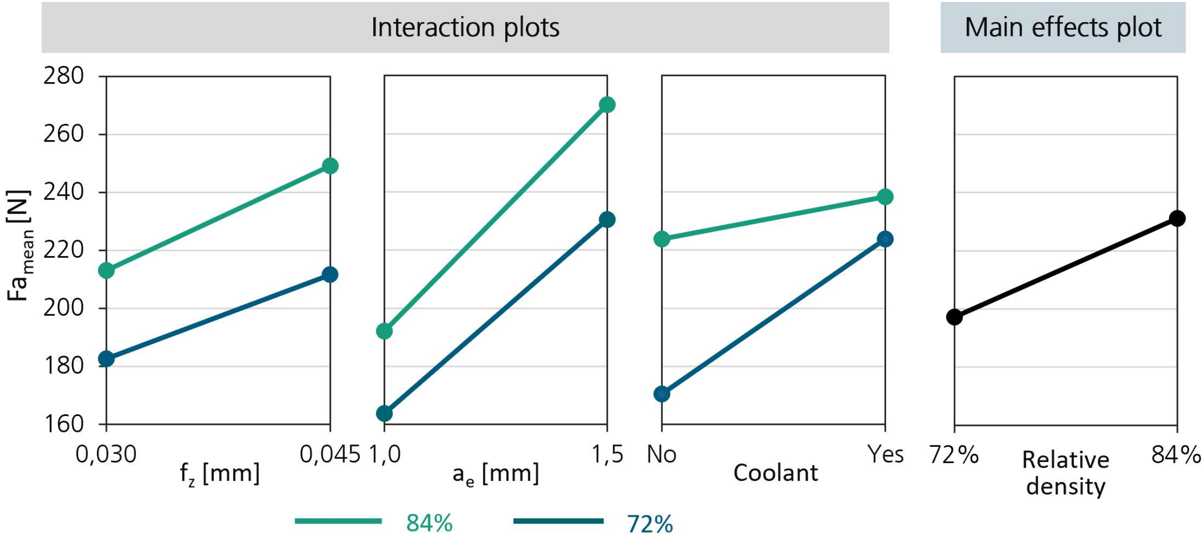

Source: Author (2024).

The interaction plots for f_z and a_e show that the curves of both porous variants run almost parallel to each other, indicating minimal interaction between relative density and f_z/a_e. This trend is consistent with the principles of cutting technology, which predict greater mechanical and thermal loads with larger values of a_e and f_z (Klocke, 2011). Moreover, the data suggests that the use of coolant has a greater impact on the mean F_a when cutting the 72% material, resulting in a 31.2% increase, compared to the 6.4% increase observed when cutting the 84% material. Further research is needed to fully understand the effects of coolant on the cutting forces.

4.3 ACCELERATIONS

The purpose of the process accelerations analysis is to quantify the vibration patterns observed when milling the two porous variants, as these oscillations have a strong influence on tool life, machinability, and surface quality (Klocke, 2011). The root mean square (RMS) was calculated for the x and y directions, which are related to the direction normal to the feed direction and to the feed motion direction, respectively, where process vibrations are most likely to occur. The RMS represents the average amplitude of the accelerations in units of acceleration g = 9.81 m/s^2. As vibrations occur in two opposite directions around the position of static equilibrium, the arithmetic mean is always approximately equal to zero. Therefore, the RMS approximates the value of the standard deviation, and can be interpreted as the amplitude of the oscillations (Li, 2023).

4.3.1 X-Axis Acceleration

Table 16 presents the ANOVA results for the RMS of acceleration in the x-direction acc_x (direction normal to the feed motion) after 200 mm of feed travel. The relative density (11.2% contribution) and cutting speed v_c (83.7% contribution) are the only two factors within the interval of significance ($\alpha = 0.05$, $p \leq 0.05$).

Table 16 – Result of the analysis of variance for the RMS of acc_x after $l_f = 200$ mm

Factors	DF	Adj. SS	Adj. MS	F-value	p-value	Contribution [%]
Rel. Density (D_r)	1	0.019561	0.019561	9.26	0.006	11.2
Hard Metal Substrate	1	0.001413	0.001413	0.67	0.422	0.8
Cutting edge radius (r_β)	1	0.001761	0.001761	0.83	0.371	1.0
Cutting speed (v_c)	1	0.145862	0.145862	69.06	0.000	83.7
Feed per tooth (f_z)	1	0.001150	0.001150	0.54	0.468	0.7
Radial depth of cut (a_e)	1	0.003114	0.003114	1.47	0.237	1.8
Feed Direction	1	0.000006	0.000006	0.00	0.957	0.0
Coolant	1	0.00137	0.00137	0.65	0.429	0.8
Error	23	0.048581	0.002112			
Total	31	0.222818				

Source: Author (2024).

In Figure 51, the main effects plot indicates that the amplitude of the oscillations was generally 22.6% higher when machining the 72% material compared to the denser variant. No interaction between v_c and relative density was identified. The v_c played a major role on the oscillations, changing the factor level from 30 to 45 m/min resulted in amplitudes 71.5% higher for the 72% material and 84.9% higher for the 84% variant.

Figure 51 – Interaction and main effects diagrams for the RMS of acc_x after $l_f = 200$ mm

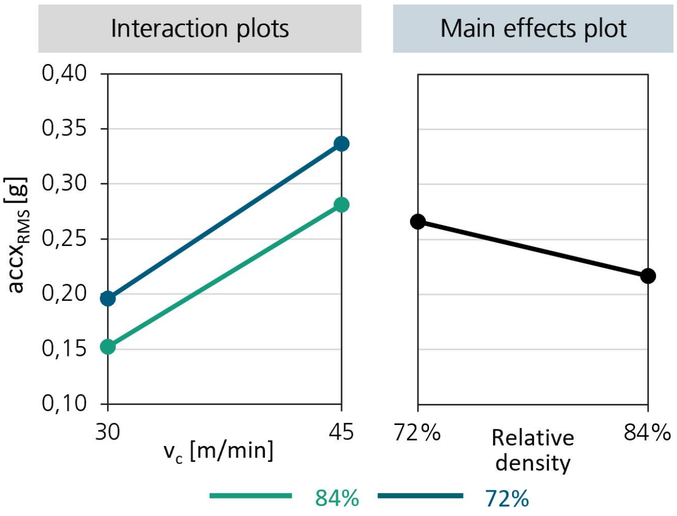

Source: Author (2024).

After l_f = 1600 mm, Table 17 shows that the significant factors for the response of acc_x are still the relative density (6.1% contribution) and v_c (86.8% contribution).

Table 17 – Result of the analysis of variance for the RMS of acc_x after l_f = 1600 mm

Factors	DF	Adj. SS	Adj. MS	F-value	p-value	Contribution [%]
Rel. Density (D_r)	1	0.012682	0.012682	8.82	0.007	6.1
Hard Metal Substrate	1	0.000411	0.000411	0.29	0.598	0.2
Cutting edge radius (r_β)	1	0.002343	0.002343	1.63	0.215	1.1
Cutting speed (v_c)	1	0.179397	0.179397	124.71	0.000	86.8
Feed per tooth (f_z)	1	0.003726	0.003726	2.59	0.121	1.8
Radial depth of cut (a_e)	1	0.003764	0.003764	2.62	0.119	1.8
Feed Direction	1	0.002161	0.002161	1.50	0.233	1.0
Coolant	1	0.002175	0.002175	1.51	0.231	1.1
Error	23	0.033085	0.001438			
Total	31	0.239743				

Source: Author (2024).

The interaction and main effects diagrams for the RMS of the acc_x after l_f = 1600 mm, in Figure 52, presented a similar trend compared to the one seen for the initial 200 mm of machined feed travel. Overall, the amplitude of the oscillations was 39.4% higher for the 72% relative density material compared to the 84% variant. No interaction was observed between cutting speed v_c and relative density. The value of RMS acc_x when milling with the higher v_c of 45 m/min was 72.6% higher for the 72% variant and 87% higher for the 84% material. The results indicate that within the selected parameters domain, process vibration increases steadily with an increase in v_c. One possible explanation for this phenomenon is that as the v_c increases, so does the momentum between the tool and the workpiece, which in turn leads to increased vibration due to the limited stiffness of the machine tool (Das; Hazarika, 2019; Li, 2023). At the same time, it is possible that built-up edge formation effect occurred during the tests. This phenomenon typically happens when machining Inconel 718 at low to medium, v_c below 50 m/min (Kümmel, 2016). As a result, cutting becomes unstable and process vibrations become stronger (Song; He; Ihara, 2023).

Moreover, the results show that the lower the relative density, the greater the vibration amplitudes. This might be explained by the greater stress differences between the local stresses in the stressed and unstressed areas of the cutting edge due to the discontinuous structure of porous Inconel 718. When the workpiece material stresses a local area of the cutting edge during machining, compressive stresses occur in the tool surface at that point. Meanwhile, due to the elasticity of the tool material and to achieve force equilibrium, tensile stresses occur in neighboring unstressed areas of the cutting edge (Klocke, 2011). If there is an abrupt structural change in the workpiece material due to porosity, uneven stress occurs, causing a greater force imbalance, which reflects in force fluctuations (Li, 2023).

Figure 52 – Interaction and main effects diagrams for the RMS of acc_x after l_f = 1600 mm

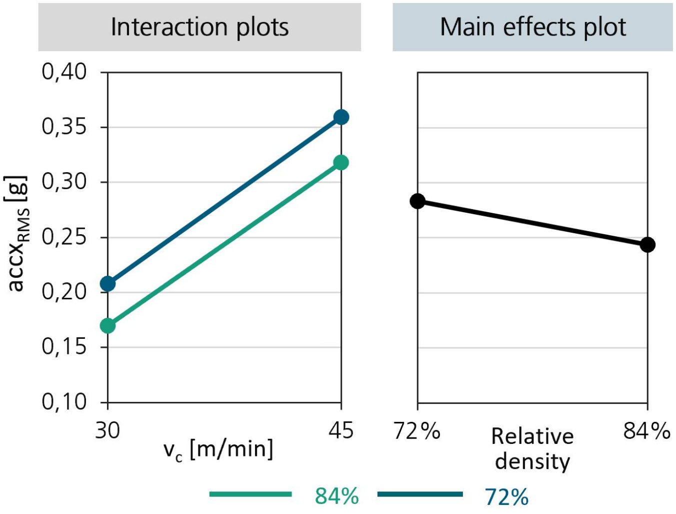

Source: Author (2024).

4.3.2 Y-Axis Acceleration

The RMS of the acc_y is used to quantify the oscillations in the y-direction (direction of feed motion). The accelerations in the x and y directions show a comparable tendency in relation to the manipulated variables with the greatest influence. The factors with the greatest influence are the relative density (D_r) and cutting speed (v_c). Table 18 shows the ANOVA results for the first 200 mm of the feed travel. The results indicate that relative density and v_c contribute 41.3% and 44.6%, respectively, to the response of the RMS acc_y.

Table 18 – Result of the analysis of variance for the RMS of acc_y after l_f = 200 mm

Factors	**DF**	**Adj. SS**	**Adj. MS**	**F-value**	**p-value**	**Contribution** [%]
Rel. Density (D_r)	1	0.041107	0.041107	15.32	0.001	41.3
Hard Metal Substrate	1	0.004354	0.004354	1.62	0.215	4.4
Cutting edge radius (r_β)	1	0.001963	0.001963	0.73	0.401	2.0
Cutting speed (v_c)	1	0.044346	0.044346	16.53	0.000	44.6
Feed per tooth (f_z)	1	0.000011	0.000011	0.00	0.949	0.0
Radial depth of cut (a_e)	1	0.001293	0.001293	0.48	0.495	1.3
Feed Direction	1	0.000180	0.000180	0.07	0.798	0.2
Coolant	1	0.006271	0.006271	2.34	0.140	6.3
Error	23	0.061718	0.002683			
Total	31	0.161242				

Source: Author (2024).

From the interaction and main effects plots in Figure 53, it was found that the amplitude of the oscillations in the y-direction was 43.4% greater when cutting the 72% relative density material compared to the 84% variant. Machining with the higher level of the cutting speed v_c led to an increase on the RMS acc_y of 19.3% when cutting with the 84% variant, while the increase was of 45.4% when cutting with the 72% relative density AM-Inconel 718.

Figure 53 – Interaction and main effects diagrams for the RMS of acc_y after l_f = 200 mm

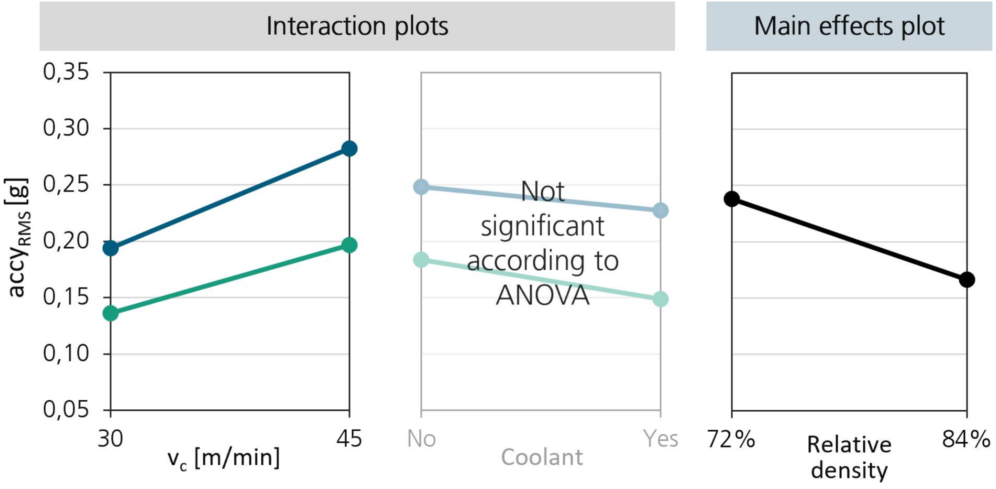

Source: Author (2024).

Table 19 presents the results of ANOVA for the final 1600 mm of machined feed travel. Now, the use of coolant (10% contribution) shows some level of significance on the response of the RMS acc_y. Together with the relative density (32.5% contribution) and cutting speed v_c (54% contribution). The same trend was also observed for the results of the intermediate 700 mm feed travel.

Table 19 – Result of the analysis of variance for the RMS of acc_y after l_f = 1600 mm

Factors	DF	Adj. SS	Adj. MS	F-value	p-value	Contribution [%]
Rel. Density (D_r)	1	0.038083	0.038083	14.28	0.001	32.5
Hard Metal Substrate	1	0.000885	0.000885	0.33	0.570	0.8
Cutting edge radius (r_β)	1	0.000573	0.000573	0.21	0.647	0.5
Cutting speed (v_c)	1	0.063396	0.063396	23.78	0.000	54.0
Feed per tooth (f_z)	1	0.000016	0.000016	0.01	0.938	0.0
Radial depth of cut (a_e)	1	0.000001	0.000001	0.00	0.984	0.0
Feed Direction	1	0.002676	0.002676	1.00	0.327	2.3
Coolant	1	0.011696	0.011696	4.39	0.047	10.0
Error	23	0.06132	0.002666			
Total	31	0.178647				

Source: Author (2024).

Finally, a 39.4% increase in the RMS values of acc_y when milling the 72% material compared to the 84% relative density variant can be seen in the interaction and main effects plots of Figure 54. Increasing the cutting speed v_c from the lower to the higher factor level caused a 42% increase in the amplitude of the oscillation in the y-direction for the 84% relative density material and 62.9% for the 72% relative density AM-Inconel 718. The small slope between the curves might be expected due to the fractional factorial experimental design. The interaction plot of coolant usage shows that the lines run almost parallel to each other. Machining with coolant appears to reduce the amplitude of the oscillations in the y-direction by 16.6% for the 84% relative density material and 22.3% for the 72% variant. Further study is required to better understand the mechanism behind the reduction of vibrations by coolants. One possible explanation is related to the lubricating effect, which reduces friction between two surfaces (Yang *et al.*, 2023). The observed trends and significance ν_c and relative density in the results of the RMS values of accelerations in the x and y directions are consistent with those reported in the investigation conducted by Li (2023, p. 99-105).

Figure 54 – Interaction and main effects diagrams for the RMS of acc_y after l_f = 1600 mm

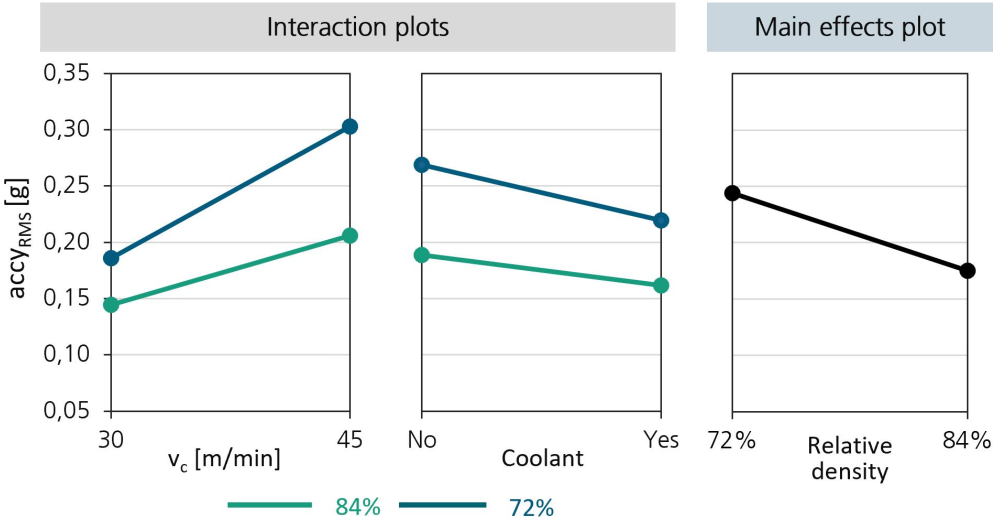

Source: Author (2024).

The results presented in this section for the process oscillations are in agreement with the interrupted cutting theory, one of the several theories used to explain the effect of porosity on the machinability of materials obtained by Powder Metallurgy (PM). According to this theory, the increased tool wear when machining such materials is result of the cyclic entry and exit of the cutting edge in the porous material, which leads to high mechanical alternating loads (Tutunea-Fatan; Fakhri; Bordatchev, 2011; Šalak; Danninger; Selecká, 2005). The process vibrations seem to affect more intensively the 72% relative density material than the 84% variant. A similar pattern was also observed by previous investigation on orthogonal cut in porous AM-Inconel 718 conducted by Li (2023).

4.4 CHIP FORMATION

Chips were collected for qualitative analysis after 200 mm of feed travel for parameter set 1 and 5 while machining both material porosities. Figure 55 illustrates the microscopic pictures and provides an overview of the chip structure. Chips in a row were obtained using the same parameter set. Both porosities produced chips with the characteristic and desirable chip comma or curling shape. The denser material, 84% relative density AM-Inconel 718, exhibited localized defects, particularly on its edges. While for the chips of the 72% relative density variant, defects were even more pronounced, resulting in an unstructured and disrupted surface. Although porosity was present in both materials, the chips of the 72% variant had larger cracks and gaps, and the chip formation was not fully continuous. This trend was observed for all chips analyzed. The variation of parameter sets did not significantly influence the chip structure, and no noticeable changes in the chip formation pattern were observed across different parameter sets. The qualitative analysis of the chips matches with the results of previous studies conducted by Li (2023, p. 106-107) and Kirchmann (2022, p. 73-75), in which similar behaviour was observed for the both porous material variants.

Figure 55 – Microscopic images of chip for Parameter Set 1 and 5 after l_f = 200 mm

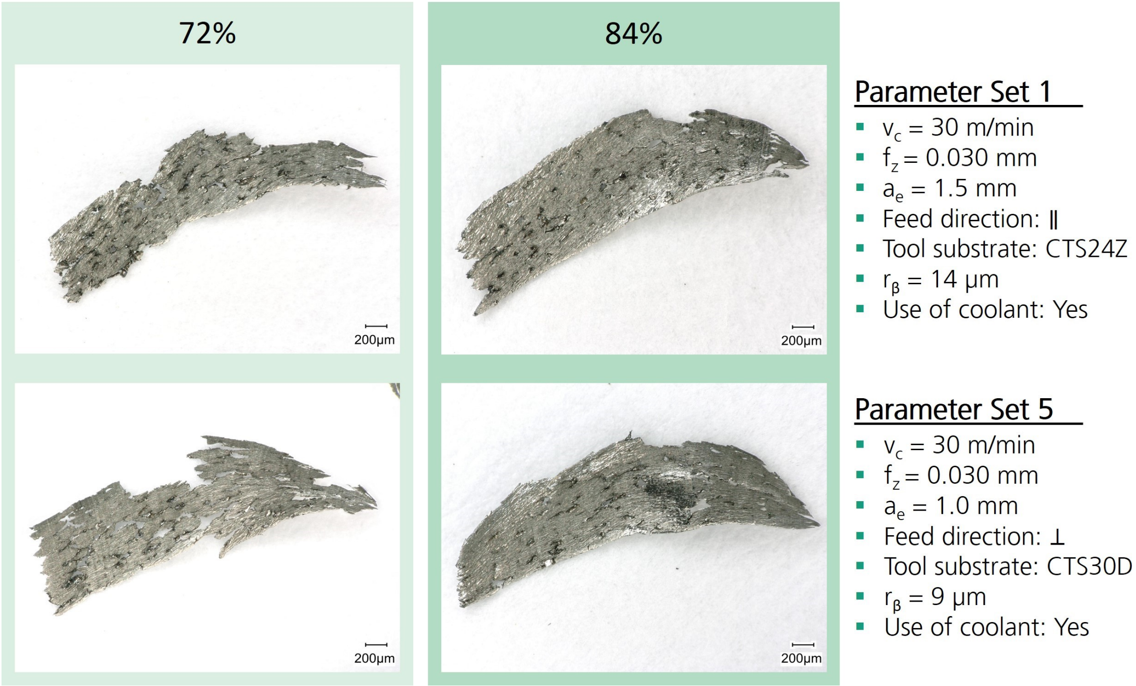

Parameter Set 1

- v_c = 30 m/min
- f_z = 0.030 mm
- a_e = 1.5 mm
- Feed direction: ∥
- Tool substrate: CTS24Z
- r_β = 14 μm
- Use of coolant: Yes

Parameter Set 5

- v_c = 30 m/min
- f_z = 0.030 mm
- a_e = 1.0 mm
- Feed direction: ⊥
- Tool substrate: CTS30D
- r_β = 9 μm
- Use of coolant: Yes

Source: Author (2024).

4.5 SURFACE QUALITY

A qualitative assessment of the workpiece's surface finishing was conducted based on images of the surface taken after the conclusion of the experimental trial. These images were captured for both material porosities, after milling the samples with the same set of parameters. The objective was to determine whether similarities or contrasts can be observed in the surface finishing. It is important to note that the surface finishing is not relevant for roughing as it is for finishing, since the finishing process comes additionally after roughing aiming to improve the quality of the machined surface and to apply fine dimensional adjustments. Figure 56 displays pictures of the machined workpiece surface obtained with the help of electronic microscopy. The first row of images shows the surface of the workpiece, which was machined parallel to the AM build-up direction using parameter set 16, and has a magnification of 50x. Both material porosities exhibit visible pores, but they appear to be more prominent and frequent on the surface of the 72% relative density material. In the second row, the images have a magnification of 100x and were taken from a workpiece machined perpendicular to the AM build-up direction using parameter set 12. The surface of the 72% relative density material also exhibited a similar trend of more visible and frequent pores. However, now on the surface of the 84% material larger pores are clearly visible. And as shown in the first row, many pores in this variant also appear to be partially clogged, but a closed layer was never formed, a behaviour also observed in the investigations conducted by Kirchmann (2022, p. 80).

Figure 56 – Microscopic images of the workpiece surface machined on parallel and perpendicular direction

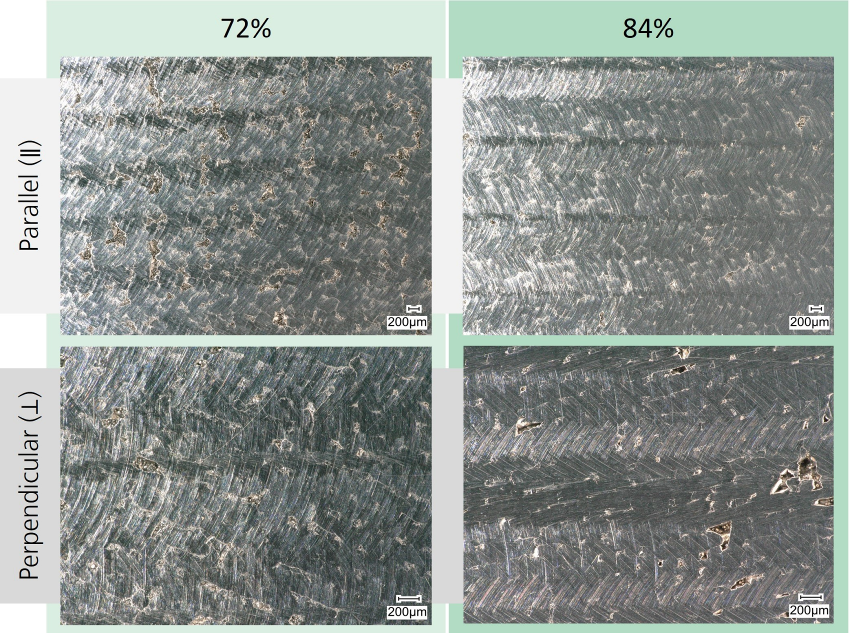

Parameter Set 16
- $v_c = 30$ m/min
- $f_z = 0.030$ mm
- $a_e = 1.0$ mm
- Tool substrate: CTS30D
- $r_\beta = 9$ µm
- Use of coolant: No

Parameter Set 12
- $v_c = 30$ m/min
- $f_z = 0.030$ mm
- $a_e = 1.5$ mm
- Tool substrate: CTS30D
- $r_\beta = 14$ µm
- Use of coolant: No

Source: Author (2024).

5 CONCLUSIONS

Additive manufacturing (AM) has several advantages over conventional manufacturing technologies and is gaining more attention in the aerospace and turbomachinery sectors, especially the Laser Powder Bed Fusion (LPBF) process. In some cases, support structures are necessary during the additive manufacturing process, but they are no longer needed once the process has been completed and must be removed, *e.g.*, by machining. The utilization of materials with induced porosity is appropriated for the support structure in the LPBF process. A porous support ensures good heat dissipation, resulting in uniform component properties, high holding forces, and shorter process time compared to conventional supports, like block and lattice structures. The nickel-chromium super alloy Inconel 718 is usually used in turbomachinery parts due to its desirable mechanical and thermal properties. However, the machinability of AM-Inconel 718 with induced porosity is not yet well understood.

The aim of this study was to investigate the influence of different process parameters on the machinability of porous AM-Inconel 718 obtained by LPBF. The study intends to contribute to the understanding of the feasibility of using porous material as support structures in the LPBF process for the manufacturing of complex aerospace components. In addition to the previously mentioned advantages, the use of such materials in the support structures has the potential to reduce material, time, and energy consumption, thereby enhancing the economic and environmental efficiency of the manufacturing process. Previous investigations have shown that chipping wear dominates when milling the porous Inconel 718 using carbide substrates commonly employed to machine this super alloy, which in its dense form is considered difficult to machine (Kirchmann, 2022; Schneider *et al.*, 2022). For this reason, this work investigated the cause-effect relationship between significant control variables and target variables on milling experiments, using Design of Experiments (DoE) and analysis of variance (ANOVA). The information gathered on the impact of the significant control variables on machinability and tool life may assist in reducing chipping and promoting uniform flank wear, as the dominant type of wear when machining such materials.

The main hypothesis of this work was to test tougher tungsten carbide tool substrates with higher concentrations of Cobalt, in order to increase their resistance to breakage and damage, helping to mitigate chipping. Eight two level control variables were studied, including relative density (D_r), cutting tool substrate, cutting edge radius (r_β), cutting speed (v_c), feed per tooth (f_z), radial depth of cut (a_e), direction of feed and the use of coolant. The results showed a significant reduction in chipping in comparison with the results obtained by Kirchmann (2022), particularly for the initial evaluated feed travel distances. The study found that the more porous material (72% relative density) showed the greatest improvement in chipping when machined with the tougher tool substrate CTS30D

(15% Co concentration), resulting in a 22% reduction in chipping wear compared to the CTS24Z substrate (12% Co concentration). The denser material (84% relative density) showed a smaller reduction of 7.5%. In addition, compared to previous research, it was possible for the first time to identify process parameter combinations that predominantly exhibited flank wear without chipping up to the investigated feed travel. These observations support the hypothesis that reduced chipping can be achieved by balancing toughness and hardness of the tool substrate. This trade-off could significantly reduce chipping without compromising the tool's resistance to abrasive wear, particularly for the 72% relative density material. The following paragraphs summarize the main conclusions for each of the examined target variables.

Abrasive-type flank wear was observed on the cutting edges at both material densities and increased with the feed travel (l_f), with greater values on the 84% relative density material than on the 72% material. This could be due to the lower volume to be machined and the lower cutting force or forming work required on the more porous variant (Schneider *et al.*, 2022). Adhesion type wear was also frequently identified on the cutting edges, which may lead to false or imprecise flank wear land (VB) measurements and impact the analysis. The main conclusions for the flank wear when milling the porous AM-Inconel are summarized below:

- Flank wear decreases as porosity increases;
- higher cutting speeds (v_c) lead to an increase in flank wear;
- the use of coolant reduces flank wear for both porosities, especially during the initial feed travel;
- at l_f = 1600 mm, flank wear was greater in the feed direction perpendicular to the AM build-up direction than in the feed direction parallel to it.

For chipping, the ANOVA results did not show any significant direct relation between porosity and chipping. Chipping was more prevalent in tools that had higher feed travels for the same volume of machined material. This is due to the use of two different radial depths of cut (a_e) in the trials, which allowed the same amount of machined material to be achieved by different feed travel distances. Additionally, it could be concluded regarding chipping that:

- As the Co concentration in the carbide substrate increases, the chipping effect decreases;
- greater radial depth of cut (a_e) results in less chipping;
- the use of coolant results in reduced chipping for the material with 84% relative density.

When examining the active force (F_a), higher forces were generally observed in lower porosity or in higher relative density. This is expected due to the higher volume of machined material and greater forming work in lower porosity. The active force values for both material porosities increased with the use of coolant. This phenomenon may be attributed to the side effects of greater cooling of the chip zone, which can result in an increase in the forming strength of the material and, thus, an increased force and power required during milling (Denkena; Tönshoff, 2011). However, further investigation is needed to confirm this. The conclusions for the active force are summarized below:

- The mean F_a decreases as porosity increases;
- higher feed per tooth (f_z) results in increased F_a values for both porosities;
- as the radial depth of cut (a_e) increases, the F_a values increase for both porosities;
- the use of coolant leads to an increase in the F_a for both porosities;
- for low feed travel, increasing the cutting edge radius (r_β) resulted in higher F_a values. Nevertheless, this result calls for further investigation, given that the two tested r_β values were relatively close to one another, due to fabrication inaccuracy, thereby making it challenging to discern their impact on the responses.

Oscillations occurred due to strongly varying force signals as porosity increased. The amplitude magnitudes of the accelerations in the directions normal to the feed motion (acc_x) and in the feed direction (acc_y) were analyzed. The conclusions for the process oscillations are very similar and presented below:

- The amplitude of the oscillations increases as the porosity increases;
- higher cutting speeds (ν_c) result in greater amplitudes of oscillations.

The mechanical alternating loads on the cutting edge support the theory of the interrupted cut. The pores that occur discontinuously result in an interrupted cut, whereby parts of the cutting edge is in contact with either a pore or a pore-free section. This results in a cyclic engagement and disengagement of the cutting tool, which in turn causes strong oscillations. The investigation revealed that cutting speed (ν_c), use of coolant and relative density had the greatest effect on flank wear, while the tool substrate, radial depth of cut (a_e), and use of coolant were particularly significant for chipping. The active force was mostly influenced by feed per tooth (f_z), radial depth of cut (a_e), use of coolant, and relative density, while the amplitude of the oscillations was influenced mainly by the cutting speed (ν_c) and relative density. Additionally, the qualitative analysis of the chips showed that as the porosity increased, the chip formation became less continuous and more susceptible to large cracks and gaps. Evaluation of the machined surface images showed more visible and frequent pores with increasing porosity. Overall, the results align with the findings of previous studies conducted by Kirchmann (2022) on milling and Li (2023) on orthogonal cut. Figure 57 presents a summary of the conclusions drawn from the quantitative analysis of this work regarding the influence of the influencing variables on the target variables.

From the presented conclusions, future investigations can derive additional insights and process optimization strategies to improve the wear behavior and machinability of

Figure 57 – Cause and effect relationships between the influencing and target factors in milling of porous AM-Inconel 718

Increase in control variables / Impact on target variables	Workpiece	Cutting tool		Milling Process				
	D_r	Co [%m]	r_β	v_c	f_z	a_e	Feed direction (∥ → ⊥)	Use of coolant (No → Yes)
Cutting tool								
Flank wear (VB)	↗	—	—	↗	—	—	↗*	↘**
Chipping (CH)	—	↘	—	—	—	↘	—	↘***
Cutting forces								
Active Force (F_a)	↗	—	↗**	—	↗	↗	—	↗
Mechanical load oscillations								
x-direction oscillation Amplitude ($accx_{RMS}$)	↘	—	—	↗	—	—	—	—
y-direction oscillation Amplitude ($accy_{RMS}$)	↘	—	—	↗	—	—	—	↘**

* The effect of the control variable on the target variable becomes significant only at the final feed travel.
** The effect of the control variable on the target variable is significant only at the initial feed travel.
*** Interaction between the control variable and relative density was observed.

↗ Increase ↘ Decrease — No significant trend

Source: Author (2024).

porous additively manufactured Inconel 718. Future research should start from the basis provided by this and previous works to develop further strategies and investigate how to reduce chipping caused by the alternating mechanical load and thus increase the economic efficiency when machining the porous AM-Inconel 718. Examples of possible improvements include selecting a suitable tool coating, textured cutting tools (Kümmel *et al.*, 2015), and conducting further investigations into the influence of cutting edge rounding, obtained through optimized brushing processes (Bergs *et al.*, 2020). Aside from that, extended investigations using more complex geometries should be conducted to assess the economic and environmental viability of the process in a real-world industry application and compared to traditional manufacturing techniques. One such example could be the manufacturing of a BLISK via LPBF with a porous support structure, using different support formats. Lastly, it is advisable to consider adjustments to the significant process parameters.

BIBLIOGRAPHY

AKHTAR, W.; SUN, J.; SUN, P.; CHEN, W.; SALEEM, Z. Tool wear mechanisms in the machining of nickel based super-alloys: A review. **Frontiers of Mechanical Engineering**, Higher Education Press, v. 9, p. 106–119, 2014.

AMERICAN SOCIETY FOR TESTING AND MATERIALS. **ASTM F2792**: Standard terminology for additive manufacturing technologies. West Conshohocken, 2012.

AMERICAN SOCIETY FOR TESTING AND MATERIALS. **ASTM B611**: Standard terminology for additive manufacturing technologies. West Conshohocken, 2017.

ANGRISH, A. A critical analysis of additive manufacturing technologies for aerospace applications. *In*: **Proceedings** of the 2014 IEEE AEROSPACE CONFERENCE, 1-8 mar. 2014, Big Sky, MT, USA. p. 1–6. Available from Internet: https://ieeexplore.ieee.org/document/6836456. Accessed on: 3 oct. 2023.

ANTONY, J. **Design of Experiments for Engineers and Scientists**. 1st. ed. San Diego: Elsevier, 2003.

BARTOLOMEIS, A. D.; NEWMAN, S. T.; JAWAHIR, I. S.; BIERMANN, D.; SHOKRANI, A. Future research directions in the machining of inconel 718. **Journal of Materials Processing Technology**, Elsevier Ltd, v. 297, n. 1, p. 1–21, 11 2021.

BERGS, T.; SCHNEIDER, S.; AMARA, M.; GANSER, P. Preparation of symmetrical and asymmetrical cutting edges on solid cutting tools using brushing tools with filament-integrated diamond grits. *In*: **Proceedings** of the 53RD CIRP CONFERENCE ON MANUFACTURING SYSTEMS 2020, 1-3 jul. 2020, Chicago. p. 873–878. Available from Internet: https://www.sciencedirect.com/science/article/pii/S2212827120305801. Accessed on: 14 apr. 2024.

BHUSHAN, B. **Principles and applications of tribology**. 2nd. ed. Hoboken, NJ: Wiley, 2013.

BLAKEY-MILNER, B. *et al*. Metal additive manufacturing in aerospace: A review. **Materials and Design**, v. 209, n. 12, p. 33, 11 2021.

CABRAL, G. F. **Modeling and Simulation of Tool Engagement and Prediction of Process Forces in Milling**. PhD Thesis in Mechanical Engineering — Rheinisch-Westfälischen Technischen Hochschule Aachen, Aachen, 2015.

CELAYA, A. *et al*. Influence of cutting edge radius on tool life in milling inconel 718. *In*: **Proceedings** of the 22ND INTERNATIONAL ESAFORM CONFERENCE ON MATERIAL FORMING, 8–10 may 2019, Vitoria-Gasteiz, Spain. p. 8–19. Available from Internet: https://ui.adsabs.harvard.edu/abs/2019AIPC.2113h0019C/abstract. Accessed on: 5 jan. 2024.

CERATIZIT. **Ceratizit Round Tool Materials - P-Line**. 114 p. 2020. Available from Internet: https://www.cbceratizit.com/files/CT%202020_EN.pdf. Accessed on: 21 dec. 2023.

CHEN, L.; XU, Q.; LIU, Y.; CAI, G.; LIU, J. Machinability of the laser additively manufactured inconel 718 superalloy in turning. **The International Journal of Advanced Manufacturing Technology**, v. 114, n. 1, p. 871–882, 1 2021.

DAS, R.; HAZARIKA, M. A study on effect of process parameters on vibration of cutting tool in turning operation. **Journal of Physics: Conference Series**, IOP Publishing, v. 1240, n. 1, p. 1–9, 6 2019. Available from Internet: https://iopscience.iop.org/article/10.1088/1742-6596/1240/1/012086. Accessed on: 10 feb. 2024.

DEGENER, W.; LUTZE, H.; SMEJKAL, E.; HEISEL, U.; ROTHMUND, J. **Spanende Formung: Theorie - Berechnung - Richtwerte**. 18. ed. München: Hanser Verlag, 2019.

DENKENA, B.; BIERMANN, D. Cutting edge geometries. **CIRP Annals**, v. 63, n. 2, p. 631–653, 04 2014.

DENKENA, B.; TöNSHOFF, H. K. **Spanen**: Grundlagen. 3rd. ed. Berlin: Springer Berlin Heidelberg, 2011.

DEUTSCHES INSTITUT FüR NORMUNG. **DIN 6583:1981-09**: Terms of cutting procedures; tool life criteria. Berlin, 1981.

DEUTSCHES INSTITUT FüR NORMUNG. **DIN 6584:1982-10**: Terms of the cutting technique; forces, energy, work, power. Berlin, 1982.

DEUTSCHES INSTITUT FüR NORMUNG. **DIN 6580:1985-10**: Terminology of chip removing; movements and geometry of the chip removing process. Berlin, 1988.

DEUTSCHES INSTITUT FüR NORMUNG. **DIN 6582:1988-02**: Terminology of cutting; additional terms for the tool, the wedge and the cutting edge. Berlin, 1988.

DEUTSCHES INSTITUT FüR NORMUNG. **DIN 8589-0:2003-09**: Manufacturing processes chip removal - part 0: General; classification, subdivision, terms and definitions. 8 p. Berlin: Beuth Verlag, 2003.

DEUTSCHES INSTITUT FüR NORMUNG. **DIN 10088-1:2014-12**: Stainless steels - part 1: List of stainless steels. Berlin, 2014.

DEUTSCHES INSTITUT FüR NORMUNG. **DIN 8580:2022-12**: Manufacturing processes - terms and definitions, division. 25 p. Berlin: Beuth Verlag, 2022.

DIETRICH, J. **Praxis der Zerspantechnik**: Verfahren, werkzeuge, berechnung. 12. ed. Wiesbaden: Springer Vieweg Wiesbaden, 2016.

DUCROUX, E.; FROMENTIN, G.; VIPREY, F.; PRAT, D.; D'ACUNTO, A. New mechanistic cutting force model for milling additive manufactured inconel 718 considering effects of tool wear evolution and actual tool geometry. **Journal of Manufacturing Processes**, Elsevier Ltd, v. 64, n. 1, p. 67–80, 4 2021.

DUTTA, B.; FROES, F. H. The additive manufacturing (am) of titanium alloys. **Metal Powder Report**, v. 72, n. 2, p. 96–106, 2017.

FRAUNHOFER-INSTITUT FüR PRODUKTIONSTECHNOLOGIE. **Additive Fertigung zur Herstellung von Triebwerkskomponenten für die Luftfahrt**. Aachen. Available from Internet: https://www.ipt.fraunhofer.de/de/presse/Pressemitteilungen/20190618-additive-fertigung-zur-herstellung-von-triebwerkskomponenten-fuer-die-luftfahrt.html. Accessed on: 18 oct. 2023.

GELMAN, A. *et al*. Discussion paper analysis of variance - why it is more important than ever. **Annals of Statistics**, Institute of Mathematical Statistics, v. 33, p. 1–53, 2005.

GIBSON, I.; ROSEN, D.; STUCKER, B.; KHORASANI, M. **Additive Manufacturing Technologies**.

GUNST, R. F.; MASON, R. L. Fractional factorial design. **WIREs Computational Statistics**, v. 1, n. 2, p. 234–244, 9 2009. Available from Internet: https://wires.onlinelibrary.wiley.com/doi/abs/10.1002/wics.27. Accessed on: 19 feb. 2024.

HABIG, K.-H. **Verschleiß und Härte von Werkstoffen**. 1. ed. München: Carl Hanser, 1980.

HEANJIA SUPER-METALS CO. **Inconel 718 for aerospace engine applications**. Available from Internet: https://super-metals.com/wp-content/uploads/2015/04/Inconel-718-Super-alloy-in-aircraft-industry.pdf. Accessed on: 15 oct. 2023.

HERZOG, D.; SEYDA, V.; WYCISK, E.; EMMELMANN, C. Additive manufacturing of metals. **Acta Materialia**, Elsevier Ltd, v. 117, p. 371–392, 9 2016. ISSN 13596454.

HORNBOGEN, E.; EGGELER, G.; WERNER, E. **Werkstoffe**: Aufbau und eigenschaften von keramik-, metall-, polymer- und verbundwerkstoffen. 10. ed. Berlin: Springer Berlin, Heidelberg, 2011.

HRECHUK, A.; BUSHLYA, V. Automated detection of tool wear in machining and characterization of its shape. *In*: **Proceedings** of the 24TH INTERNATIONAL CONFERENCE ON WEAR OF MATERIALS, 16-20 apr. 2023, Banff, Canada. p. 204–214. Available from Internet: https://www.sciencedirect.com/science/article/pii/S004316482300145X. Accessed on: 22 feb. 2024.

HU, B.; III, R. W.; ROPAR, S.; NEILAN, A. The effect of porosity on machinability of pm materials. *In*: **Proceedings** of the POWDERMET 2016, 5-8 jun. 2016, Boston, USA. Boston, p. 1–15.

INTERNATIONAL ORGANIZATION FOR STANDARDIZATION. **ISO8688-2**: Tool-life testing in milling - part 2: End milling. Geneva, 1989.

INTERNATIONAL ORGANIZATION FOR STANDARDIZATION. **ISO3685:1993-11**: Tool-life testing with single-point turning tools. Geneva, 1993.

INTERNATIONAL ORGANIZATION FOR STANDARDIZATION. **ISO/ASTM 52900:2021**: Additive manufacturing - general principles - fundamentals and vocabulary. Geneva, 2021.

JäRVINEN, J. P. *et al*. Characterization of effect of support structures in laser additive manufacturing of stainless steel. *In*: **Proceedings** of the 8TH INTERNATIONAL CONFERENCE ON LASER ASSISTED NET SHAPE ENGINEERING LANE 2014, 8-11 sep. 2014, Fürth. p. 72–81. Available from Internet: https://www.sciencedirect.com/science/article/pii/S1875389214002442. Accessed on: 07 jan. 2024.

KAYA, M.; SUNAY, N.; KAYNAK, Y.; PıTıR, F. Comparison of finite element and empirical model prediction of surface residual stress in inconel 718 parts fabricated by laser powder bed fusion additive manufacturing. **Journal of Additive Manufacturing Technologies**, v. 1, n. 3, p. 529–535, 2021.

KHAN, S. A. *et al*. An in-depth analysis of tool wear mechanisms and surface integrity during high-speed hard turning of aisi d2 steel via novel inserts. **International Journal of Advanced Manufacturing Technology**, Springer Science and Business Media Deutschland GmbH, v. 122, p. 4013–4028, 10 2022.

KHANNA, N. *et al*. Review on machining of additively manufactured nickel and titanium alloys. **Journal of Materials Research and Technology**, v. 15, n. 1, p. 3192–3221, 11 2021. Available from Internet: https://www.sciencedirect.com/science/article/pii/S2238785421010772. Accessed on: 21 oct. 2023.

KIRCHMANN, S. **Untersuchung der Zerspanbarkeit von porösem, additiv hergestelltem Inconel 718**. Master's Degree in Aerospace Engineering — Fachhochschule Aachen, Aachen, 2022.

KISTLER GROUP. **Cutting Force**. Available from Internet: https://www.kistler.com/US/en/cutting-force/C00000102. Accessed on: 17 mar. 2024.

KISTLER INSTRUMENTE AG. **Data sheet Charge Amplifier Type 5011B**. 1-6 p. 2005. Available from Internet: www.kistler.com. Accessed on: 16 jan. 2024.

KISTLER INSTRUMENTE AG. **Data sheet 3-Component Dynamometer type 9255B**. 1-4 p. 2009. Available from Internet: www.kistler.com. Accessed on: 16 jan. 2024.

KLOCKE, F. **Manufacturing process 1**: Cutting. 1st. ed. Aachen: Springer Berlin, Heidelberg, 2011.

KLOCKE, F. *et al*. Technological and economical assessment of alternative process chains for blisk manufacture. *In*: **Proceedings** of the 15TH MACHINING INNOVATIONS CONFERENCE FOR AEROSPACE INDUSTRY (MIC 2015), 18-19 nov. 2015, Hannover. p. 67–72. Available from Internet: https://www.sciencedirect.com/science/article/pii/S2212827121011100. Accessed on: 28 jul. 2023.

KROL, T.; ZAEH, M.; SEIDEL, C. Optimization of supports in metal-based additive manufacturing by means of finite element models. *In*: **Proceedings** of the 23RD ANNUAL INTERNATIONAL SOLID FREEFORM FABRICATION SYMPOSIUM - AN ADDITIVE MANUFACTURING CONFERENCE, SFF 2012, 6-8 aug. 2012, Austin. p. 707–718. Available from Internet: https://repositories.lib.utexas.edu/items/06f6b165-2cc6-494a-af39-5711aa43097f. Accessed on: 8 jan. 2024.

KUMAR, P. *et al*. Influence of laser processing parameters on porosity in inconel 718 during additive manufacturing. **International Journal of Advanced Manufacturing Technology**, Springer London, v. 103, n. 1, p. 1497–1507, 4 2019.

KÜMMEL, J. **Detaillierte Analyse der Aufbauschneidenbildung bei der Trockenzerspanung von Stahl C45E mit Berücksichtigung des Werkzeugverschleißes**. PhD Thesis in Applied Materials — Karlsruher Institut für Technologie (KIT), 2016.

KÜMMEL, J. *et al*. Study on micro texturing of uncoated cemented carbide cutting tools for wear improvement and built-up edge stabilisation. **Journal of Materials Processing Technology**, v. 215, n. 1, p. 62–70, 01 2015.

LACHMAYER, R.; RETTSCHLAG, K.; KAIERLE, S. **Konstruktion für die Additive Fertigung 2020**. 1st. ed. Heidelberg: Springer Vieweg Berlin, Heidelberg, 2021.

LEDOLTER, J.; SWERSEY, A. J. **Testing 1-2-3: Experimental Design with Applications in Marketing and Service Operations**. 1st. ed. Stanford: Stanford Business Books, 2007.

LI, Y. **Untersuchung der Zerspanbarkeit und Werkstoffstruktur von mittels PBF-LB/M hergestelltem Inconel 718 mit gezielt eingestellter Porosität**. Master's Degree in Manufacturing Technology — RWTH Aachen University, Aachen, 2023.

MANI, M.; LYONS, K.; GUPTA, S. Sustainability characterization for additive manufacturing. **Journal of research of the National Institute of Standards and Technology**, National Institute of Standards and Technology, v. 119, n. 2, p. 419–428, 09 2014.

MATHEWS, P. G. **Design of experiments with MINITAB**. 1st. ed. Milwaukee, USA: ASQ Quality Press, 2005. 499 p.

MEYER, R.; KRUEGER, D. **A Minitab Guide to Statistics**. 3rd. ed. New Jersey: Pearson Education, 2005. 429 p.

MINITAB. **Minitab® 20 Support**: What is an interaction? Available from Internet: https://support.minitab.com/en-us/minitab/20/help-and-how-to/statistical-modeling/anova/supporting-topics/anova-models/what-is-an-interaction/. Accessed on: 17 mar. 2024.

MINITAB. **Minitab® 21 Support**: Available 2-level factorial designs. Available from Internet: https://support.minitab.com/en-us/minitab/21/help-and-how-to/statistical-modeling/doe/supporting-topics/factorial-and-screening-designs/available-2-level-factorial-designs/. Accessed on: 12 mar. 2024.

MINITAB. **Minitab® 21 Support**: What is a main effects plot? Available from Internet: https://support.minitab.com/en-us/minitab/21/help-and-how-to/statistical-modeling/anova/supporting-topics/basics/what-is-a-main-effects-plot/. Accessed on: 16 jan. 2024.

MINITAB. **Minitab® 21 Support**: Overview for interaction plot. Available from Internet: https://support.minitab.com/en-us/minitab/21/help-and-how-to/statistical-modeling/anova/how-to/interaction-plot/before-you-start/overview/. Accessed on: 15 jan. 2024.

MINITAB. **Minitab® 21 Support**: Analysis of variance table for one-way anova. Available from Internet: https://support.minitab.com/en-us/minitab/21/help-and-how-to/statistical-modeling/anova/how-to/one-way-anova/interpret-the-results/all-statistics-and-graphs/analysis-of-variance-table/. Accessed on: 22 feb. 2024.

NAJMON, J. C.; RAEISI, S.; TOVAR, A. Review of additive manufacturing technologies and applications in the aerospace industry. *In*: FROES, F.; BOYER, R. (Ed.). **Additive Manufacturing for the Aerospace Industry**. Cambridge: Elsevier, 2019. p. 7–31.

NATIONAL INSTRUMENTS. **NI cDAQ-9178 Specifications**. Available from Internet: https://www.ni.com/docs/en-US/bundle/cdaq-9178-specs/page/specs.html. Accessed on: 24 jan. 2024.

OIMOEN, S. **Classical Designs: Full Factorial Designs**. 25 p. 2019. Available from Internet: https://www.afit.edu/stat/statcoe_files/Classical%20Designs-Full%20Factorial%20Designs_Final.pdf. Accessed on: 15 dec. 2023.

ONDřEJ, H.; MIROSLAV, Z.; TOMáš, B. The influence of cutting edge radius on force load when milling inconel 718. *In*: **Proceedings** of the 29TH DAAAM INTERNATIONAL SYMPOSIUM ON INTELLIGENT MANUFACTURING AND AUTOMATION, 24-27 oct. 2018, Zadar, Croatia. p. 822–828. Available from Internet: https://dspace5.zcu.cz/bitstream/11025/33829/1/119.pdf. Accessed on: 5 jan. 2024.

OPITZ, H.; BRAMMERTZ, P.-H.; KOHLHAGE, E. H. **Untersuchungen zum Leistungsvergleich der Feinbearbeitungsverfahren**. 1st. ed. Wiesbaden: VS Verlag für Sozialwissenschaften, 1963. 66 p.

RAHMAN, M.; SEAH, W.; TEO, T. The machinability of inconel 718. **Journal of Materials Processing Technology**, v. 63, n. 1, p. 199–204, 1 1997. Available from Internet: https://www.sciencedirect.com/science/article/pii/S0924013696026246. Accessed on: 8 jun. 2023.

SCHEDLER, W. **Hartmetall für den Praktiker**: Aufbau, herstellung, eigenschaften und industrielle anwendung einer modernen werkstoffgruppe. 10. ed. Düsseldorf: Plansee TIZIT GmbH VDI, 1988.

SCHLEIFENBAUM, H.; MEINERS, W.; WISSENBACH, K.; HINKE, C. Individualized production by means of high power selective laser melting. **CIRP Journal of Manufacturing Science and Technology**, v. 2, n. 3, p. 161–169, 2010.

SCHNEIDER, S. A. M. *et al.* Machinability analysis for milling of additively manufactured inconel 718 with specifically induced porosity. *In*: **Proceedings** of the MACHINING INNOVATIONS CONFERENCE FOR AEROSPACE INDUSTRY (MIC) 2022, 30 nov.-1 dec. 2022, Hannover. p. 51–58. Available from Internet: https://papers.ssrn.com/sol3/papers.cfm?abstract_id=4259357#. Accessed on: 12 aug. 2023.

SCHNEIDER, S. A. M. *et al.* Machinability study in orthogonal cutting of additively manufactured inconel 718 with specifically induced porosity. *In*: **Proceedings** of the 11TH CIRP GLOBAL WEB CONFERENCE (CIRPE 2023), 24-26 oct. 2023, Cape Town. p. 168–173. Available from Internet: https://www.sciencedirect.com/journal/procedia-cirp/vol/115/suppl/C. Accessed on: 01 nov. 2023.

SECO TOOLS. **Tool Wear Patterns and how to optimize them**. Available from Internet: https://www.secotools.com/article/122073?language=en. Accessed on: 15 oct. 2023.

SOCIETY OF AUTOMOTIVE ENGINEERS. **AMS5662P**: Nickel alloy, corrosion- and heat-resistant, bars, forgings, rings, and stock for forgings and rings 52.5ni - 19cr - 3.0mo - 5.1cb (nb) - 0.90ti - 0.50al - 18fe consumable electrode or vacuum induction melted 1775 °f (968 °c) solution heat treated, precipitation-hardenable. Warrendale, 2022.

SONG, X.; HE, W.; IHARA, T. A novel approach for dry cutting inconel 718 in a more sustainable and low-cost way by actively and purposely utilizing the built-up layer. **Micromachines**, Multidisciplinary Digital Publishing Institute (MDPI), v. 14, 9 2023.

SVANTESSON, R. **Optimization of support structures for laser powder bed fusion by Design for AM**. Master's Degree in Product Development — Chalmers Uiversity of Technology, Gothenburg, 2021.

TEPYLO, N.; HUANG, X.; PATNAIK, P. C. Laser-based additive manufacturing technologies for aerospace applications. **Advanced Engineering Materials**, Wiley-VCH Verlag, v. 21, 11 2019. Available from Internet: https://onlinelibrary.wiley.com/doi/abs/10.1002/adem.201900617. Accessed on: 13 aug. 2023.

TUTUNEA-FATAN, O. R.; FAKHRI, M. A.; BORDATCHEV, E. V. Porosity and cutting forces: From macroscale to microscale machining correlationsg. **Proceedings of the Institution of Mechanical Engineers, Part B: Journal of Engineering Manufacture**, v. 225, n. 5, p. 619–630, 5 2011.

VALDEZ, M.; KOZUCH, C.; FAIERSON, E. J.; JASIUK, I. Induced porosity in super alloy 718 through the laser additive manufacturing process: Microstructure and mechanical properties. **Journal of Alloys and Compounds**, Elsevier Ltd, v. 725, n. 1, p. 757–764, 11 2017.

VIEREGGE, G. **Zerspanung Der Eisenwerkstoffe**. Oberthal: Verlag Stahleisen, 1959.

VOLPATO, G. M.; TETZLAFF, U.; FREDEL, M. C. A comprehensive literature review on laser powder bed fusion of inconel superalloys. **Additive Manufacturing**, v. 55, p. 102871, 7 2022. Available from Internet: https://www.sciencedirect.com/science/article/pii/S2214860422002706. Accessed on: 20 nov. 2023.

WOOD, P. *et al*. Machinability of inconel718 alloy with a porous microstructure produced by laser melting powder bed fusion at higher energy densities. **Materials**, v. 13, n. 24, p. 1–13, 12 2020.

YANG, K. Z. *et al*. Application of coolants during tool-based machining - a review. **Ain Shams Engineering Journal**, v. 14, n. 1, p. 1–17, 5 2023.

YOUSSEF, H. A.; EL-HOFY, H. **Machining technology: machine tools and operations**. Boca Raton: CRC Press, 2008.

ŠALAK, A.; DANNINGER, H.; SELECKá, M. **Machinability of Powder Metallurgy Steels**. 1st. ed. Cambridge: Cambridge International Science Publishing, 2005.

APPENDIX A – PARAMETER SETS WITH MINIMAL CHIPPING

Figure 58 – Wear development on the cutting edges under milling of 84% material using parameter set 2

Parameter Set 2

Relative density = 84% / v_c = 30 m/min / f_z = 0.045 mm / a_e = 1.0 mm

Cutting direction: ǁ / Tool substrate: CTS30D / r_β = 14 µm / Use of coolant: No

Source: Author (2024).

Figure 59 – Wear development on the cutting edges under milling of 84% material using parameter set 14

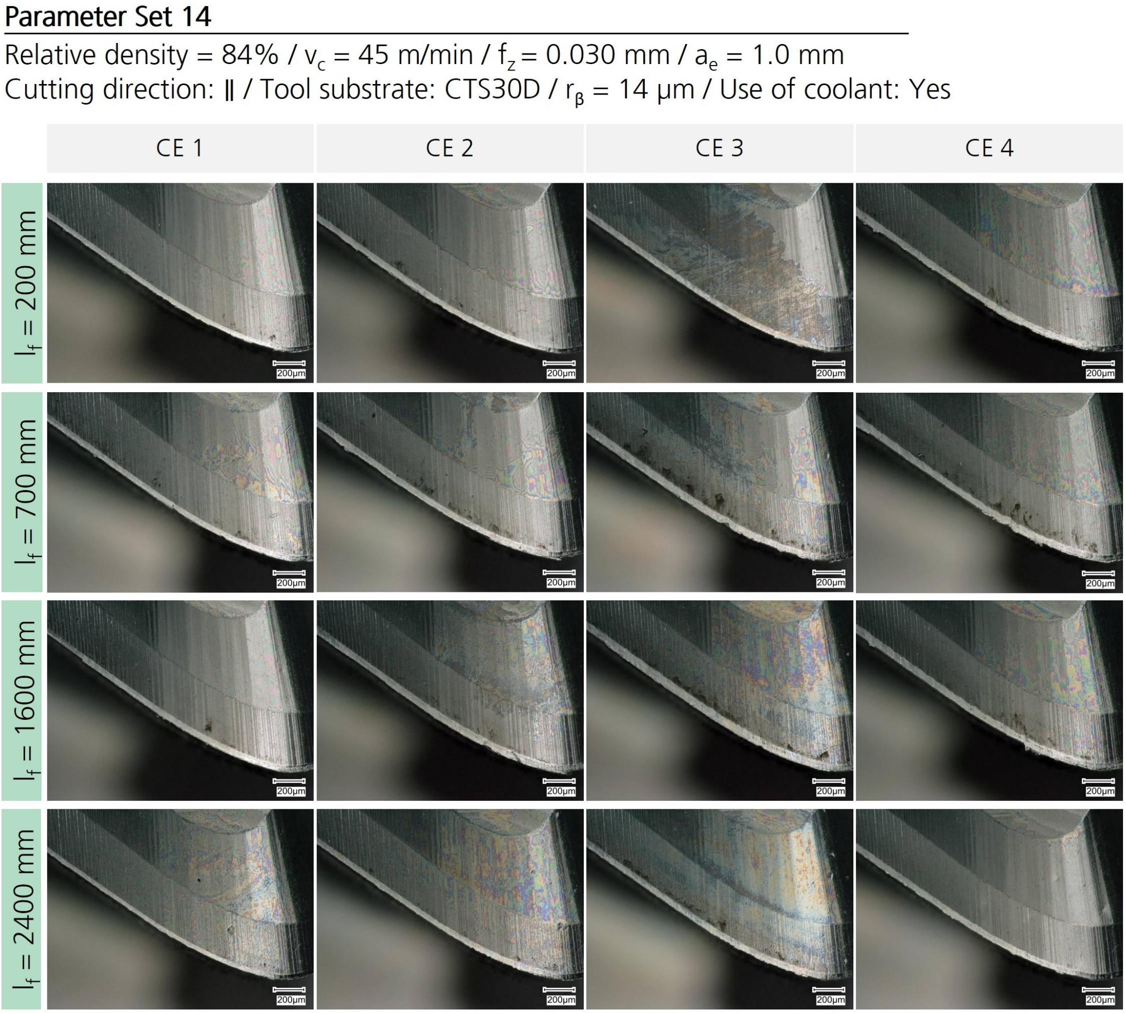

Source: Author (2024).